ไคโตซานดัดแปรเพื่อเพิ่มสมบัติการเกาะติดเยื่อเมือกสำหรับระบบนำส่งยาที่ระบบทางเดินอาหาร

นางสาวเมธาวี ศรีละพันธ์

MODIFIED CHITOSAN TO ENHANCE MUCOADHESIVE PROPERTIES FOR
GASTROINTESTINAL DRUG DELIVERY SYSTEM

Miss Metawee Srilaphan

A Thesis Submitted in Partial Fulfillment of the Requirements
for the Degree of Master of Science Program in Petrochemistry and Polymer Science
Faculty of Science
Chulalongkorn University
Academic Year 2009

| Thesis Title | MODIFIED CHITOSAN TO ENHANCE MUCOADHESIVE PROPERTIES FOR GASTROINTESTINAL DRUG DELIVERY SYSTEM |
| --- | --- |
| By | Miss Metawee Srilaphan |
| Field of Study | Petrochemistry and Polymer Science |
| Thesis Advisor | Associate Professsor Nongnuj Muangsin, Ph.D. |
| Thesis Co-Advisor | Nalena Praphairaksit, D.V.M., Ph.D. |

Accepted by the Faculty of Science, Chulalongkorn University in Partial Fulfillment of the Requirements for the Master's Degree

……………………………………… Dean of the Faculty of Science

(Professor Supot Hannongbua, Dr.rer.nat.)

THESIS COMMITTEE

………………………………………….. Chairman

(Associate Professor Sirirat Kokpol, Ph.D.)

………………………………………..……. Thesis Advisor

(Associate Professsor Nongnuj Muangsin, Ph.D.)

………………………………………….. Thesis Co-Advisor

(Nalena Praphairaksit, D.V.M., Ph.D.)

………………………………………….. Examiner

(Assistant Professor Warinthorn Chavasiri, Ph.D.)

………………………………………….. External Examiner

(Assistant Professor Thongdee Leksopee, Ph.D)

เมธาวี ศรีละพันธ์ : ไคโตซานดัดแปรเพื่อเพิ่มสมบัติการเกาะติดเยื่อเมือกสำหรับระบบ
นำส่งยาที่ระบบทางเดินอาหาร (MODIFIED CHITOSAN TO ENHANCE
MUCOADHESIVE PROPERTIES FOR GASTROINTESTINAL DRUG DELIVERY
SYSTEM) อ.ที่ปรึกษาวิทยานิพนธ์หลัก: รศ.ดร.นงนุช เหมืองสิน, อ.ที่ปรึกษาวิทยานิพนธ์
ร่วม: อ.สพญ.ดร.นลินา ประไพรักษ์สิทธิ์, 183 หน้า.


งานวิจัยนี้มีแนวคิดที่จะดัดแปรไคโตซานเพื่อเพิ่มสมบัติเกาะติดเยื่อเมือกที่กระเพาะอาหาร
เพื่อใช้ในระบบนำส่งยา พร้อมทั้งมีความสามารถในการหน่วงการปลดปล่อยและเพิ่ม
ประสิทธิภาพในการออกฤทธิ์ของยา พอลิเมอร์ที่สังเคราะห์ได้มีสมบัติเกาะติดเยื่อเมือกจึงเพิ่ม
โอกาสให้ยาสามารถปลดปล่อยเข้าไปถึงเชื้อได้มากขึ้น และไม่เป็นพิษต่อเซลล์ มีความสามารถใน
การละลายและบวมตัวที่ดี ทนต่อกรดในกระเพาะอาหาร พิสูจน์เอกลักษณ์ของไคโตซานที่ทำการ
ดัดแปรแล้วด้วยเทคนิค NMR, FT-IR และ DSC ศึกษาสมบัติเกาะติดเยื่อเมือกที่สภาวะ pH 1.2 ซึ่ง
เป็นสภาวะเดียวกันกับกระเพาะอาหาร พบว่าที่ pH 1.2 ไคโตซานดัดแปรมีสมบัติเกาะติดเยื่อเมือก
ได้ดีกว่าไคโตซาน และความสามารถในการละลายและการบวมตัวดีกว่าไคโตซาน จึงนำพอลิเมอร์
ที่ได้มาใช้ควบคุมปลดปล่อยตัวยาในสภาวะเลียนแบบที่กระเพาะอาหารและลำไส้เล็ก โดยใช้ยา
แอม็อกซิซิลลินและยาโซเดียมไดโครฟีแนคเป็นต้นแบบยาในการทดลอง และใช้สูตรผสมของ
แอลจิเนตเป็นเมทริกซ์สำหรับการเตรียมบีด และใช้ไคโตซานและไคโตซานดัดแปรเป็นส่วน
เคลือบบีด ซึ่งจะพบว่ายาที่เคลือบด้วยไคโตซานดัดแปรสามารถหน่วงการปลดปล่อยยาได้นานถึง
5 ชั่วโมง ซึ่งสูตรผสมที่เตรียมได้นี้นับว่าเป็นทางเลือกใหม่สำหรับการรักษาได้อย่างมีประสิทธิภาพ

สาขาวิชา  ปิโตรเคมีและวิทยาศาสตร์พอลิเมอร์     ลายมือชื่อนิสิต.................................................
ปีการศึกษา    2552                                                  ลายมือชื่ออ.ที่ปรึกษาวิทยานิพนธ์หลัก..............
                                                                             ลายมือชื่ออ.ที่ปรึกษาวิทยานิพนธ์ร่วม................

# # 4972445423: MAJOR  PETROCHEMISTRY AND POLYMER SCIENCE

KEYWORDS: CHITOSAN / GLUCONOLACTONE / CAPROLACTONE / MUCOADHESIVE POLYMER

METAWEE SRILAPHAN: MODIFIED CHITOSAN TO ENHANCE MUCOADHESIVE PROPERTIES FOR GASTROINTESTINAL DRUG DELIVERY SYSTEM. THESIS ADVISOR: ASSOC. PROF. NONGNUJ MUANGSIN, Ph.D., THESIS CO-ADVISOR: NALENA PRAPHAIRAKSIT, D.V.M., Ph.D., 183 pp.

The objective of this research is to modify chitosan to enhance mucoadhesive properties of chitosan in order to apply to drug delivery system, to controlled release and increase drug efficiency. The synthetic polymers with improved mucoadhesive properties provide more chance for drug to release on to the *H. pylori*. In addition, this polymer is non-toxic, has high solubility and swelling, and can tolevate acid in the  stomach. The modified chitosan are characterized by NMR, FT-IR and DSC. The mucoadhesive properties of modified chitosan were studied at pH 1.2 which is the same condition as in the stomach. At pH 1.2, we found that the modified chitosan has a better mucoadhesive abilities than chitosan. From these reasons, we applied this polymer to controlled release of drug in the simulated gastrointestinal system. We used amoxicillin trihydrate and sodium diclofenac as drug model. Furthermore, alginate was used as a metrix polymer for beads preparation and chitosan and modified chitosan were used to coated on beads. The coated modified chitosan beads can controlled release up to 5 hours. In summary, it can be concluded that the beads coated with modified chitosan offer a novel alternative for the effective treatment of peptic ulcer.

Field of Study : Petrochemistry and Polymer Science       Student's Signature _____

Academic Year : 2009 _____       Advisor's Signature _____

                                                       Co-Advisor's Signature _____

# ACKNOWLEDGEMENTS

I would like to express my deepest appreciation and gratitude to my advisor, Associate Professor Dr. Nongnuj Muangsin, for providing valuable suggestion, guidance, encouragement and supportive throughout the entire period of conducting this thesis. I would like to express my thanks to my co-advisor Dr. Nalena Praphairaksit, Department of Biology, Faculty of Science, Srinakarinwirot University for all the assistances.

I would like to express deep appreciation to Associate Professor Dr. Sirirat Kokpol, Assistant Professor Dr. Warinthorn Chavasiri and Assistant Professor Dr. Thongdee Leksopee, attending as the chairman and members of my thesis committee, respectively, for their kind guidance, helpful discussions and valuable suggestions throughout my study.

A special appreciation is also to the Program of Petrochemistry and Polymer Science, Faculty of Science, Chulalongkorn University and Naional Center of Excellence for Petroleum, Petrochemicals, and Advanced Materials (NCE-PPAM), for provision of experimental facilities.

Finally, I would like to express thank to my family for their care and supports to make my study successful and my good friends whose names are not mentioned here for their love. Thanks are also due to everyone who has contributed suggestion and supports throughout my research.

# CONTENTS

# LIST OF TABLES

# LIST OF FIGURES

# LIST OF ABBREVIATIONS

| | |
|---|---|
| % | percentage |
| cm | centimeter |
| $cm^{-1}$ | unit of wave number |
| conc. | concentration |
| Chi | chitosan |
| MCC | chitosan-caprolactone modified |
| MCG | chitosan-gluconolactoe modified |
| °C | centrigrae degree |
| DSC | Differential scanning calorimeter |
| FTIR | Fourier Transform Infrared |
| UV | Ultraviolet |
| NMR | Nuclear Mangnetic Resonance |
| SEM | Scanning Electron Microscope |
| EE | entrapment efficiency |
| g | gram |
| min | minute |
| ml | milliliter |
| mg | milligram |
| pH | power of hydrogen ion or the negative logarithm (base ten) |
| w/v | weight/volume |
| v/v | volume/volume |

# CHAPTER I

# INTRODUCTION

## 1.1 Introduction

Mucoadhesive polymers are natural or synthetic macromolecules which could attach to mucosal surface. The mucoadhesive polymers have received considerable attention in pharmaceutical field since 1980s [1]. Nowadays, interests of studying mucoadhesive polymer have been to improve the efficiency of drug delivery systems at the mucous membranes level due to many advantages, such as the ability to prolong the residence time for sustained release within the specific location of drug [2]. Mucoadhesive polymers also exhibit permeation enhance properties are used, the intensified contact with the mucosa would provide the prerequisite for an increased epithelial for many drugs mediated by the polymeric carrier system, leading to an improved patient compliance [3].

Mucoadhesion of polymer with mucous membranes were based on the formation of non-covalent bond such as hydrogen bonds and ionic interaction or physical entanglement between the mucus layer and polymer [4]. For example, thiolate polymer or thiomer which is a thiol containing polymer, is a new mucoadhesive polymer drug delivery system. It showed strong mucoadhesive properties, because the thiol groups in the thiomer can formed disulfide bonds with the mucous membranes [5]. Poly(acrylates) is a carbomers which have mucoadhesive force with mucous membranes via hydrogen bonds, whereas chitosan seems to bind to the mucous membranes via ionic interactions between their primary amino substructures and sialic acid and sulfonic acid substructures of the mucus [6].

Some of the polymeric structural characteristics necessary for mucoadhesive polymer can be summarized as follows: 1) strong hydrogen bonding groups, e.g., carboxyl, hydroxyl, amino and sulfate groups, 2) strong anionic or cationic charges, 3) high molecular weight, 4) chain flexibility, 5) surface energy properties favoring spreading onto mucus and 6) nontoxic, nonabsorbable and noninteracting with the drug [7]. Other polymers that have mucoadhesive properties such as poly(acrylic

acid), deacetylated gellan gum, derivatised with thiol groups on their side chain, chitosan and chitosan derivative are able to increased the epithelial permeability for many drugs [8].

One of interesting mucoadhesive polymer is chitosan or poly[β-(1→4)-2-amino-2-deoxy-D-glucopyranose] (Figure 1.1). It is a polysaccharide obtained by N-deacetylation of chitin. Chitosan is a biocompatible, mucoadhesive, non-toxic, biodegradable polymer. It is widely used in pharmaceutical, medicine and biomaterial field [9,10]. Chitosan have high mucoadhesive properties due to the ability to form, depending on the pH, chemical bonds such as hydrogen bonds or ionic interaction between the positively charged amino groups of chitosan and the negatively charged of glycoproteins or mucins [11].
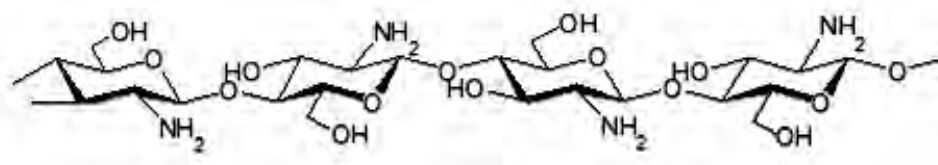


**Figure 1.1** Structure of chitosan

Modifying chitosan has been the approach to improve its mucoadhesive. Examples of modified chitosan are as follows:

Bernkop-Schnurch et al. [12] modified chitosan with 2-iminothiolane to obtained chitosan-4-thio-butyl-amidine (chitosan-TBA) (Figure 1.2a). It showed high mucoadhesive properties.



(a)                                                      (b)

(c)                                              (d)
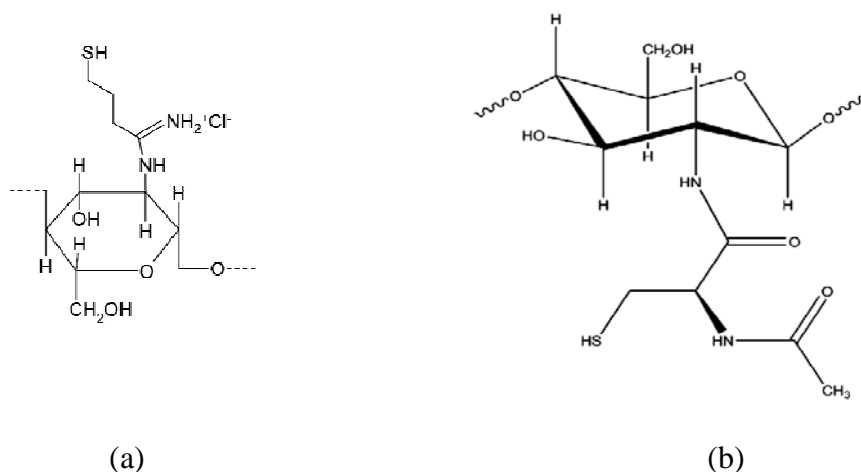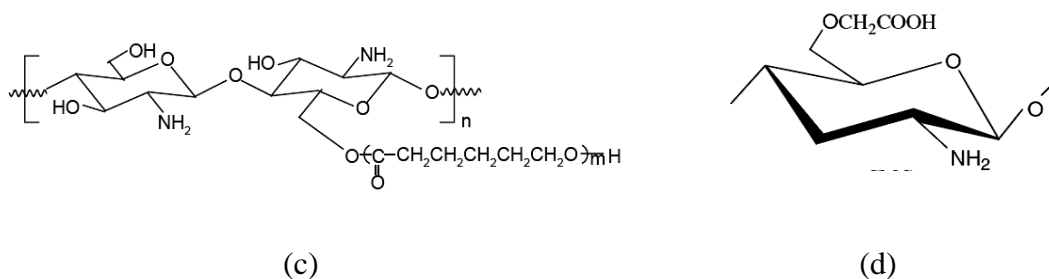
**Figure 1.2** Structures of (a) chitosan-4-thio-butyl-amidine, (b) chitosan-*N*-acetyl cysteine, (c) chitosan-g-polycaprolactone and (d) carboxymethyl chitosan

Schmitz et al. [2] synthesized and characterized a thiolated polymer by covalent attachment of N-acetyl cysteine to chitosan (Figure 1.2b). It showed strong mucoadhesive and cohesive properties.

Roldo et al. [3] reported the effect of the degree of modification and the polymer chain length on the mucoadhesive properties of thiolated chitosan derivatives obtained from chitosan and 2-iminothiolane (Figure 1.3).



glucosamine                              N-acetylglucosamine

N-(4-thio-1-imino-butyl) glucosamine
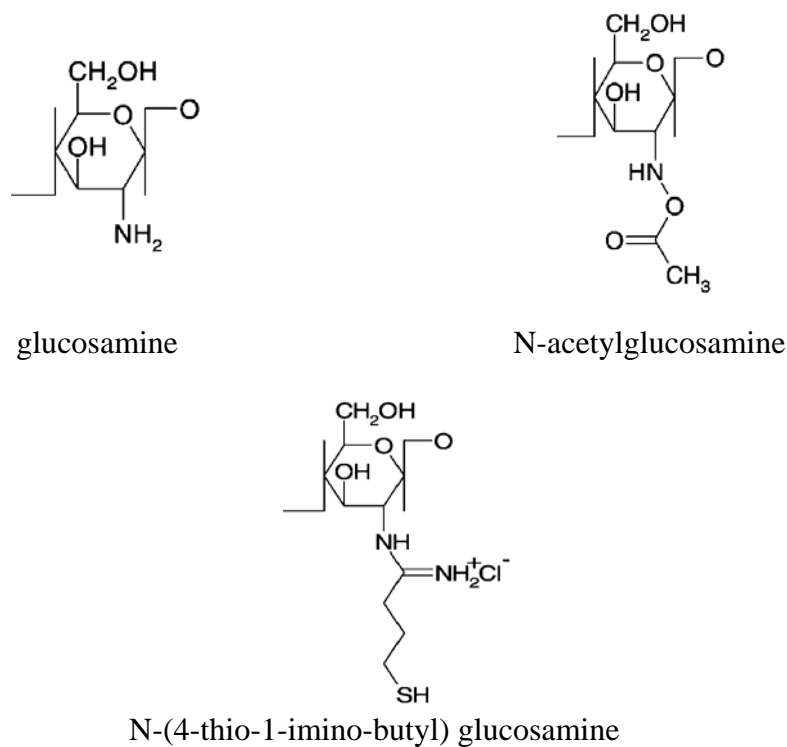
**Figure 1.3** Structure monomers on which chitosan-TBA derivatives are based

Liu et al. [13] grafted ε-caprolactone onto chitosan under microwave irradiation. The product has large amount of free amino groups and hydrophobic polycaprolactone side chain (Figure 1.2c), therefore it was anticipated as a degradable amphoteric material.

Chen et al. [14] prepared carboxymethyl chitosan by crosslinking with glutaraldehyde (Figure 1.2d). The hydrogel showed typical amphoteric character responding to pH of the external medium.

Therefore, in this work, we aim to improve mucoadhesive property of chitosan by grafting gluconolactone and caprolactone onto chitosan chain.

Gluconolactone (Glu) (Figure 1.4) is a naturally occurring food additive used as a sequestrant, an acidifier, or a curing, picking, or leavening agent. It is a lactone (cyclic ester) of D-gluconic acid [15]. The modified of chitosan was done by gluconolactone to improve properties of unmodified chitosan. The product obtained chitosan - gluconolactone (MCG) has large amount of free amino and hydroxyl groups, high molecular weight, hydrophilic side chain, chain flexibility and surface energy properties favoring spreading onto mucus.
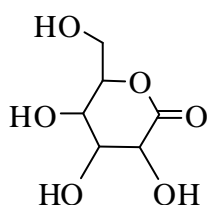


**Figure 1.4** Chemical structure of gluconolactone

γ-Caprolactone (Figure 1.5) is occasionally found as a volatile component of human urine. γ-Caprolactone has been found in the polar fraction of human blood [16]. The modified of chitosan by γ-Caprolactone to improve properties of unmodified chitosan. The product obtained chitosan - caprolactone (MCC) has large amount of free amino groups, high molecular weight, hydrophobic side chain, chain flexibility and surface energy properties favoring spreadind onto mucus.
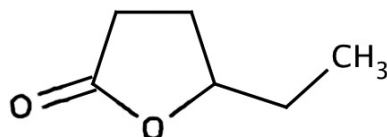
**Figure 1.5** Chemical structure of γ-Caprolactone

Recently, the use of chitosan and modified chitosan for controlled release of drug delivery system have been widely studied. Advantages of chitosan have been to prolong gastric residence time, controlled release of drugs within the gastrointestinal tract, helps to reduce dosing frequency and total dose. In addition, there has been considerable interest to improved properties of chitosan to enhance mucoadhesive properties in the preparation of pharmaceutical products.

In order to study a pharmaceutical application potential of modified chitosan as a drug delivery system, the drug delivery system were prepared in various pharmaceutical formulations, such as capsules, tablets, micro/nano capsules, etc. In a gastrointestinal drug delivery system, typically using amoxicillin trihydrate (AMX) and sodium diclofenac (DFNa) as model drug for delivery at the stomach (pH 1.2) and the intestinal tract (pH 7.4), respectively.

Amoxicillin (α-amino-hydroxybenzylpenicillin) (Figure 1.6) is a broad spectrum *β*-lactam antibiotic, which is effectively used to treat bacterial infections caused by susceptible microorganism. Amoxicillin is susceptible to degradation by *β*-lactamase producing bacteria, and may be given with clavulanic acid to decrease its susceptibility. Amoxicillin was selected as a model drug because it is widely used to treat *Helicobacter pylori* infection, the major causative agents of peptic ulcer [17].
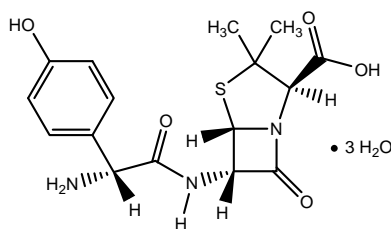


**Figure 1.6** Chemical structure of amoxicillin trihydrate

However, some other report trials indicated that the therapies cannot completely eradicate *H. pylori* and suggested that the therapeutic effect needs more investigation [18].

The reasons for the incomplete eradication are probably due to the short residence time of antimicrobial agents in the stomach and the inability to adhere to the gastric mucosa layer or epithelial cell surfaces where *H. pylori* exists. Furtheremore, the antimicrobial agent such as amoxicillin has short residence time in the stomach and may be degraded by gastric acid [19]. Therefore, some researcher had prepared and improve amoxicillin formulations, such as floating tablets [20], mucoadhesive tablet [21], mucoadhesive microspheres [22]., which were able to reside in stomach for an extended period of time for more effective *H. pylori* eradication.

Sodium diclofenac (DFNa) (Figure 1.7) is a non-steroidal anti-inflammatory drug (NSAID) which is widely used in the long-term treatment of antirheumatic, analgesic, osteoarthritis and antipyretic activity. It has a short half-life in plasma (1-2 hours). The most common adverse effects of drug are gastritis, peptic ulceration and depression of renal function [23, 24].
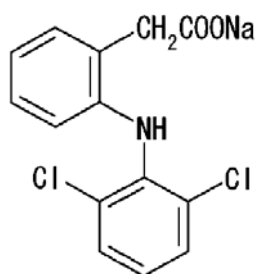


**Figure 1.7** Chemical structure of sodium diclofenac

The use of polymeric matrix for controlled release of drug in the pharmaceutical development is consider. Hydrophilic polymers have gained a lot of attention owing to its excellent ability and simplicity to form the bead such as alginate (Alg), by dropping an aqueous sodium alginate solution into a calcium chloride solution [25]. The use of hydrophilic polymer for the delivery of drug has proven to be advantageous over the conventional drug delivery systems.

Alginate is a natural anionic polysaccharide found mainly in brown seaweeds. It consisted of linear block copolymer of β-D-mannuronic acid and α-L-guluronic acid. Alginate has been known to from gel immediately when contact with calcium ion [26], from this property it is used in a wide variety of applications especially in food and pharmaceutics manufactures.

Alginate-calcium chloride is rapidly fromed by gelation of alginic acid in the presence of calcium ions and is able to incorporate some compounds such as drug or polysaccharides in the gel matrix [27].

In this research, the chitosan - gluconolactone (MCG) and chitosan - caprolactone (MCC) were synthesized using a simple method with gluconolactone and caprolactone. The obtained MCG and MCC, with large amount of free hydroxyl groups, hydrophobic and hydrophilic side chain, high molecular weight, chain flexibility. The chemical structure of chitosan and modified chitosan were characterization by FT-IR, DSC, ^{1}H-NMR, swelling behavior. Additionally, the release profiles of a model drug (AMX and DFNa) from beads were characterization and studied in simulated gastric and intestinal media, respectively.

## 1.2 The objectives of this research

1) To improve mucoadhesive properties of chitosan for gastric drug delivery system
2) To modify bead formulation based on sodium alginate coated with chitosan or modified chitosan to obtain the effective controlled release.
3) To study release behavior of beads in gastric-intestine simulated condition.

## 1.3 The scope of research

The scope of this research was carried out by stepwise investigation as follows:

1) Review literatures survey for related research work.
2) Prepare of chitosan-caprolactone (MCC) and chitosan-gluconolactone (MCG)

3) Characterization the physical chemical properties of chitosan and modified chitosan such as $^1$H-NMR, FT-IR, DSC, degree of substitution, mucoadhesive properties, swelling properties, solubility.

4) Prepare the beads of amoxicillin and sodium diclofenac.

5) Determine the encapsulation efficiency of beads.

6) Study the morphology of the beads using SEM.

7) Study the swelling behavior of the beads in simulated gastric-intestine fluids.

8) Study the release behavior of the beads in simulated gastric-intestine fluids by using UV-VIS and HPLC method.

9) Summarize the results.

```
                        ┌─────────────────┐
                        │    Chitosan     │
                        └─────────────────┘
                                 │
                        ┌─────────────────┐
                        │  Modification   │
                        └─────────────────┘
                                 │
               ┌─────────────────┴─────────────────┐
   ┌───────────────────────┐         ┌───────────────────────┐
   │ Chitosan : caprolactone│         │ Chitosan : gluconolactone│
   │        (MCC)          │         │        (MCG)          │
   └───────────────────────┘         └───────────────────────┘
               │                                 │
   ┌───────────────────────┐         ┌───────────────────────┐
   │Pharmaceutical applications│     │   Characterization    │
   └───────────────────────┘         └───────────────────────┘
```

Chitosan

Modification

Chitosan : caprolactone (MCC)

Chitosan : gluconolactone (MCG)

Pharmaceutical applications

Characterization

Gastrointestinal Tract

- % substitution: NMR

- NMR, IR, DSC

- Physical properties: solubility, swelling behavior

- Mucoadhesive property: chitosan, modified chitosan

Stomach (pH 1.2)

Intestinal tract (pH 7.4)

Beads

Amoxicillin trihydrate (AMX)

Sodium diclofenac (DS)

Characterisation

% Drug content

Release profile

- FT- IR, DSC, TGA, SEM

- Swelling behavior

- Floating

% encapsulation efficiency (%EE)

pH 1.2

pH 7.4

**Figuer 1.8** Flow chart of methodology

# CHAPTER II

# BACKGROUND AND LITERLATURE REVIEWS

## 2.1 Mucoadhesive polymer

Mucoadhesive polymers are synthetic or natural macromolecules which are capable of attaching to mucosal surfaces [1]. A number of charged and neutral polymers has been classified as mucoadhesive, since they are known to bind very strongly to mucus via non-covalent bonds such as hydrogen bonds, van der Waal's forces, and ionic interactions. Therefore mucoadhesive polymer has been interesting as a promising strategy to prolong the residence time and improve the specific localization of drug delivery systems on various membranes [28].

### 2.1.1 The mucoadhesive interactions

*Chemical bonds*

Mucins are large, extracellular glycoproteins with molecular masses ranging from 0.5 to 20 MDa. Mucins contain large amounts of carbohydrates primarily N-acetylgalactosamine, N-acetylglucosamine, fucose, galactose, traces of mannose, sialic acid (N-acetylneuraminic acid) and sulfate.

For adhesion to accur, molecule must bond across the interface. These bonds can arise in the following way [29].

1. Ionic bonds

A bond formed by the interaction between two oppositely charged ions (e.g. in a salt crystal).

2. Covalent bonds

A bond formed by the sharing of pairs of electrons between atoms. These are also strong bonds (e.g. thiomer).

3. Hydrogen bonds

A bond is the interaction of a hydrogen atoms with an electronegative atoms such as oxygen, fluorine or nitrogen. The hydrogen bond is stronger than Van – der – Waals bonds and weaker than ionic or covalent bonds.

4. Van – der – Waals bonds

The Van – der – Waals bonds are weak compared the chemical bonds. The bond formed of interaction from dipole – dipole and dipole – induced dipole attractions in polar molecule, and dispersion forces with non – polar substances.

5. Hydrophobic bonds

The bond that occur when non – polar groups are present in an aqueous solution. Water molecule adjacent to non – polar groups form hydrogen bonded structure, which lowers the system entropy. There is therefore an increase in the tendency of non – polar groups to associate with each other to minimize this effect.

*Theories of adhesion*

The adhesion mucin and mucoadhesive polymers is explained by the various theories based on the molecular attractive and repulsive forces [30,31,32].

1. Electronic theory

Electron transfer occurs between the two forming a double layer of electric at the interface, with subsequent adhesion due to attractive forces between glycoprotein mucin network and the bioadhesive material.

2. Wetting theory

The ability of bioadhesive polymer to spread spontaneously onto surface and develop intimate contact with the mucus membranes.

3. Adsorption theory

This theory has results from molecular contact between two material and the surface forces such as hydrogen bonding and van der waals' forces.

4. Diffusion theory

The adhesion arises from the interdiffusion of the polymers chains across an adhesive interface. This process is driven by concentration gradients and is affected by the available molecular chain lengths and their mobilities. The depth of interpenetration depends on the diffusion coefficient and the time of contact.

5. Mechanical theory

The adhesion was thought to occur on a rough surface by an interlocking of a liquid adhesive. However, rough surfaces also provide an increased surface area available for interaction along with an enhanced viscoelastic and plastic dissipation of

energy during joint failure, which are thought to be more important in the adhesion process than a mechanical effect.

      6.   Fracture theory

When adhesive bond failure at the interface, this theory suggests that true interfacial failure seldom occurs. However, failure normally occurs at the weakest component, which is typically a cohesive failure within one of the adhering surfaces.

2.1.2 Mucoadhesion dosage forms

"Bioadhesion" is a term of adhesive phenomena where at least one of the adherents is biological tissue. An adhesive bond may form with the epithelial cell layer, the continuous mucus layer or a combination of the two [33].

"Mucoadhesion" is a term used for a bioadhesive phenomenon where the biological substrate is a mucosal surface [30].

In considering the mechanism of mucoadhesion, the mucoadhesive bond formation are possible (Figure 2.1). These include:
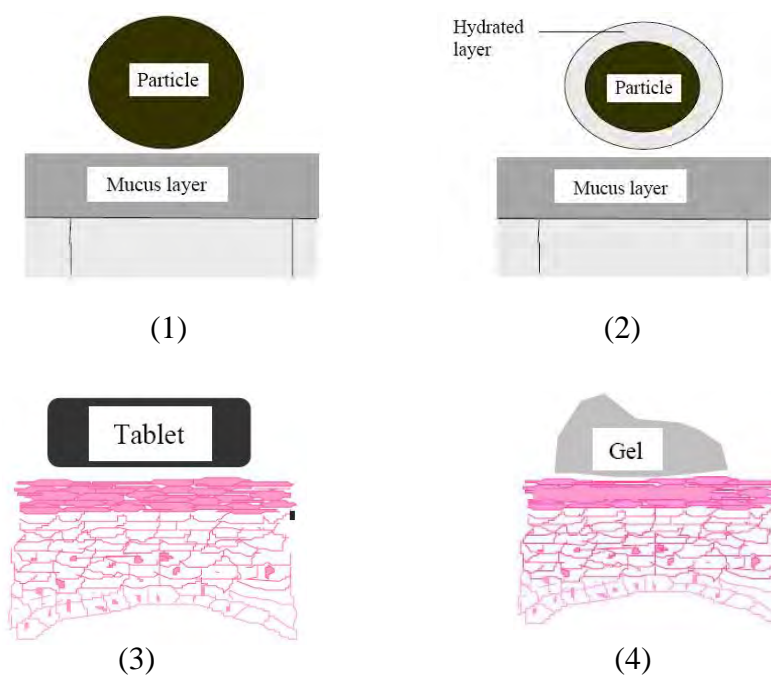


**Figure 2.1** Some scenarios where mucoadhesion occur

(1) Dry or partially hydrated dosage forms contacting surfaces with substantial mucus layers (typically particulates administered into the nasal cavity).

(2) Fully hydrated dosage forms contacting surfaces with substantial mucus layers (typically particulates of many 'First Generation' mucoadhesives that have hydrated in the luminal contents on delivery to the lower gastrointestinal tract).

(3) Dry or partially hydrated dosage forms contacting surfaces with thin/discontinuous mucus layers (typically tablets or patches in the oral cavity or vagina).

(4) Fully hydrated dosage forms contacting surfaces with thin/discontinuous mucus layers (typically aqueous semisolids or liquids administered into the oesophagus or eye).

In the study of adhesion generally, the adhesive process have been two steps identified [34], the interaction between mucoadhesive materials and a mucous membrane are shown in Figure 2.2 [35].

Step 1 Contact stage: An intimate contact (wetting) occurs between the mucoadhesive and mucous membrane

Step 2 Consolidation stage: Various physicochemical interaction occur to consolidate and strengthen the adhesive joint, leading to prolonged adhesion.
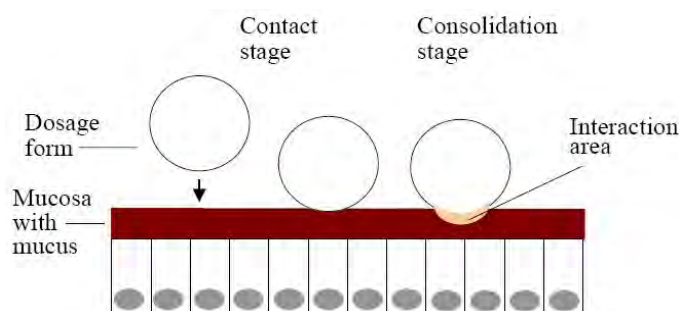


**Figure 2.2** The two stages in mucoadhesive

**2.2 Controlled drug release system**

Controlled drug release system occurs when a polymer is combined with a drug or other active agent in such a way that the active agent is released from the material in a predesigned manner. The release of the active agent may be constant over a long period, the advantages of controlled-delivery system can include the maintenance of drug level within a desired rang (Figure 2.3) [36].
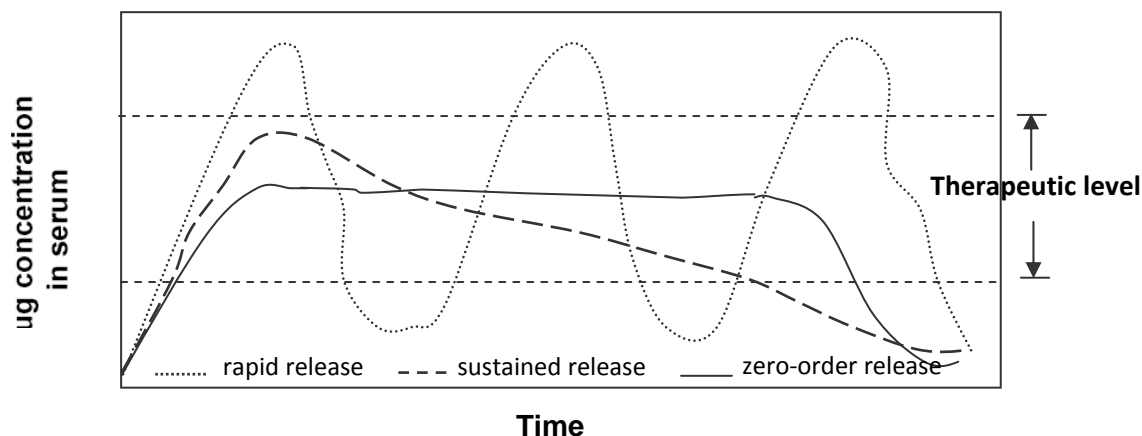


**Figure 2.3** Hypothetical serum drug concentrations of various oral dosage forms

2.2.1 Controlled – release mechanism [37]

There are three mechanisms the drug can be released from a delivery system: diffusion, swelling, and degradation. Any or all of these mechanisms may occur in a given release system.

1. Diffusion controlled release

When the drug or other active agent passes through pores in the polymer matrix into the external environment, it causes the diffusion as shown in Figures 2.4. The diffusion rate will decrease when the release continues as the result of the active agent has a longer distance to travel and a longer diffusion time to release.
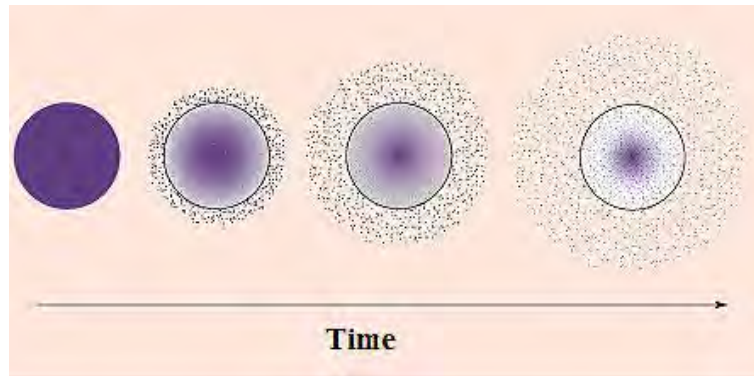
**Figure 2.4** Diffusion release from a typical matrix drug delivery system

2.    Swelling controlled release

The initial materials of the swelling controlled release system are dry. After put the materials in the body, it will absorb water and other fluids to swell. When the swelling occurs, the aqueous solvent content in the formulation as well as the polymer mesh size are increase. Therefore, the drug will diffuse through the swollen network into the external environment. The swelling controlled are shown in Figure 2.5a and 2.5b for reservoir and matrix systems, respectively.
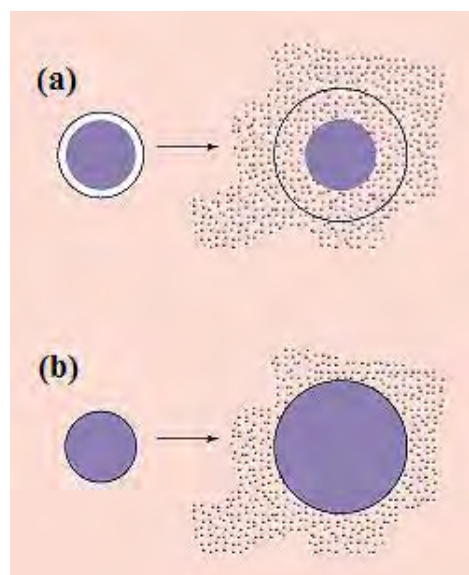


**Figure 2.5**. Drug delivery from (a) reservoir and (b) matrix swelling-controlled release systems.

The polymer's swelling ability can be changed by changing the environment surrounding the delivery system. These environment factor are pH, temperature and ionic strength. The polymer's structure changes are reversible and repeatable upon additional changes in the external environment. For example in Figure 2.6, the drug delivery occurs upon an increase in the pH of the environment.
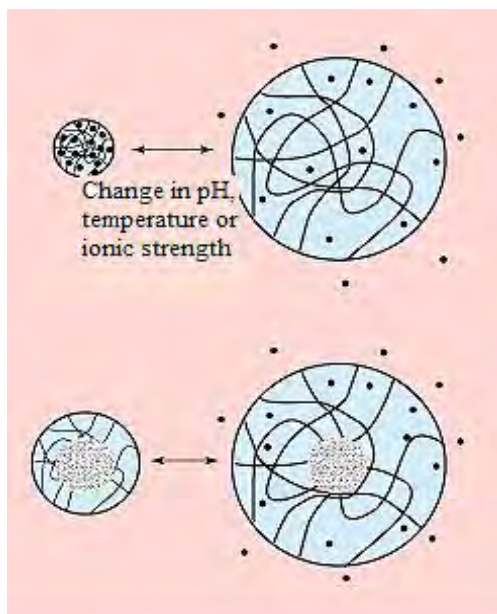


**Figure 2.6** Drug delivery from environmentally sensitive release systems

3. Biodegration controlled release

Degradation may take place through bulk hydrolysis, in which the polymer degrades in a fairly uniform manner throughout the matrix, as shown schematically in Figure 2.7a. For some degradable polymers, most notably the polyanhydrides and polyorthoesters, the degradation occurs only at the surface of the polymer, resulting in a release rate that is proportional to the surface area of the drug delivery system (Figure 2.7b)
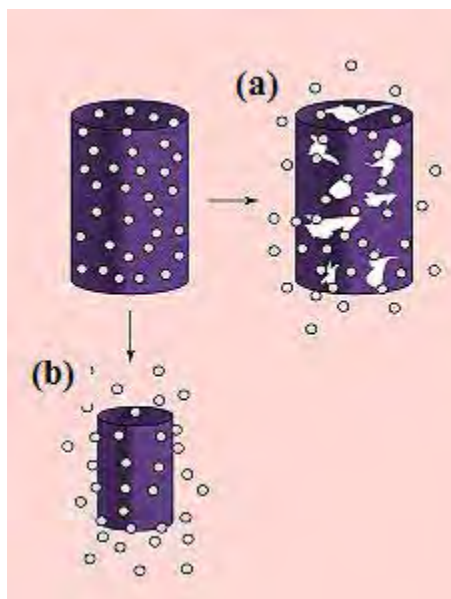
**Figure 2.7** Drug delivery from (a) bulk-eroding and (b) surface-eroding biodegradable systems

## 2.3 Polyelectrolyte complexs (PEC)

Polyelectrolyte complexs (PEC) are formed between oppositely charged particles (e.g. polymer-polymer, polymer-drug and polymer-drug-polymer). These are formed due to electrostatic interaction between oppositely charged polyions. The polyelectrolyte complexes formed between a polycationic polymer such as chitosan and polyanionic polymer such as alginate, pectin and carrageenan [38]. For example of polyelectrolyte complexes, the mixture of poly (acrylic acid)-chitosan, chitosan-alginate and chitosan-carrageenan.

## 2.4 Chitosan

Chitosan, a polycationic biopolymer, was discovered by Rouget in 1859 and gave a name by Hoppe-Seyler in 1894. Chitosan obtained by deacetylation with an alkaline treatment of acetamide group at the C-2 position in the 2-acetamido-2-deoxy-D-glucopyranose unit.

Chemically, chitosan is a linear polysaccharides consists of 2-acetamido-2-deoxy-(1-4)-β-D-glucopyranose residue (D-glucosamine units) and has small or moderate amount of *N*-acetyl-D-glucosamine units. The hydrogen bonding in chitosan

due to the presence of OH and $NH_2$ groups causes the chains flexibility and mucoadhesive properties. Furthermore, the cationic polyelectrolyte nature of chitosan can provide a strong electrostatic interaction with mucus or negatively charged mucosal surfaces, reinforcing the important mucoadhesive properties that have been demonstrated for chitosan-base materials [39]. It is widely used in food processing, medicine and biomaterial field. It becomes an interesting material in pharmaceutical applications due to its biodegradability and biocompatibility, and low toxicity. Chitosan has found wide applications in conventional pharmaceutical devices as a potential formulation excipient. The use of chitosan in novel drug delivery as mucoadhesive, peptide and gene delivery.
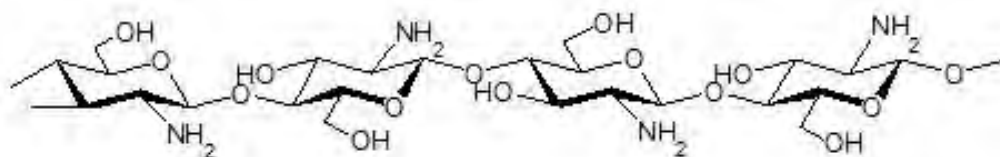


**Figure 2.8** Chemical structure of chitosan

2.4.1 Chitosan in pharmaceutical application

Chitosan has a good candidate for biomedical application such as blood anticoagulants, wound healing accelerators, preparation against parasites and drug delivery in gastrointestinal tract (GI). Due to its positive charges at physiological pH, chitosan can bind to the negatively charges and thus make it bioadhesive to for example, mucus, fatty acid and lipid. Consequently, they can increase the retention time at the site of application and so can be used for the prolonged release of drug in small intestine. Moreover, it is potentially suitable for use in dietary food because it can significantly reduce the cholesterol, triglyceride level and blood glucose.

**2.5 Alginate**

Alginate is a natural polysaccharide obtained from brown seaweeds, and it is partly responsible for the flexibility of the seaweed. Alginate is the term used for the salts of alginic acid and its derivatives. Alginate chain are multiblock copolymers composed of 2 monomeric units, β-D-Mannuronic acid (M) and α-L-Guluronic acid (G) and alternating G/M block, the structure are shown in Figure 2.9.
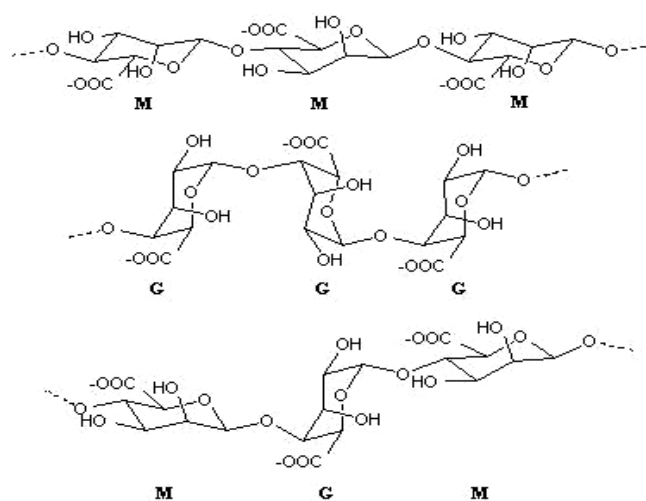


**Figure 2.9** The structure of the chemical units of alginate (M = mannuronic acid and G = guluronic acid)

Alginate is consist of blocks of similar and strictly alternating sequnce such as MMMMM, GGGGG and GMGMG. The primary function of the alginate are as thermally stable cold setting gelling agents in the presence of calcium ions. Gelling depends on the ion binding with the control for the production of homogeneous gels. High G content produces strong brittle gels with good heat stability, whereas high M content produces weaker more elastic gel and high MGMG content zips with $Ca^{2+}$ ions to reduces shear [27].

2.5.1 Alginate uses

The alginates is used in pharmaceutical and foods industry that based on three main properties. Firstly, it has ability to increase the viscosity of aqueous solutions. Moreover, its property is to form gels when a calcium salt is added to a aqueous solution of sodium. The gel is formed by chemical reaction at low temperature, displacerment of calcium ions into sodium ions is occurred to form the alginate, and holds themselves together to result in a gel. Finally, the third property of alginates is capable to forms of sodium or calcium alginate films and calcium alginates fibers. As the previous properties, alginates are widely use in many applications for example, the textile printing, food and pharmaceutical uses.

So, the alginate is spreadly used in the controlled release of drugs and other chemicals. Some applications, in which used the alginate, the active ingredient is displaced in a calcium alginate bead and slowly released when the bead is exposed in the appropriate environment [39].

## 2.6 Amoxicillin

Amoxicillin (α-amino-hydroxybenzylpenicillin) is a semisynthetic, orally absorbed, broad spectrum antibiotic that belongs to a class of antibiotics called penicillins. It is widely used in a standard eradication treatment of *H. Pylori* infection combined with a second antibiotic and an acid-suppressing agent.

2.6.1 Physicochemical properties [40]

Amoxicillin appears as a white, partially odorless, crystalline powder and is sparingly soluble in water.
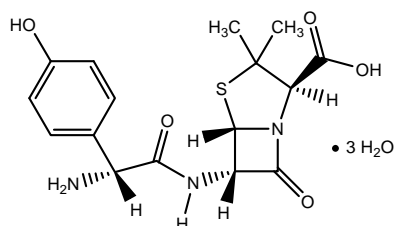


**Figure 2.10** Chemical structure of amoxicillin trihydrate

IUPAC name                    :7-[2-amino-2-(4-hydroxyphenyl)-acetyl]amino-
                              3.3-dimethyl-6-ox-2-thia-5-azabicyclo[3.2.0]
                              heptanes-4-carboxylic acid trihydrate

Empirical formula             : $C_{16}H_{19}N_3O_5S.3H_2O$

Molecular weight              : 419.46

CAS No.                       : 61336-70-7

2.6.2 Uses and indications [41, 42]

Treatment of ear, nose, throat, lower respiratory tract, gastric ulcer, skin and skin structure, and acute uncomplicated gonorrhea infections caused by susceptible strains of specific organisms.

2.6.3 Side effect of amoxicillin [41]

Central nervous system (CNS): Headache, somnolence, hyperactivity, anxiety, insomnia, confusion, convulsions, behavior changes, dizziness

Dermatologic: Fixed drug eruption, acute exanthematous pustulosis, erythematous maculopapular rashes occur frequently in patients with infectious mononucleosis, erythema multiforme, stevens-Johnson syndrome, exfoliative dermatitis, toxic epidermal necrolysis, hypersensitivity vasculitis, urticaria

Gastrointestinal: Nausea, vomiting, diarrhea, hemorrhagic colitis, generalized abdominal cramps, pseudomembranous colitis, tooth discoloration (brown, yellow or gray; rare)

Hematologic: Anemia, hemolytic anemia, thrombocytopenia, leucopenia, thrombocytopenia purpura, eosinophilia, agranulocytosis

Hepatic: Moderate elevates AST (SGOT) and ALT (SGPT), cholestatic jaundice, hepatic cholestasis, acute cytolytic hepatitis

Immunologic: Mucocutaneous candidiasis, vulvovaginal mycotic infection

## 2.7 Sodium Diclofenac

Sodium diclofenac (DFNa) is a widely used non-steroidal anti-inflammatory drug (NSAIDs) that exhibits antirheumatic, analgesic, osteoarthritis and antipyretic activities. DFNa was manufactured and marketed under the proprietary name Voltaren[®].

### 2.7.1 Physicochemical properties [43]

DFNa, as the sodium salt, is a faintly yellowish white to light beige, virtually odoless, slightly hygroscopic crystalline powder. It is freely soluble in methanol, sparingly soluble in water, very slightly soluble in acetonitrile, and insoluble in chloroform and in 0.1N HCl.
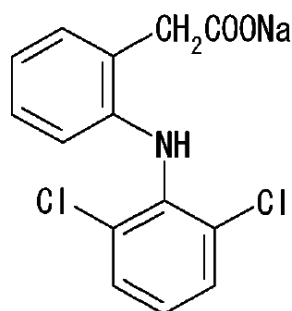


**Figure 2.11** Chemical structure of sodium diclofenac

IUPAC name : Monosodium-2-(2,6-dichloroanilino)phenylacetate

Empirical formula : $C_{14}H_{10}Cl_2NO_2Na$

Molecular weight : 318.13

CAS No. : 15307-79-6

2.7.2 Uses and indication [18]

DFNa has been used in human medicine for many years. It possesses analgesic, antipyretic, and anti-inflammatory activities by inhibition of prostaglandin synthesis (cyclo-oxygenase). The drug has been used for the long-term symptomatic treatment of rheumatoid arthritis, osteoarthritis, ankylosing spondylitis and primary nocturnal enuresis. It may also be useful for short-term treatment of acute musculoskeltal injury, and dysmenorrheal

2.7.3 Side effect of DFNa [18, 19]

Central nervous system (CNS): Headache, drowsiness, dizziness, insomnia

Dermatologic: Pruritus, eczema, stevens-Johnson syndrome, erythema multiforme, allergic purpura,toxic epidermal necrolysis, bullous eruptions

Gastrointestinal: Diarrhea, nausea, vomiting, constipation

Hematologic: Anemia, hemolytic anemia, thrombocytopenia, leucopenia, thrombocytopenia purpura, eosinophilia, agranulocytosis

Hepatic: Jaundice, fatal fulminant hepatitis

## 2.8 Gluconolactone

Gluconolactone (Glu) is the inner ester of gluconic acid formed by the removal of water. Glu is used effectively in various food processing applications such as a sequestrant, an acidifier, or a curing, picking, or leavening agent. Pure gluconolactone is a white adorless crystalline powder.
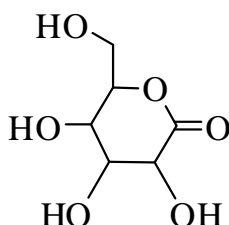


**Figure 2.12** Chemical structure of gluconolactone

IUPAC name          : D-Gluconic acid δ-lactone

Empirical formula    : $C_6H_{10}O_6$

Molecular weight    : 178.14

CAS No.           : 90-80-2

## 2.9 γ-Caprolactone

γ-Caprolactone is occasionally found as a volatile component of human urine. γ-Caprolactone has been found in the polar fraction of human blood. Biological fluids such as blood and urine have been shown to contain a large number of components, some of them volatiles (low boiling point) apparently present in all individuals, while others such are much more variable.
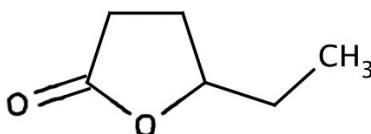


**Figure 2.13** Chemical structure of γ-caprolactone

IUPAC name          : 5-ethyloxolan-2-one

Empirical formula    : $C_6H_{10}O_2$

Molecular weight    : 114.14

CAS No.           : 695-06-7

# CHAPTER III

# EXPERIMENT

## 3.1 Materials

The following materials were obtained from commercial suppliers.

### 3.1.1 Model drugs

- Amoxicillin trihydrate (Chumchon Pharmaceutical, Thailand)

- Sodium diclofenac (compliment from Metallergy and Material Science Research Institute (MMRI))

### 3.1.2 Polymers and chemicals

- Alginic acid sodium salt from brown algae, Lot No. 1256646 (Fluka, UK)

- Chitosan, food grade, Lot No. 497613, M. W. 500,000 – 1,000,000. Deacetylation 95% (Bonafides, Thailand)

- Gluconolactone, Lot No. 038K0029 (Sigma, USA)

- γ-Caprolactone, Lot No. 396143/1 (Fluka, UK)

- Mucin from porcine stomach, Type II, Lot No. 018K0079 (Sigma, USA)

- Acetonitrile, HPLC grade (Merck, Germany)

- Calcium chloride, AR grade (Merck, Germany)

- Lactic acid (UCS, Thailand)

- Methanol, HPLC grade (Merck, Germany)

- Hydrochloric acid fuming 37%, AR geade (Merck, Germany)

- Sodium hydroxide, AR grade (Merck, Germany)

- Sodium hydrogen phosphate, AR grade (Merck, Germany)

- Potassium chloride, AR grade (Merck, Germany)

- Potassium dihydrogen phosphate, AR grade (Merck, Germany)

- Potassium bromide, AR grade (Merck, Germany)

## 3.2 Instruments

The instruments used in this study are listed in Table 3.1

**Table 3.1** Instruments

| Instrument | Manufacture | Model |
| --- | --- | --- |
| Analytical balance | Mettler | AT200 |
| HPLC | ThermoFinnigan | P4000 |
| UV-VIS Spectrophotometer 800 | Perkin Elmer | Lambda |
| Fourier transform infrared spectrometer | Perkin Elmer | Spectrum One |
| Scanning electron microscope | Philips | XL30CP |
| Digital camera | Olympus | SP-500UZ |
| Horizontal shaking water-bath | Lab-line instruments | 3575-1 |
| pH-meter | Metrohm | 744 |
| Ultrasonic bath | Ney Ultrasonik | 28 H |
| Differential scanning calorimeter | NETZSCH | DSC 7 |
| Micropipette (100-10000 µl) | Mettler Toledo | Volumate |

**3.3 Methods**
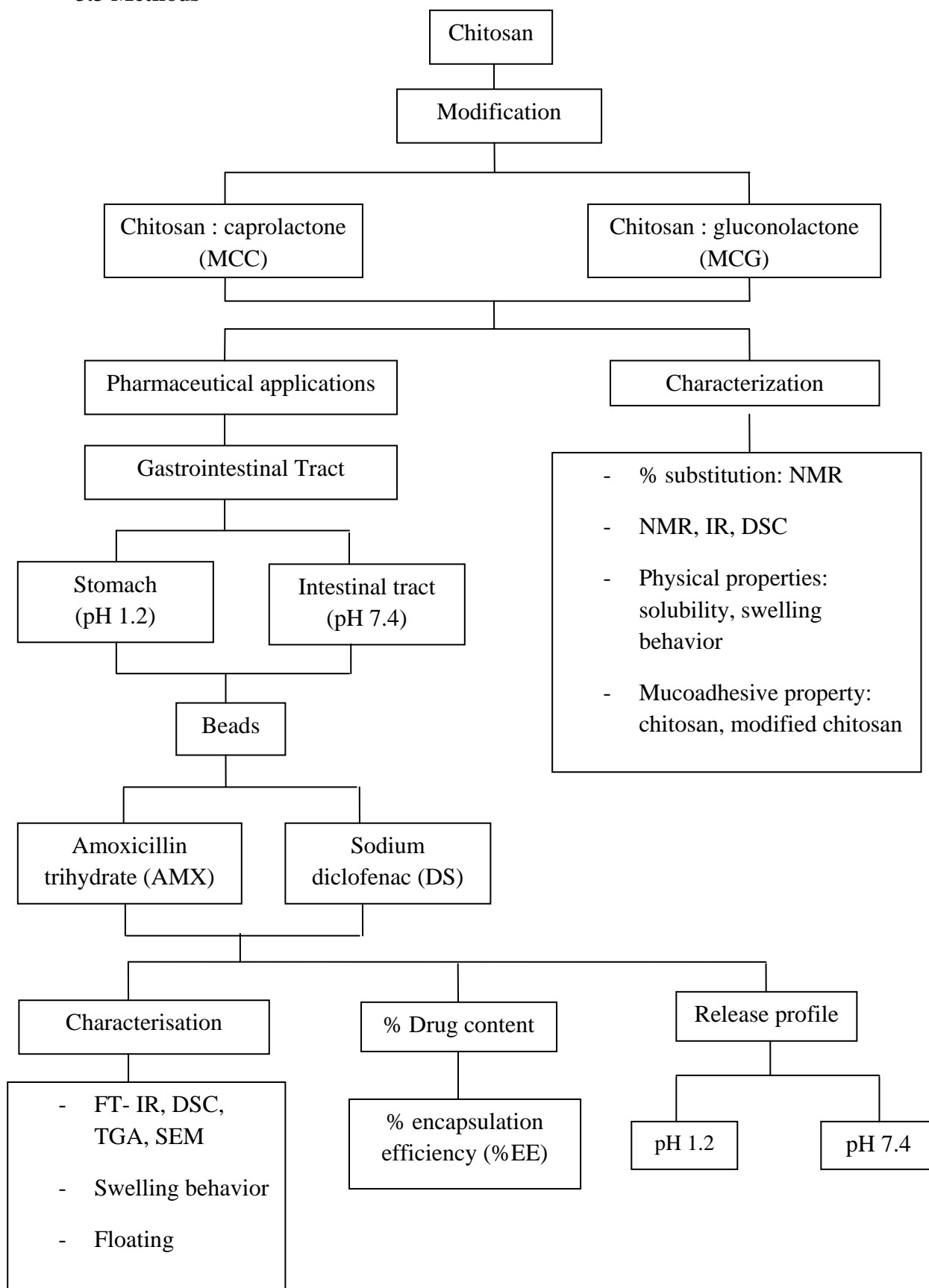


**Figuer 3.1** Flow chart of methodology

### 3.3.1 Preparation of modified chitosan (m-CS)

In the work, chitosan was modified with caprolactone and gluconolactone as follows.

### 3.3.1.1 Preparation of chitosan – caprolactone (MCC)

1 g of chitosan was dissolved in 100 ml of 1% aqueous lactic acid to yield 1% w/v chitosan solution. The suspension was stirred at room temperature overnight until completely dissolved. 0.1 g of caprolactone was added in the solution to make 0.1:1 of Cap:Chi (MCC 0.1). The mixture was stirred at room temperature for 12 –14 hours. The reaction mixture was adjusted to pH 7.0 with 15% w/v NaOH. The mixture was precipitated in an excess of acetone and air dried [44]. The preparation of another three different ratios of Cap:Chi was similar to the above procedure. The weight ratio of chitosan and caprolactone were shown in Table 3.2.
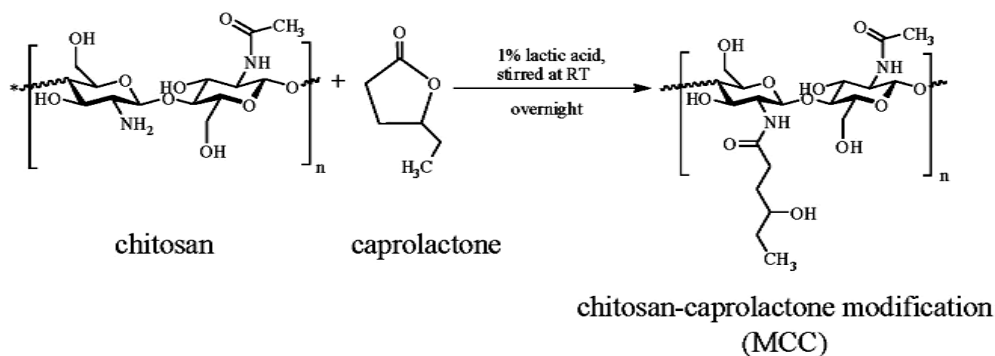


**Figure 3.2** Reaction scheme of chitosan-caprolactone modification (MCC)

### 3.3.1.2 Preparation of chitosan – gluconolactone (MCG)

Modified chitosan with gluconolactone was prepared using a similar procedure of above mentioned for the chitosan-caprolactone preparation, except only using gluconolactone instead of caprolactone. The weight ratio of chitosan and gluconolactone for another three diffirent ratios were shown in Table 3.2.
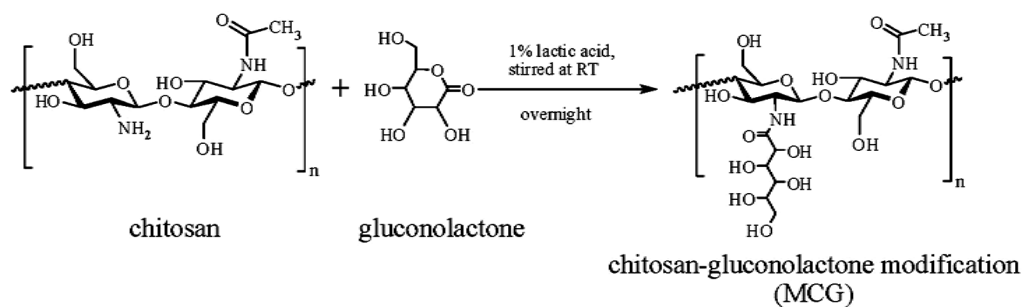
**Figure 3.3** Reaction scheme of chitosan-gluconolactone modification (MCG)

**Table 3.2** Mass ratio (w/w) of chitosan : caprolactone (MCC) and chitosan: gluconolactone (MCG)

| Formulation | Chitosan (g) : Caprolactone (g) | Formulation | Chitosan (g) : Gluconolactone (g) |
|:---:|:---:|:---:|:---:|
| MCC 0.1 | 1 : 0.1 | MCG 0.1 | 1 : 0.1 |
| MCC 0.3 | 1 : 0.3 | MCG 0.3 | 1 : 0.3 |
| MCC 0.7 | 1 : 0.7 | MCG 0.7 | 1 : 0.7 |
| MCC 1 | 1 : 1 | MCG 1 | 1 : 1 |

3.3.1.3 Characterization of modified chitosan

*Nuclear Magnetic Resonance (*[1]*H-NMR)*

^{1}H-NMR spectra were recorded on a Mercury 400 MHz spectrometer. Chitosan and the modified chitosan were dissolved in 2% $d_4$ acetic acid in $D_2O$.

*Infrared Spectroscopy  (FT-IR)*

FT-IR spectra were recorded in KBr discs on a Perkin Elmer Spectrum One spectrometer under dry air at room temperature. The sample was mixed with potassium bromide in agate mortar and pestle. The mixture was then transferred to a hydraulic pressing machine and pressed into a thin disc. The KBr pellets were scanned between 4000 and 400 cm$^{-1}$.

*Differential Scaning Calorimetry (DSC)*

Accurately weigh of the sample was placed into the aluminum pan and sealed. An empty pan was used as a reference. DSC chromatograms were obtained with NETZSCH DSC 7. All samples were run at a temperature range of 30– 300 °C and heating rate of 10 °C/min.

3.3.1.4 Solubility test

Solubility of the chitosan and modified chitosan (MCC and MCG) was determined by the method reported by Xie, Liu and Chen, 2007 [45]. 0.1 g of each sample was dissolved in 10 g of $H_2O$, then stirred at room temperature for 4 h. Undissolved materials were separated and washed with acetone, then dried in an oven at 40°C under a vacuum until the weight was constant. The residue was accurately weigh. Solubility (Sa) was calculated using the following equation:

$$S_a = \left[\frac{0.1 - W_1}{0.1}\right] \times 100\%$$

$W_1$: is the weight of undissolved materials (g). The experiments were carried out three times. The values were reported as the mean values with standard deviation.

3.3.1.5 Swelling study of chitosan and modified chitosan (MCC and MCG)

Chitosan film was prepared as follows. 1 g of chitosan was dissolved in 100 ml of 1% aqueous lactic acid to yield 1% w/v chitosan solution, poured on a tray (10.3 x 15.5 x 1.7 cm), and then air dried. Modified chitosan films were prepared using a similar procedure of above mentioned for the chitosan film preparation, except for using modified chitosan instead of chitosan.

Chitosan and modified chitosan films were cut into a circular with a diameter of 5.0 mm and immersed respectively in $H_2O$, 0.1 N HCl (pH 1.2) and phosphate buffer (pH 7.4). The swelling properties were determined by measuring the

change of the diameters of the film. The swelling ratio for each sample determined at time t was calculated from the following equations [46].

$$S_w = \frac{D_t - D_0}{D_0}$$

where $D_t$ was the film diameter at time t and $D_0$ was the initial film diameter. The experiments were carried out three times. The values were reported as the mean values with standard deviation.

3.3.1.6 Determination of degree of substitution of chitosan (DS) by NMR spectroscopy

*Degree of substitution*

Modified chitosan was dissolved in 2% $d_4$ acetic acid in $D_2O$. $^1$H-NMR spectra were recorded on a Mercury 400 MHz spectrometer. Degree of substitution was calculated from the peak of $^1$H-NMR spectra using the method reported by M.R. Thatte, 2004 [44].

The degree of subsitution of MCC was calculated using the signal intensities obtained from the $^1$H NMR.

For example, degree of subsitution of MCC 0.1 using the intensities of $^1$H NMR spectrum was calculated from the peak area at 3.35 – 3.55 ppm of –$CH_{2b}$-, –$CH_c$- and $H_3$ – $H_6$ proton against 0.83 - 0.85 ppm of –$CH_{2d}$- proton as follow equation:

Where Y was degree of substitution

$$Y = \frac{4_{sugar} \times 100}{3[\frac{Intregrate\ due\ to\ b, c, 3, 4, 5, 6}{Intregrate\ due\ to\ d} - \frac{2}{3}]}$$
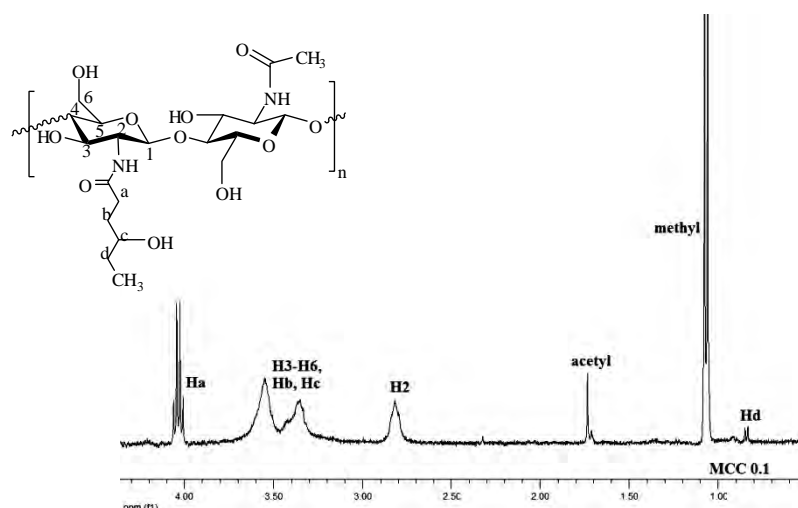
**Figure 3.4** Stucture of MCC and ^{1}H NMR spectrum of MCC 0.1

The degree of subsitution of MCG was calculated using the signal intensities obtained from the ^{1}H NMR.

For example, degree of subsitution of MCG 0.1 using the intensities of ^{1}H NMR spectrum was calculated from the peak area at 3.50 -3.70 ppm of –$CH_{2c}$- and $H_3$ – $H_6$ proton against 3.84 ppm of –$CH_a$- proton as follow equation:

.

$$Y = \frac{4_{sugar} \times 100}{\dfrac{Intregrate\ due\ to\ c, 3, 4, 5, 6}{Intregrate\ due\ to\ a} - 2}$$
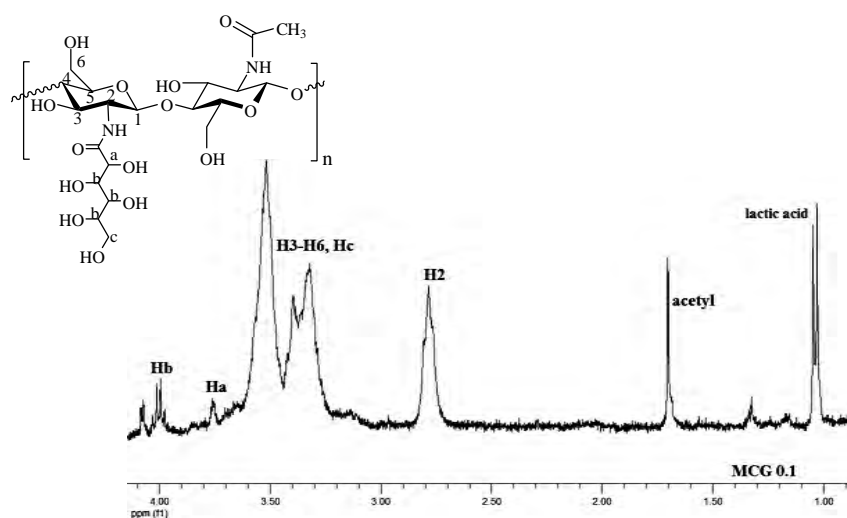


**Figure 3.5** Stucture of MCG and ^{1}H NMR spectrum of MCG 0.1

### 3.3.1.7 Mucoadhesive analysis

Mucoadhesive characteristics of the polymer were evaluated using the method of Hassan and Gallo, 1989 [47]. The viscosities of 0.1% w/v of each polymer, 15% w/v mucin and mixtures of 15% w/v mucin/0.1% polymer in 0.1 N HCl (pH 1.2) were measured at 37 °C by using an Oswald viscometer (Tamson, TV 4000). Dried mucin was hydrated with 0.1 N HCl by gentle stirring for 3 hours at 25 C° to yield a dispersion of 20% w/v. Chitosan was dissolved in 10% lactic acid to yield a 4% w/v stock solution and then diluted with 0.1 N HCl to yield 0.1% w/v. Modified chitosan was prepared in 0.1 N HCl to yield a 0.1% w/v solution. The viscosities of mixture 15% w/v mucin/0.1% polymer were prepared in either 0.1 N HCl (pH 1.2) for 15 mins. All viscosity experiments were repeated three time.

Viscosity component of bioadhesion ($\eta_b$) was calculated from the following equation:

$$\eta_b = \eta_t - (\eta_m + \eta_p)$$

Where $\eta_t$ is the viscosity of the system, $\eta_m$ and $\eta_p$ are the individual viscosity of mucin and polymer, respectively.

### 3.3.1.8 Inhibition of chitosan and modified chitosan against bacteria

Antibacterial activity of the chitosan and modified chitosan against *E. coli* (Gram-negative) and *S. aureus* (Gram-positive) was evaluated by using agar well diffusion method. The *E. coli* and *S. aureus* were obtained from Department of Medical Sciences (Thailand). Firstly, a representative bacteria single colony was picked off, placed in nutrient broth (peptone 5 g, beef extract 3 g, agar 17 g in distilled water 1000 ml; pH 7.0-7.2) and incubated at 37 °C for 24 hours. Then the obtained fresh culture where bacterial cells grew luxuriantly was ready for antibacterial test. Lastly, 10 mg of sample were dissolved in 1% lactic acid 1 ml. A volume of 20 µl solution of microbe suspension and 20 µl solution of sample were orderly added into the petri dishes. All the petri dishes were incubated at 37 °C for 24 hours and take out of photograph. The experiments were repeated for three times.

*Inhibition of AMX – Alg/MCC beads and AMX – Alg/MCG beads against bacteria*

Accurately weighed quantities of 10 mg of dried beads were immersed in 25 ml of 1% lactic acid to dissolve the drug dispersed inside the beads. A volume of 20 µl solution of microbe suspension and 20 µl solution of sample at 2 hours were orderly added into the petri dishes. All the petri dishes were incubated at 37 °C for 24 hours and take out of photograph. The experiments were repeated for three times.

### 3.3.2 Pharmaceutical applications

#### 3.3.2.1 Preparation of the drugs - loaded polymer beads

In order to study a pharmaceutical application potential of modified chitosan as a drug delivery system, the beads were prepared in various formulations using amoxicillin trihydrate (AMX) and diclofenac sodium (DS) as a drug model. Amoxicillin trihydrate, an antibiotic used for treatment of *H.pylori* in the stomach, is the representation model drug for studying the drug delivery system in stomach (pH 1.2). Diclofenac sodium, a NSAIDs drug, is the most common model drug used for studying the controlled release systems in the intestinal tract (pH 7.4). The properties of drug loaded beads, e.g. encapsulation efficiency, swelling properties, morphology and drug release profiles were investigated and compared to the results obtained from the pure alginate beads and nature chitosan/alginate beads.

The procedures of the bead preparation are as follows:

*DFNa loaded pure alginate beads.*

Formulation A1, 4% w/v alginate solution was prepared by dissolved 4 g of sodium alginate in 100 ml water. The specific amount of sodium diclofenac given in Table 3.3 was dissolved in minimal water and then added into the alginate solution by a homogenizer. The alginate/sodium diclofenac mixture was dropped through 18G needle into a 4% aqueous calcium chloride solution as a coagulant. The beads were immersed for 30 minutes, filtered and washed with DI water and then air dried.
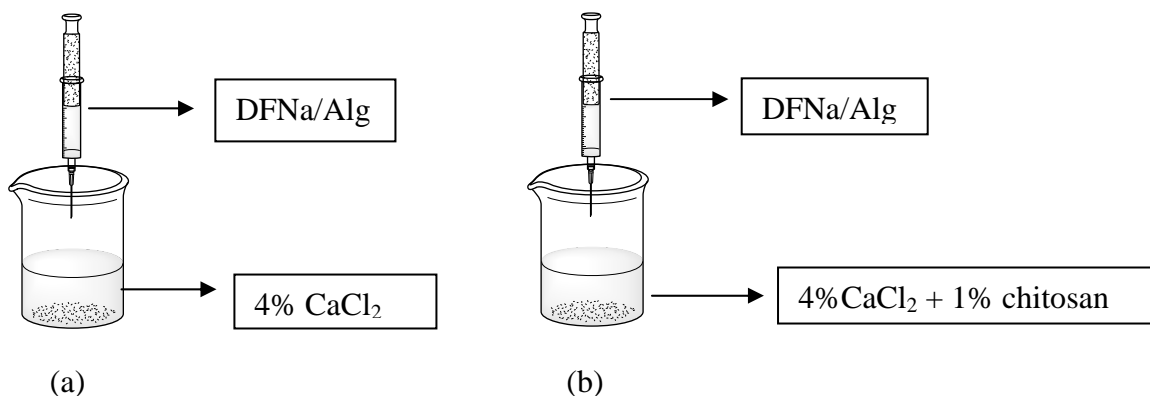
**Figure 3.6** Preparation of (a) DFNa loaded pure alginate beads and (b) DFNa loaded polymer beads

*DFNa loaded pure chitosan beads*

Formulation A2, 1% w/v chitosan solution was prepared by dissolved 1 g of chitosan in 100 ml in 1% v/v lactic acid. The specific amount of sodium diclofenac given in Table 3.3 was dissolved in minimal water and then added into the 1% w/v chitosan solution by a homogenizer. The chitosan/sodium diclofenac mixture was dropped through 18G needle into a 4% aqueous sodium hydroxide solution as a coagulant. It could not form the bead.

*DFNa loaded polymer beads*

Formulation B (ALG/CS beads), the aqueous mixtures of 4% alginate and 4% sodium diclofenac according to the given ratio in Table 3.3. The mixture of alginate/sodium diclofenac dropped through 18G needle into a solution mixed with 1% w/v chitosan dissolved in 1% v/v lactic acid. The beads were immersed for 30 minutes, filtered and washed with DI water and then air dried.

Formulations C – J, the mixture of this formation was prepared using a similar procedure of above mentioned for the formulation B preparation, except only using MCC and MCG instead of chitosan.

*AMX loaded polymer beads*

The formulations of amoxicillin trihydrate loaded polymer beads were prepared in the similar procedures for sodium diclofenac-loaded Alg/CS beads .

**Table 3.3** The compositions of drug loaded-polymer/Alginate represented in weigth ratio. (DFNa = Sodium diclofenac, AMX = Amoxicillin trihydrate, MCC = Chitosan-Caprolactone and MCG = Chitosan-Gluconolactone)

| Formulations | | Ratio of composition | | | Formulation | | Ratio of composition | | |
|---|---|---|---|---|---|---|---|---|---|
| | | DFNa | Alginate | Polymer | | | AMX | Alginate | Polymer |
| A1 | Pure alginate | 1 | 1 | 0 | K1 | Pure alginate | 1 | 1 | 0 |
| A2 | Pure chitosan | 1 | 0 | 1 | K2 | Pure chitosan | 1 | 0 | 1 |
| B | Chitosan | 1 | 1 | 0.5 | L | Chitosan | 1 | 1 | 0.5 |
| C | MCC0.1 | 1 | 1 | 0.5 | M | MCC 0.1 | 1 | 1 | 0.5 |
| D | MCC0.3 | 1 | 1 | 0.5 | N | MCC 0.3 | 1 | 1 | 0.5 |
| E | MCC0.7 | 1 | 1 | 0.5 | O | MCC 0.7 | 1 | 1 | 0.5 |
| F | MCC1 | 1 | 1 | 0.5 | P | MCC 1 | 1 | 1 | 0.5 |
| G | MCG0.1 | 1 | 1 | 0.5 | Q | MCG 0.1 | 1 | 1 | 0.5 |
| H | MCG0.3 | 1 | 1 | 0.5 | R | MCG 0.3 | 1 | 1 | 0.5 |
| I | MCG0.7 | 1 | 1 | 0.5 | S | MCG 0.7 | 1 | 1 | 0.5 |
| J | MCG1 | 1 | 1 | 0.5 | T | MCG 1 | 1 | 1 | 0.5 |

3.3.2.2 Encapsulation efficiency

*Encapsulation efficiency of sodium diclofenac-loaded alginate beads*

Accurately weighed quantities of 100 mg of dried ground beads were immersed in 250 ml of phosphate buffer pH 7.4 in an erlenmeyer flask to dissolve the drug dispersed inside the beads. After sonicatation, the solution was collected and determined the encapsulation efficiency by UV- VIS spectrophotometer at 276 nm [48].

*Encapsulation efficiency of amoxicillin-loaded alginate beads.*

Accurately weighed quantities of 100 mg of dried ground beads were transferred into a 100 ml volumetric flask with distilled water to a volume of 90 ml. The suspension was sonicated for 60 minutes. Then, distilled water was added to adjust the volume to 100 ml. The suspension was filtered through 0.45 μm nylon membrane filter, 20 µl of filtrate was withdrawn and determined the encapsulation efficiency by HPLC. The conditions for HPLC assay were as follows:

> HPLC apparatus;
> Mobile phase: phosphate buffer (0.01 M, pH 6.0): acetonitrile (90:10)
> Pump: ThermoFinnigan P4000
> Detector: UV6000LP (UV detector)
> column:Pinnacle II C18 5 µm 200x4.6 mm
> flow rate: 1 ml/min

The encapsulation efficiency was calculated according to the following equation. All experiments were performed in triplicates [49].

$$EE(\%) = \frac{Actual\ drug\ content}{Theoretical\ drug\ content} \times 100\%$$

### 3.3.2.3 Morphological characterization of the beads

*Scanning electron microscope (SEM)*

The surfaces and inner part of the beads were observed by scanning electron microscope (XL30CP, Philips, Japan). In the preparation of SEM examination, the samples were mounted on stub and coated by gold under vacuum before observation. The photographs were taken at different magnifications.

*Infrared Spectroscopy  (FT-IR)*

The infrared spectra of all beads were recorded in KBr discs on a Perkin Elmer Spectrum One spectrometer. The dried sample was mixed with potassium bromide in agate mortar and pestle. The mixture was then transferred to a hydraulic pressing machine and pressed into a thin disc. The KBr pellets were scanned between 4000  and 400 cm$^{-1}$.

*Differential Scaning Calorimetry (DSC)*

Accurately weighed of the sample were placed into the aluminum pan and sealed. An empty pan was used as a reference. DSC chromatograms were obtained with NETZSCH DSC 7. All sample were run at a temperature range of 30–300 °C and heating rate of 10 °C/min.

### 3.3.2.4 Swelling properties

The swelling behaviors were observed by measuring the change of diameters of the beads in a 0.1 N HCl pH 1.2 and pH 7.4. then was determined by measuring the change of the diameters of the beads. The swelling ratio for each sample determined at time t was calculated from the following equations [46].

$$S_w = \frac{D_t - D_0}{D_0}$$

Where $D_t$  is the diameter of the beads at time (t) and $D_0$ is the initial diameter of the dried beads.

3.3.2.5 *In vitro* drug release

*Drug release behavior in SGF (pH 1.2)*

*Drug release of sodium diclofenac-loaded alginate beads*

Accurately weighed quantities of 100 mg beads were suspended in 250 ml of 0.1 N HCl pH 1.2 in a conical flask. The flask was then placed in a shaken water bath at a speed of 50 strokes/minute with the temperature maintained at $37 \pm 1$ °C. Samples of 5 ml were withdrawn at 0, 0.25, 0.5, 1, 1.5, 2, 4, 6, 8 and 24 h, and replaced by the same volume of fresh dissolution medium. Sample was determined by a UV- VIS spectrophotometer at 276 nm.

*Drug release of amoxicillin-loaded alginate beads*

Accurately weighed quantities of 100 mg beads were suspended in 250 ml of 0.1 N HCI pH 1.2 in a conical flask. The flask was then placed in a shaken water bath at a speed of 50 strokes/minute with the temperature maintained at $37 \pm 1$ °C. Samples of 3 ml were collected and neutralized with 1 ml of NaOH solution at 0, 0.5, 1, 2, 4, 6 and 24 h, and replaced by the same volume of fresh dissolution medium. The sample then filtered through a 0.45 µm nylon membrane filter and determined by a HPLC assay as the same conditions described in section 3.3.2.2.

*Drug release behavior in SIF (pH 7.4)*

*Drug release of sodium diclofenac-loaded alginate beads*

Accurately weighed quantities of 100 mg beads were placed into conical flask with 250 ml of 0.1 M phosphate buffer saline (pH 7.4) and incubated at $37 \pm 1$ °C under shaking speed of 50 strokes/minute. Samples of 5 ml were withdrawn at 0, 0.25, 0.5, 1, 1.5, 2, 4, 6, 8 and 24 h, and replaced by the same volume of fresh dissolution medium. Sample was determined by a UV- VIS spectrophotometer at 276 nm.

*Drug release of amoxicillin-loaded alginate beads*

Accurately weighed quantities of 100 mg beads were placed into conical flask with 250 ml of 0.1 M phosphate buffer saline (pH 7.4) and incubated at 37 ± 1 °C under shaking speed of 50 strokes/minute. Samples of 3 ml were collected at 0, 0.5, 1, 2, 4, 6 and 24 h, and replaced by the same volume of fresh dissolution medium. The sample then filtered through a 0.45 µm nylon membrane filter and determined by a HPLC assay as the same conditions described in section 3.3.2.2.

# CHAPTER IV

# RESULTS AND DISCUSSION

## 4.1 Syntesis of MCC and MCG

Modify chitosan to improve mucoadhesive properties of chitosan in order to apply to drug delivery system. The lactone derivatives of chitosan were synthesized using caprolactone and gluconolactone according to the reaction scheme as shown in Figures 4.1 – 4.2 and the ratio of chitosan:lactone are listed in Table 3.1.

Lactone addition will generated a hydroxyl group in the side chain which respect to the nitrogen of chitosan. The reaction exploits the fact that the primary amine in chitosan is more nucleophilic than the hydroxyls. Therefore selective of N-acylation is possible to attain.
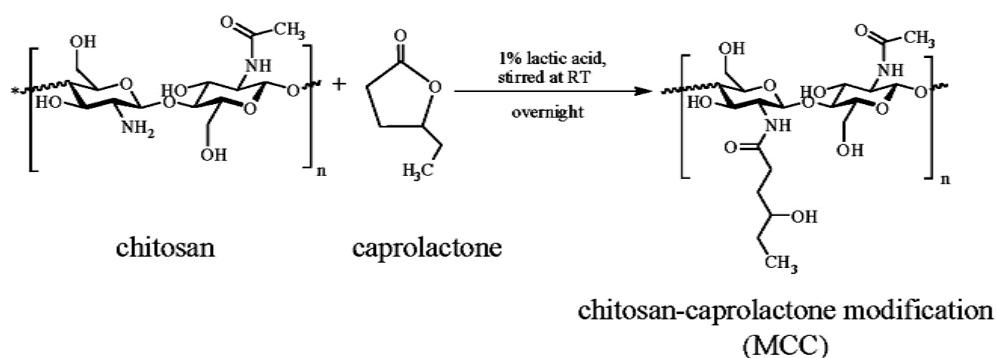


**Figure 4.1** Reaction scheme of chitosan-caprolactone addition
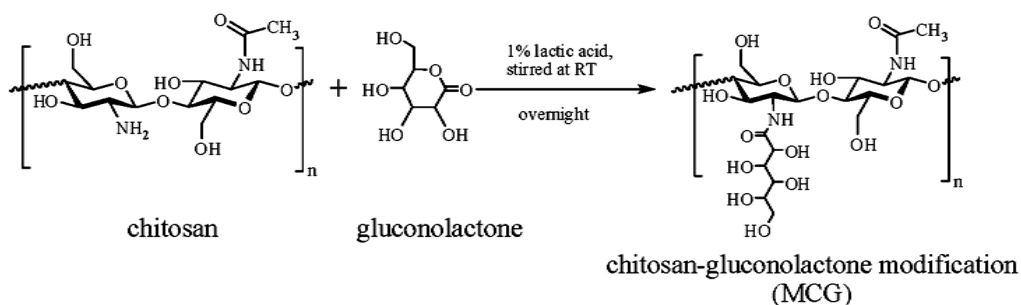


**Figure 4.2** Reaction scheme of chitosan-gluconolactone addition

The results obtained from these reactions appeared as pale yellow powder and amorphous. The products were characterized by $^1$H-NMR, FT-IR and DSC.

**4.2 Characterization and physical properties of chitosan and modification of chitosan**

4.2.1 Nuclear Magnetic Resonance ($^1$H – NMR) of MCC and MCG

4.2.1.1 $^1$H NMR spectrum of MCC

The $^1$H NMR spectra of chitosan and MCC in 2%(w/w) $d_4$ acetic acid in $D_2O$ are shown in Figure 4.4.

The $^1$H NMR spectrum of chitosan is shown in Figure 4.4a, the signal at 1.69 ppm corresponds to acetyl proton. A singlet at 2.80 ppm was attributed to $H_2$. The signals due to the hydrogen atoms ($H_3$ – $H_6$) in the chitosan ring were observed around 3.34 – 3.54 ppm. The $H_1$ proton was not observed in most cases as it was overlapped by the signals of $D_2O$.

The $^1$H NMR spectrum of MCC 0.1 (Figure 4.4b), showed that the quartet $H_a$ is represented by the signal at 4.04 ppm ($J$=8.0 Hz). Signals due to the $H_3$ – $H_6$ in the chitosan ring and $H_b$ and $H_c$ of the caprolactone were observed about 3.35 – 3.54 ppm. The signal at 2.80 ppm represents the $H_2$. The signal due to acetyl proton appears at 1.73 ppm. The appearances of new proton positions of caprolactone were observed a doublet at 0.85 ppm for $H_d$ ($J$=8.0 Hz) and at 1.06 ppm for methyl. These results clearly confirmed that MCC has been successfully prepared. The $^1$H NMR spectrum of MCC 0.3, MCC 0.7 and MCC 1 are shown in Figure 4.4c to 4.4e, the results are similar to that of MCC 0.1.

4.2.1.2 Degree of substitution of MCC

The degree of substitution of MCC (table 4.2) was calculated using the signal intensities obtained from the $^1$H NMR. $^1$H NMR technique is determined the changing nuclear magnetic moment in the hydrogen nucleus under the external magnetic field. So, the different hydrogen positions were shown the different relative signal positions. There were the two reasons using $^1$H NMR to characterize MCC. The first, the proton signals in MCC were shifted from the unmodified chitosan, because the caprolactone part was grafted into the chitosan chain. The other reason is when the ratios of caprolactone were varied, the quantities of characteristic proton of MCC were changed. The intensity of proton signal has been directly proportional to the increasing number hydrogen atoms.

In this work, the integrated intensity of the new $H_d$ signal position of caprolactone and the $H_3 - H_6$ proton signal of chitosan in the modified chitosan was used to compare to that of the $H_3 - H_6$ proton signals of the native chitosan.
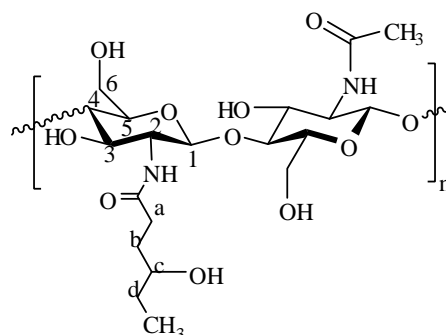


**Figure 4.3** Chemical structure of MCC

$^1$H NMR spectrum of MCC was used to compared the intensities of the – $CH_{2b}$-, –$CH_c$- and $H_3 - H_6$ proton signals with that of the –$CH_{2d}$- proton.

For example, degree of subsitution of MCC 0.1 using the intensities of $^1$H NMR spectrum were calculated from the peak area at 3.35 – 3.55 ppm of –$CH_{2b}$-, –$CH_c$- and $H_3 - H_6$ proton against 0.83 - 0.85 ppm of –$CH_{2d}$- proton as follow:

$$Y = \frac{4_{sugar} \times 100}{3[\dfrac{Intregrate\ due\ to\ \text{b, c}, 3, 4, 5, 6}{Intregrate\ due\ to\ \text{d}} - \dfrac{2}{3}]}$$

where, $Y$ is the degree of substitution. The detailed calculation was given in appendices A.

Using equation above, degree of subsitution for MCC are 5.71, 7.63, 7.77 and 9.42% for MCC 0.1, MCC 0.3, MCC 0.7 and MCC 1, respectively (Table 4.1). The results showed that the degree of subsitution of MCC increased with increasing ratio of caprolactone.
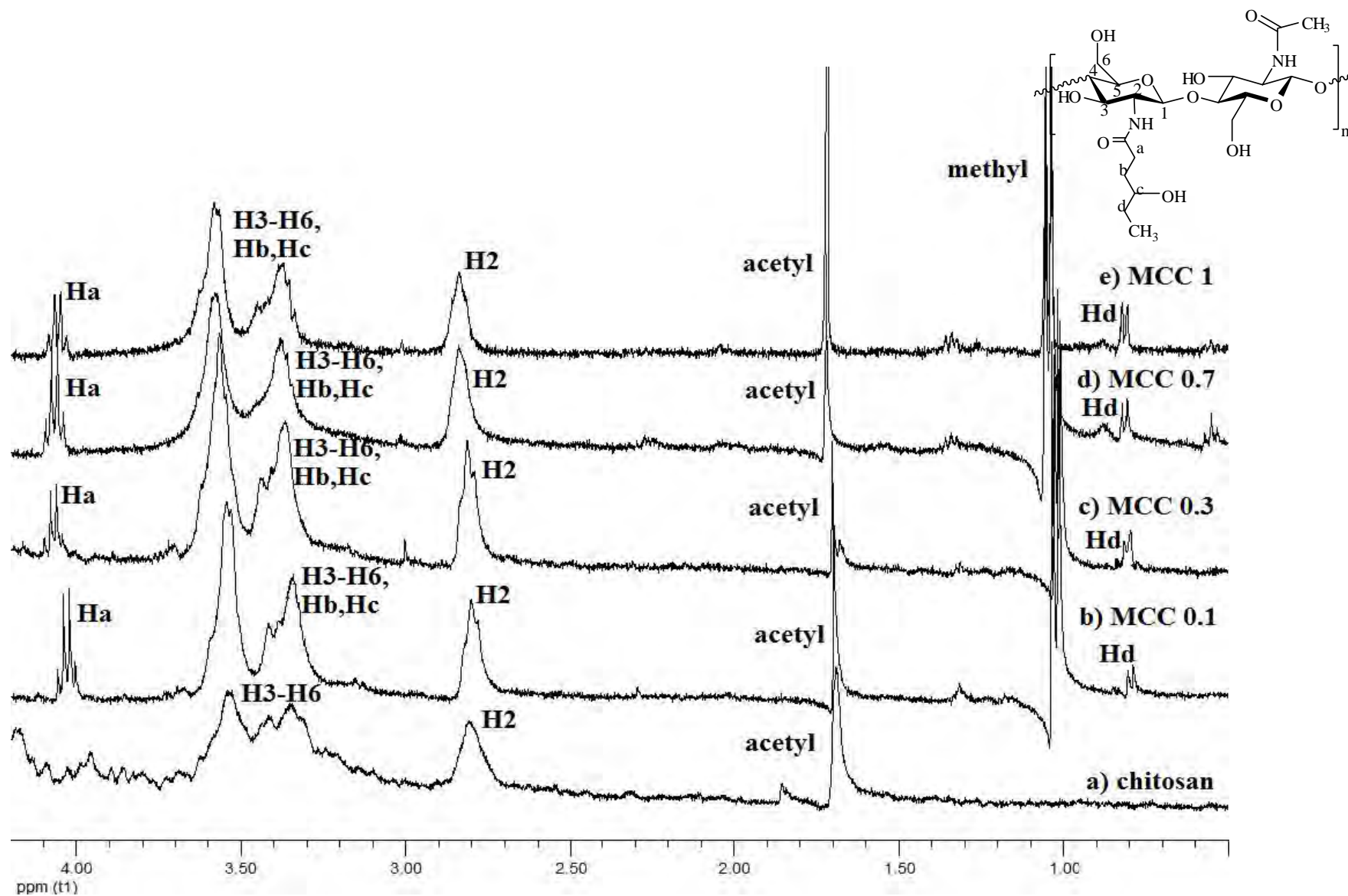
**Figure 4.4** $^{1}$H NMR spectrum of (a) Chitosan, (b) MCC 0.1, (c) MCC 0.3, (d) MCC 0.7, (e) MCC 1

**Table 4.1** $^1$H NMR chemical shifts (ppm) and integrations of chitosan and MCC

| Positions | Chitosan | | MCC 0.1 | | MCC 0.3 | | MCC 0.7 | | MCC 1 | |
|---|---|---|---|---|---|---|---|---|---|---|
| | δ (ppm) | Integrate | δ (ppm) | Integrate | δ (ppm) | Integrate | δ (ppm) | Integrate | δ (ppm) | Integrate |
| H1 | * | | * | | * | | * | | * | |
| Hd | - | - | 0.83 - 0.85 | 1.00 | 0. 78 – 0.80 | 0.41 | 0.88 – 0.89 | 1.00 | 0.78 – 0.80 | 1.00 |
| methyl | - | - | 1.06 – 1.08 | 5.81 | 1.1 - 1.12 | 0.77 | 1.1 - 1.12 | 3.97 | 1.01 – 1.03 | 2.78 |
| acetyl | 1.69 | 1.00 | 1.63 | 2.65 | 1.77 | 0.62 | 1.77 | 1.33 | 1.76 | 2.69 |
| H2 | 2.80 | 1.44 | 2.80 | 6.05 | 2.86 | 1.75 | 2.87 | 4.95 | 2.76 | 3.73 |
| H3 - H6, Hb- Hc | 3.34 – 3.54 | 5.20 | 3.35 – 3.55 | 24.02 | 3.39 - 3.58 | 7.44 | 3.40 – 3.60 | 17.83 | 3.28 - 3.50 | 14.83 |
| Ha | - | - | 4.04-4.06 | 2.77 | 4.06-4.08 | 1.00 | 4.07 – 4.08 | 1.93 | 3.97 – 3.99 | 1.96 |
| %subsitution[a] | - | | 5.71 | | 7.63 | | 7.77 | | 9.42 | |

*H1 was overlap with the signal of $D_2O$.

%subsitution[a] by $Y = \dfrac{4_{sugar} \times 100}{3[\frac{Intregrate\ due\ to\ b,c,3,4,5,6}{Intregrate\ due\ to\ d} - \frac{2}{3}]}$

4.2.1.3 $^1$H NMR spectrum of MCG

The $^1$H NMR spectrum of chitosan and MCG in 2%(w/w) $d_4$ acetic acid in D$_2$O are shown in Figure 4.6.

The $^1$H NMR spectra of chitosan is shown in Figure 4.6a, signals due to the hydrogen atoms (H$_3$ – H$_6$) in the chitosan ring were observed around 3.34 – 3.54 ppm. A singlet at 2.80 ppm was attributed to H$_2$. The H$_1$ proton was not observed in most cases as it was overlapped by the signal of D$_2$O. The signal at 1.69 ppm was assigned to acetyl proton [50].

The $^1$H NMR spectrum of gluconolactone (Figure 4.6f), signal of H$_{3'}$ – H$_{4'}$ and H$_{6'}$ were observed about 3.40 – 3.80 ppm, at 3.9 ppm for H$_{2'}$ and at 4.23 ppm for H$_{5'}$.

The $^1$H NMR spectrum of MCG 0.1 (Figure 4.6b) is the representative NMR spectra for the modified chitosan with the various ratios of gluconolactone. The appearances of new proton positions of gluconolactone were observed singlet at 3.77 ppm and a quartets at 3.99 ppm, may be due to H$_a$ and H$_b$ ($J$=4.0 Hz), respectively. The multiplets from 3.32 to 3.51 ppm attributed to H$_3$ –H$_6$ and H$_c$. A singlet at 2.79 ppm was assigned to H$_2$. The acetyl proton was showed at 1.70 ppm. The proton of lactic acid was observed at 1.05 ppm. These results confirmed that the MCG were successfully prepared. The $^1$H NMR spectrum of MCG 0.3, MCG 0.7 and MCG 1 are shown in Figure 4.6c to 4.6e, the results are similar to that of MCG 0.1.

4.2.1.4 Degree of substitution of MCG

The degree of subsitution of MCG (table 4.2) can be calculated using the signal intensities obtained from the $^1$H NMR as mentioned above in section 4.2.1.2.
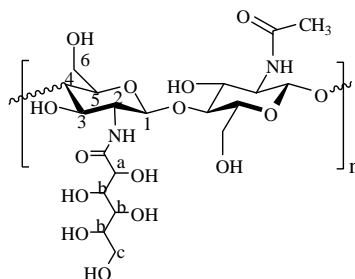


**Figure 4.5** Chemical structure of MCG

$^1$H NMR spectrum of MCG was used to compare the intensities of the $-CH_{2c}$- and $H_3 - H_6$ proton signal with that of the $-CH_a$- proton as the following equation (the detailed calculation was given in appendices A):

$$Y = \frac{4_{sugar} \times 100}{\dfrac{Intregrate \ due \ to \ c, 3, 4, 5, 6}{Intregrate \ due \ to \ a} - 2}$$

Where, $Y$ is the degree of substitution

For example, degree of substitution of MCG 0.1 was calculated from the set of the peak area around 3.32 -3.51 ppm which contribute to the proton of $-CH_{2c}$- and $H_3 - H_6$ protons against the peak area at 3.77 ppm of $-CH_a$- proton as follow the calculation was given in appendices A.

Using equation above, degree of subsitution of the four different ratio of MCG are 23.85, 20.34, 22.73 and 25.41% for MCG 0.1, MCG 0.3, MCG 0.7 and MCG 1, respectively (Table 4.2). The results showed that the degree of substitution of MCG were similar for all ratios of MCG 0.1 to MCG 1.
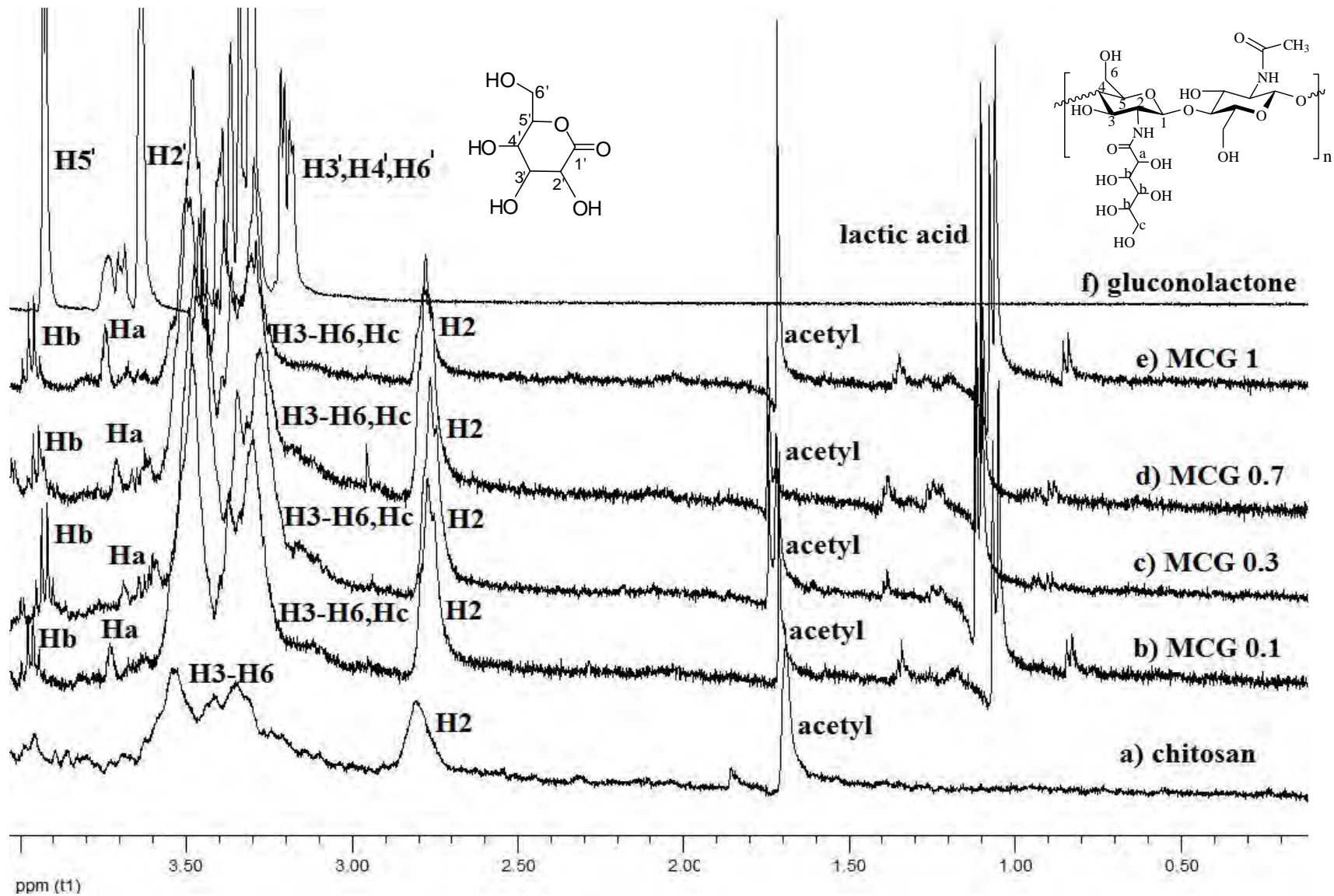
**Figure 4.6** $^1$H NMR spectrum of (a) chitosan, (b) MCG 0.1, (c) MCG 0.3, (d) MCG 0.7, (e) MCG 1, (f) Gluconolactone

**Table 4.2** ^{1}H NMR chemical shifts (ppm) and integrations of chitosan and MCG

| Positions | Chitosan | | MCG 0.1 | | MCG 0.3 | | MCG 0.7 | | MCG 1 | |
|---|---|---|---|---|---|---|---|---|---|---|
| | δ (ppm) | Integrate | δ (ppm) | Integrate | δ (ppm) | Integrate | δ (ppm) | Integrate | δ (ppm) | Integrate |
| H1 | * | | * | | * | | * | | * | |
| acetyl | 1.69 | 1.00 | 1.70 | 2.05 | 1.81 | 1.42 | 1.80 | 1.09 | 1.49 | 0.98 |
| H2 | 2.80 | 1.44 | 2.79 | 4.85 | 2.89 | 2.92 | 2.88 | 3.40 | 2.58 | 2.03 |
| H3 - H6, Hc | 3.34 – 3.54 | 5.20 | 3.32-3.51 | 18.77 | 3.43-3.64 | 11.48 | 3.41-3.62 | 15.09 | 3.10 – 3.32 | 10.82 |
| Ha | - | - | 3.77 | 1.00 | 3.86 | 0.53 | 3.85 | 0.77 | 3.56 | 0.61 |
| Hb | - | - | 3.99-4.00 | 1.54 | 4.10-4.12 | 1.00 | 4.12 | 1.00 | 3.80 | 1.00 |
| %subsitution[a] | - | | 23.85 | | 20.34 | | 22.73 | | 25.41 | |

*H1 was overlap with the signal of $D_2O$.

%subsitution[a] by $Y = \dfrac{4_{sugar} \times 100}{\dfrac{Intregrate\ due\ to\ c,3,4,5,6}{Intregrate\ due\ to\ a} - 2}$

4.2.2 Infrared Spectroscopy (FT - IR)

FTIR spectroscopy was used to determine the chemical interaction of the samples as displayed in Figure 4.7 to 4.8. Peak assignments of chitosan and MCCs are given in Table 4.3. Interactions between chitosan and carprolactone was determined by comparing IR transmission signals of pure components with the mixed system.

**Table 4.3** Peak positions and assignments of chitosan and MCCs

| Assignment | Chitosan | MCC 0.1 | MCC 0.3 | MCC 0.7 | MCC 1 |
|---|---|---|---|---|---|
| $\nu$ O-H + $\nu$ N-H | 3434 | 3434 | 3433 | 3409 | 3432 |
| $\nu$ CH$_3$ + $\nu$ CH$_2$ | 2920 | 2924 | 2926 | 2921 | 2922 |
| $\nu$ C-H | 2877 | 2878 | 2879 | 2879 | 2879 |
| $\nu$ C=O (amide I) | - | - | - | - | - |
| $\delta$ N-H (NH$_2$) | 1601 | 1595 | 1591 | 1593 | 1594 |
| $\delta$ CH$_3$ + $\delta$ CH$_2$ | 1422 | 1416 | 1415 | 1417 | 1417 |
| $\delta$ CH$_3$ + $\delta$ CH$_2$ | 1383 | 1382 | 1382 | 1383 | 1383 |
| $\nu$ C-N (amide III) | 1324 | 1319 | 1318 | 1319 | 1320 |
| $\nu$ C-O-C | 1154 | 1154 | 1154 | 1154 | 1154 |
| $\nu$ C-O(-COH-) | 1075 | 1076 | 1075 | 1079 | 1077 |
| $\nu$ C-O(-CH$_2$OH) | 1032 | 1033 | 1034 | 1034 | 1033 |
| $\nu$ ring | 897 | 898 | 898 | 898 | 896 |

$\nu$ = stretching, $\delta$ = bending

Figure 4.7(a) shows the IR spectrum of chitosan. The broad absorption band at 3434 cm$^{-1}$ resulted from the –NH and –OH stretching vibrations. The weak band at about 2920 cm$^{-1}$ corresponded to the –CH– stretching. The bands at 1601, 1383 cm$^{-1}$ were assigned to the –NH$_2$ bending and -CH$_3$ bending, respectively. The band of carbonyl appeared around 1601 cm$^{-1}$ and it might be overlaped with –NH$_2$ bending band because of the electron withdrawing of amino groups in the chitosan, they could pull electron from the adjacent carbonyl group by inductive effect. As the result, the carbonyl group revealed the characteristic carbonyl stretching band at lower the reciprocal wavenumber than a typical stretching band of carbonyl. The band at 1154

cm$^{-1}$ was the asymmetric stretching of C-O-C bridge. The band at 1075, 1035 cm$^{-1}$ were assigned to the C-O stretching vibration of C$_3$-OH and C$_6$-OH, respectively [51].

Figure 4.7(b) shows the IR spectrum of MCC 0.1. The band at around 3434 cm$^{-1}$ was due to the stretching vibration of O-H bonded to N-H. The band at around 2922 cm$^{-1}$ was assigned to –CH stretching vibration. The band at 1595 cm$^{-1}$ and 1319 cm$^{-1}$ attributed to amide II and amide III (mainly –NH$_2$ bending and C–N stretching), respectively. The chemical interaction band of –NH$_2$ and C-N were shifted from the original position. The band at around 1382 cm$^{-1}$ was due to –CH$_3$ bending and the band at 1154 cm$^{-1}$ attribute to the C-O-C stretching.

Figure 4.7(c) shows the IR spectrum of MCC 0.3. The wide absorption band around 3433 cm$^{-1}$, was due to the stretching vibration of N-H group bonded to –OH group. The band at around 2926 cm$^{-1}$ was due to –CH stretching vibration. The band at 1382 cm$^{-1}$ was due to –CH$_3$ bending. The absorption band at 1591 cm$^{-1}$ and 1318 cm$^{-1}$ were assigned to -NH$_2$ bending and C–N stretching vibration of amide group. The band at 1075, 1032 cm$^{-1}$ were assigned to the C-O stretching vibration of C$_3$-OH and C$_6$-OH, respectively.

Figure 4.7(d) shows the IR spectrum of MCC 0.7. The band at around 3409 cm$^{-1}$ was assigned to O-H and N-H stretching vibration. The band at 1383 cm$^{-1}$ was due to –CH$_3$ bending and distinct band at 1154 cm$^{-1}$ attributed to the C-O-C stretching. The band shifted from original position band at 1601 and cm$^{-1}$ 1324 cm$^{-1}$ to the wavenumber 1593 cm$^{-1}$ and 1319 cm$^{-1}$ was corresponded to –NH$_2$ bending and C–N stretching. The band at 1454 cm$^{-1}$ was due to –CH$_3$ bending and the band at 1417 cm$^{-1}$ was due to –CH$_2$ bending.

Figure 4.7(e) shows the IR spectrum of MCC 1. The absorption band around 3432 cm$^{-1}$ was due to the stretching vibration of N-H group bonded to O-H group. The band at around 2922 cm$^{-1}$ was due to –CH stretching. The band at 1594 cm$^{-1}$ and 1320 cm$^{-1}$ were assigned to amide II and amide III (–NH$_2$ bending and C–N stretching), respectively. The absorption band at 1154 cm$^{-1}$ attributed to C-O-C stretching. The band at 1417 cm$^{-1}$ was due to -CH$_3$ bending and the band at 1452 cm$^{-1}$ was due to –CH$_2$ bending.
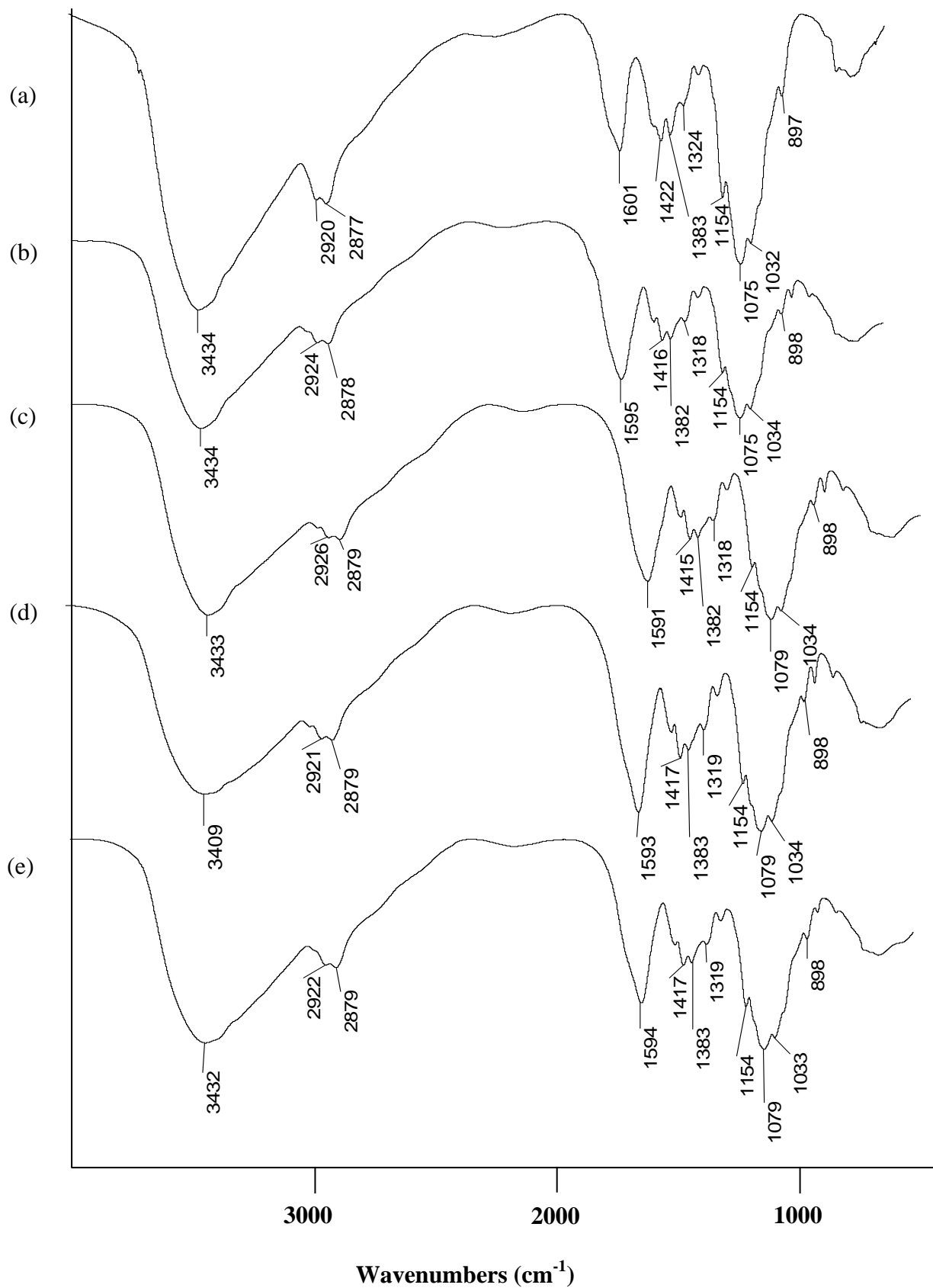
**Figure 4.7** IR spectra of (a) Chitosan, (b) MCC 0.1, (c) MCC 0.3, (d) MCC 0.7, (e) MCC 1

FTIR spectroscopy of MCGs was displayed in Figure 4.8. Peak assignments of chitosan and MCCs are given in Table 4.4. Interaction between chitosan and gluconolactone was determined by comparing IR transmission signals of pure components with the mixed system.

**Table 4.4** Peak positions and assignments of chitosan and MCGs

| Assignment | Chitosan | MCG 0.1 | MCG 0.3 | MCG 0.7 | MCG 1 |
|---|---|---|---|---|---|
| $\nu$ O-H + $\nu$ N-H | 3434 | 3433 | 3428 | 3433 | 3433 |
| $\nu$ CH$_3$ + $\nu$ CH$_2$ | 2920 | 2928 | 2928 | 2926 | 2929 |
| $\nu$ C-H | 2877 | 2883 | 2882 | 2884 | 2886 |
| $\nu$ C=O (amide I) | - | - | - | - | - |
| $\delta$ N-H (NH$_2$) | 1601 | 1590 | 1593 | 1599 | 1601 |
| $\delta$ CH$_3$ + $\delta$ CH$_2$ | 1422 | 1416 | 1416 | 1416 | 1413 |
| $\delta$ CH$_3$ + $\delta$ CH$_2$ | 1383 | 1383 | 1383 | 1384 | 1383 |
| $\nu$ C-N (amide III) | 1324 | 1318 | 1316 | 1317 | 1315 |
| $\nu$ C-O-C | 1154 | 1153 | 1152 | 1152 | 1154 |
| $\nu$ C-O(-COH-) | 1075 | 1077 | 1078 | 1078 | 1079 |
| $\nu$ C-O(-CH$_2$OH) | 1032 | 1033 | 1035 | 1035 | 1037 |
| $\nu$ ring | 897 | 896 | 896 | 894 | 891 |

$\nu$ = stretching, $\delta$ = bending

Figure 4.8(a) shows the IR spectrum of chitosan, the characteristic peak of chitosan was in the same Figure 4.7(a) as mentioned above.

Figure 4.8(b) shows the IR spectrum of MCG 0.1. The wide absorption band at 3433 cm$^{-1}$, was due to the stretching vibration of N-H group bonded to O-H group. The band at 2928 cm$^{-1}$ was due to the –CH stretching vibration. The band at 1590 cm$^{-1}$ and 1318 cm$^{-1}$ were assigned to amide II and amide III (–NH$_2$ bending and C–N stretching), respectively. The absorption band at 1153 cm$^{-1}$ attributed to C-O-C stretching. The band at 1416 cm$^{-1}$ was due to -CH$_3$ bending and the band at 1453 cm$^{-1}$ was due to –CH$_2$ bending.

Figure 4.8(c) shows the IR spectrum of MCG 0.3. The wide absorption band around 3428 $cm^{-1}$ was assigned to the stretching vibration of N-H group bonded to –OH group. The band at 1383 $cm^{-1}$ was due to $-CH_3$ bending. The absorption band at 1593 $cm^{-1}$ and 1316 $cm^{-1}$ were assigned to $NH_2$ bending and C–N stretching vibration of amide group. The band at 1152 $cm^{-1}$ might be due to asymmetric stretching of C-O-C.

Figure 4.8(d) shows the IR spectrum of MCG 0.7. The band at around 3433 $cm^{-1}$ attributed to O-H and N-H stretching vibration. The band at around 2926 $cm^{-1}$ was assigned to –CH stretching. The band at 1384 $cm^{-1}$ was due to $-CH_3$ bending and distinct band at 1152 $cm^{-1}$ attributed to the C-O-C stretching. The band shifted from original position band at 1601 and $cm^{-1}$ 1324 $cm^{-1}$ to the wavenumber 1599 $cm^{-1}$ and 1317 $cm^{-1}$ was corresponded to $-NH_2$ bending and C–N stretching.

Figure 4.8(e) shows the IR spectrum of MCG 1. The wide band around 3433 $cm^{-1}$ was due to the stretching vibration of O-H bonded to N-H and the band at around 2929 $cm^{-1}$ was assigned to –CH stretching vibration. The band at 1601 $cm^{-1}$ and 1315 $cm^{-1}$ attributed to amide II and amide III (mainly $-NH_2$ bending and C–N stretching), respectively. The band at 1383 $cm^{-1}$ was due to $-CH_3$ bending. The band at 1079, 1037 $cm^{-1}$ assigned to the C-O stretching vibration of $C_3$-OH and $C_6$-OH, respectively.
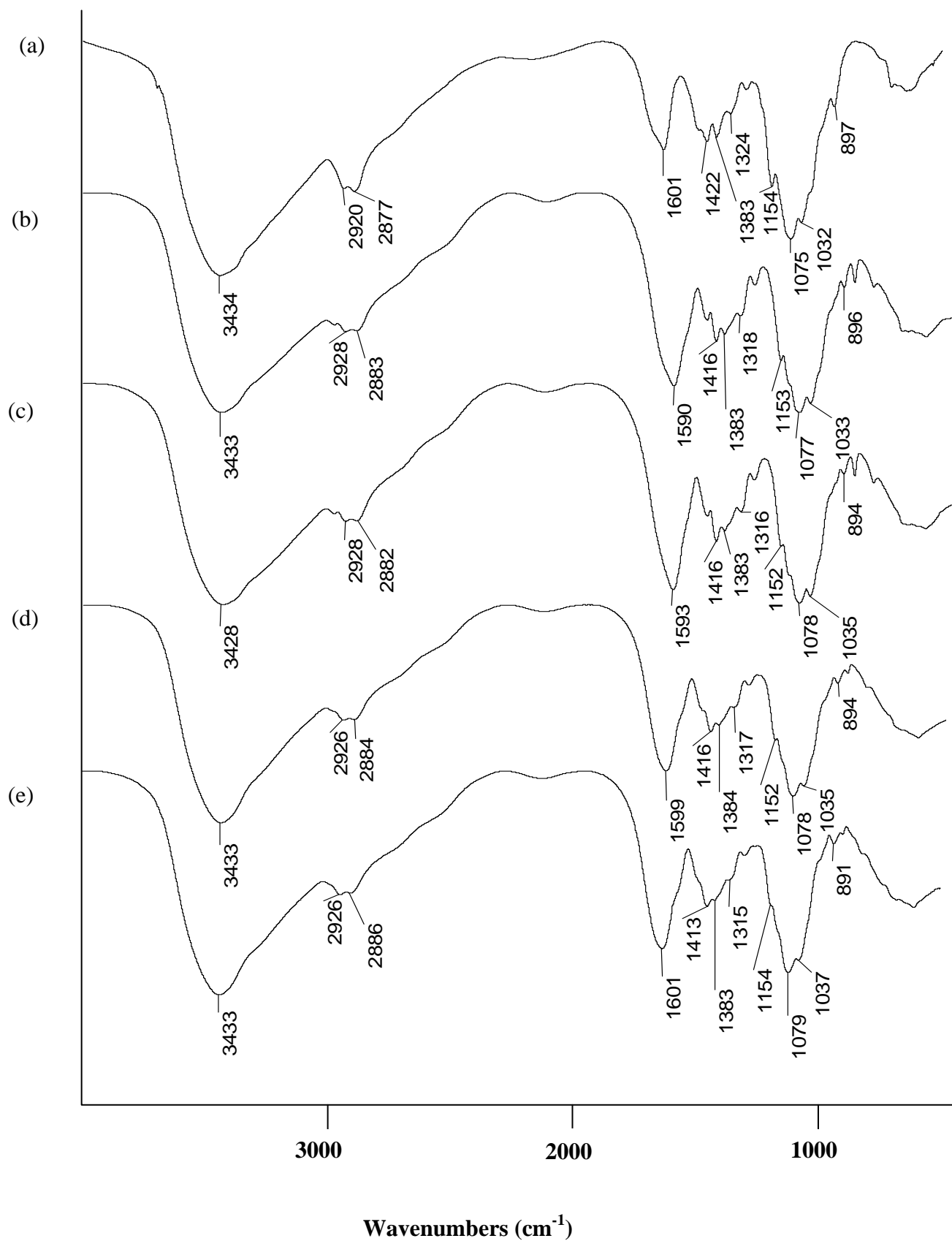
**Figure 4.8** IR spectra of (a) Chitosan, (b) MCG 0.1, (c) MCG 0.3, (d) MCG 0.7, (e) MCG 1

4.2.3 Solubility test

The solubility of chitosan and modified chitosan in water at room temperature are shown in Figure 4.9 and Table 4.5. The results showed that all MCC and MCG can dissolved in water, the solubility of MCC 1 reached 83.09 mg/ml and MCG 1 reached 73.09 mg/ml, which are greater than that of chitosan (6.26 mg/ml). It suggested that MCC and MCG is a good water soluble polymer. After grafting of caprolactone and gluconolactone onto chitosan backbones, hydrogen bonding and crystallinity of the native chitosan were reduced, while water solubility increased [52]. When the ratio of caprolactone and gluconolactone were increase to more than 20% by weight, there was no effect on the solubility.
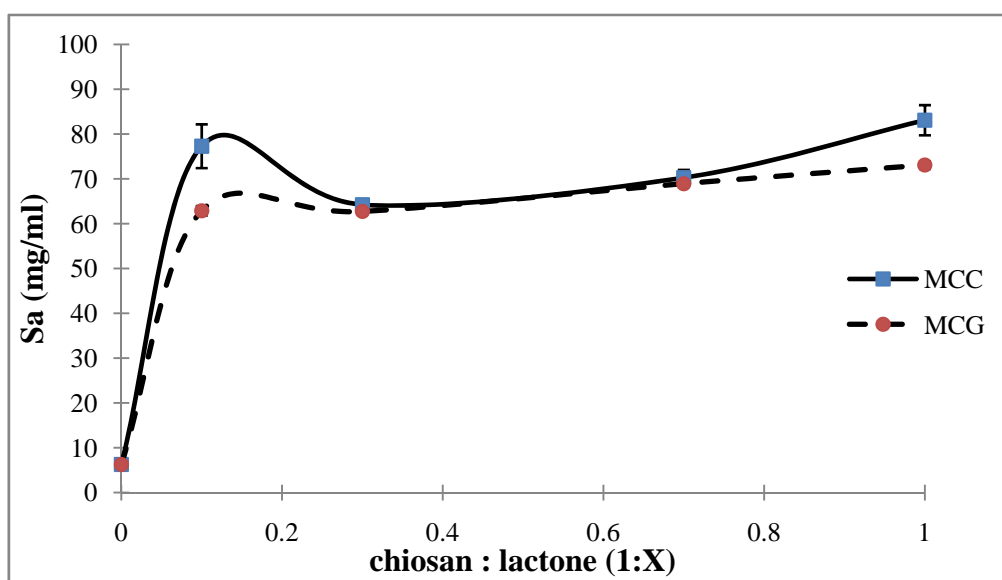


**Figure 4.9** The water solubility of MCC and MCG

Solubility in various pH

The solubility of chitosan and modified chitosan in various pH were measured using a UV spectrophotometer as shown in Figure 4.10. The transparency of chitosan solution gradually decreased from high at pH 6 (90.45%) to practically insoluble at pH higher than 7 (18.48%). Furthermore, MCCs and MCGs solutions showed good transparency at all pH levels. The transparency of MCGs solution slightly decreased from high at pH 6.2 (99.87%) to practically insoluble at pH higher than 7 (74.80%).

The transparency of MCCs solution slightly decreased from high at pH 6.2 (99.48%) to practically insoluble at pH higher than 7.2 (71.80%).

(a)



(b)
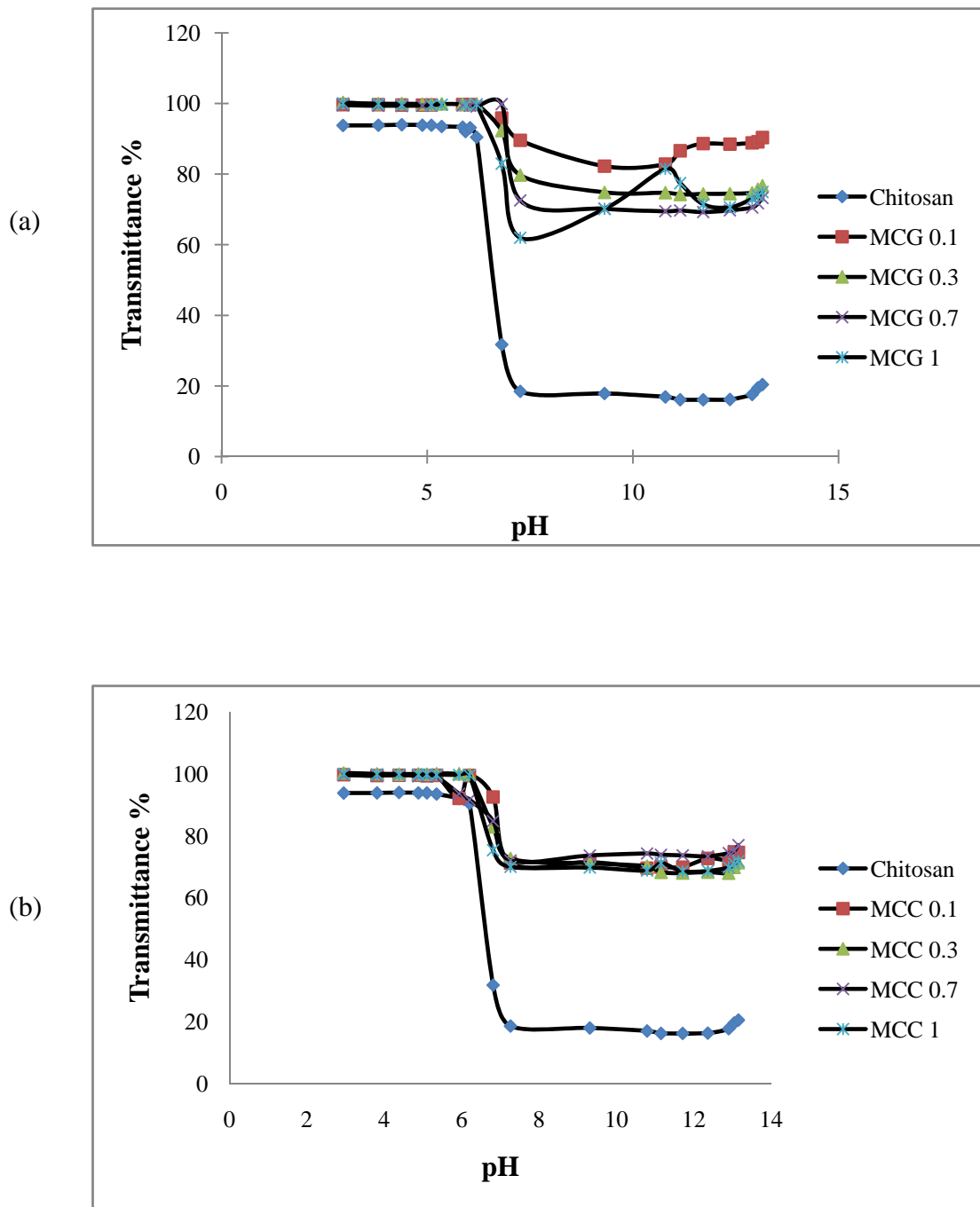


**Figure 4.10** The solubility in various pH of MCG and MCC

**Table 4.5** The water solubility (Sa) and component of bioadhesion of chitosan and modified chitosan

|  | Sa (mg/ml) ± SD | Component of bioadhesion $(\eta_b)$ [a] |
|---|---|---|
| Chitosan | 6.26 ± 0.78 | 24.55 ± 0.76 |
| MCC 0.1 | 77.29 ± 4.88 | 39.55 ± 0.64 |
| MCC 0.3 | 64.24 ± 0.57 | 38.34 ± 0.35 |
| MCC 0.7 | 70.28 ± 1.72 | 31.73 ± 0.40 |
| MCC 1 | 83.09 ± 3.36 | 27.34 ± 0.29 |
| MCG 0.1 | 62.88 ± 1.04 | 25.48 ± 0.16 |
| MCG 0.3 | 62.73 ± 0.51 | 13.83 ± 0.26 |
| MCG 0.7 | 68.92 ± 0.68 | 37.69 ± 0.08 |
| MCG 1 | 73.09 ± 0.85 | 51.50 ± 0.18 |

[a] By Oswald viscometer

### 4.2.4 Mucoadhesive Properties

The condition for studying mucoadhesive at pH 1.2 in order to simulate the condition in the stomach.

### 4.2.4.1 Mucoadhesive of MCC

The mucoadhesion studies of chitosan and MCC in 0.1 N HCl (pH 1.2) at 37°C are shown in Table 4.5 and Figure 4.11(a). The results showed that MCC 0.1 had higher bioadhesion component at 39.55 cps than 24.55 cps of the chitosan. The interactions of MCC with mucin appear to be both electrostatic force, via the $NH_3^+$ groups on MCC with the $COO^-$ groups on the mucin carbohydrate side chain and hydrophobic force, via the $-CH_3$ groups on acetylated chitosan residues with the $-CH_3$ groups on mucin side chains [53]. When increasing the quantity of caprolactone above the ratio of 0.1, the quantity of $-NH_3^+$ decreased and the hydrophobic part of caprolactone increased. Therefore, the interactions between MCC and mucin decreased.

### 4.2.4.2 Mucoadhesive of MCG

The mucoadhesion studies of chitosan and MCG in 0.1 N HCl (pH 1.2) at 37°C are shown in Table 4.5 and Figure 4.11(b), The mucoadhesion studies of ratio 1:1 have the bioadhesion component at 51.50 cps which displayed a higher mucoadhesive property than that of the chitosan. Generallly, mucin reacted efficienctly with hydroxyl group. When chitosan was modified by increasing the hydroxyl group, the component of interactions were enhanced due to the reaction of mucin with $-OH$ group of MCG and the $-NH_3^+$ group on chitosan.

It can be concluded the modified chitosan with gluconolactone has been more hydroxyl groups than modified chitosan with caprolactone, bioadhesion force of MCG was higher than MCC. Increasing of the hydroxyl groups that can participating strong, intermolecular interactions between $-OH$, $-NH_3^+$ groups in mucin.
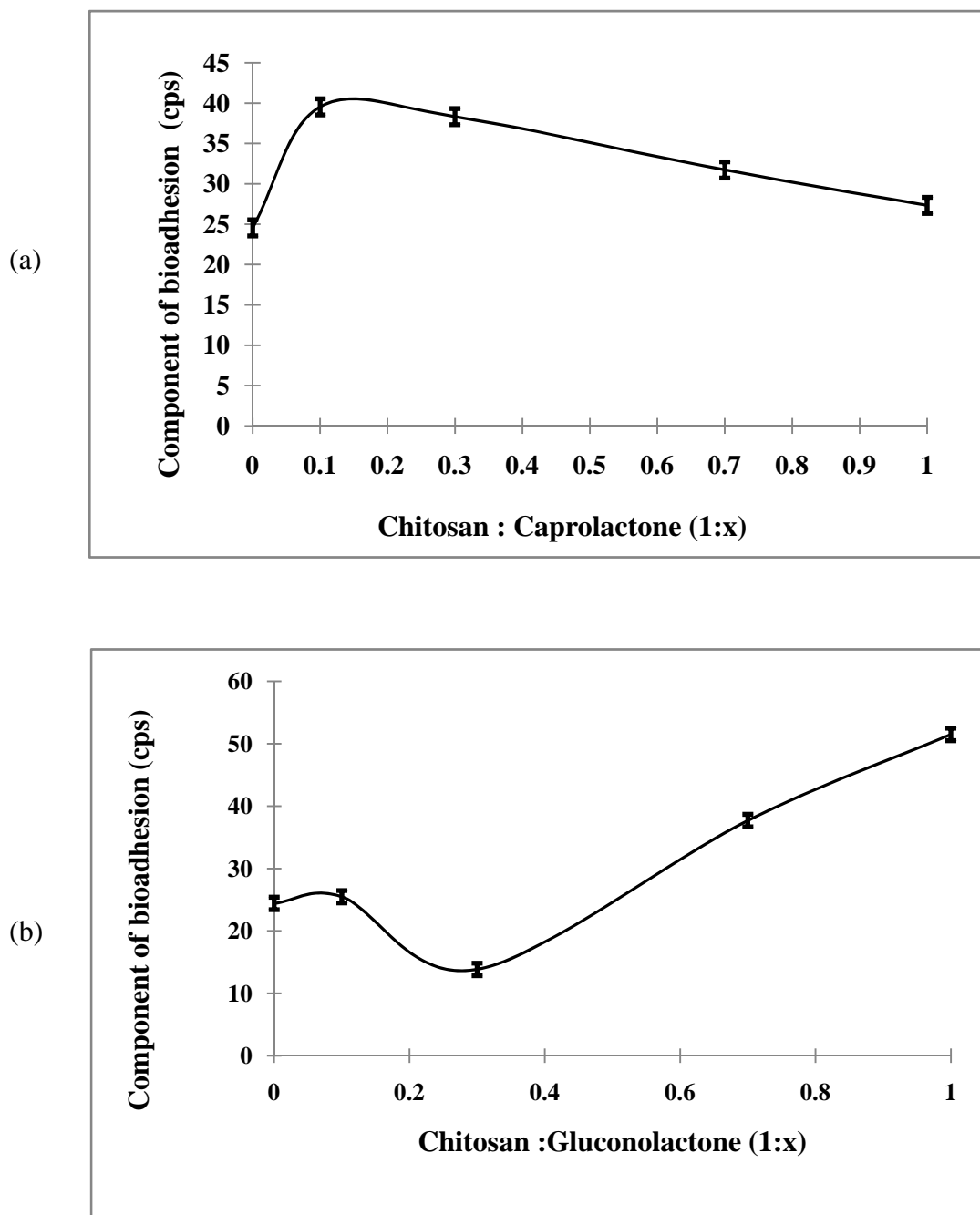
**Figure 4.11** Effect of the ratio of polymer on the component of bioadhesion (a) MCC, (b) MCG in pH 1.2

4.2.5 Swelling Analysis

4.2.5.1 Swelling study of MCC

The swelling ratio of chitosan and MCC in $H_2O$ are shown in Figures 4.12(a). MCC 1 showed a high swelling ratio in water with the swelling ratio of 5.2 at 2 minute after immersing in DI water. Chitosan showed the swelling ratio of 1.5 in the same condition. MCC in $H_2O$ consisted of the hydrophobicity of caprolactone side chains, reduce hydrogen bonding, and crystallinity [52].

The swelling ratio of chitosan and MCC in 0.1 N HCl pH 1.2 are shown in Figure 4.12(b). The swelling ratio of MCC 1 reached 4.2 which is greater than chitosan (1.5) and were constant around 2 minute after immersing in 0.1 N HCl pH 1.2. The swelling ratio of MCC because the dominant charge in the film are the protonated amino group [54].

The swelling ratio of chitosan and MCC in phosphate buffer 7.4 are shown in Figure 4.12(c). The swelling ratio was measured at 1.5 and 3.6 in chitosan and MCC 1, respectively. The swelling ratio of MCC in phosphate buffer 7.4 was lower than swelling ratio in $H_2O$ and 0.1 N HCl pH 1.2 because the amino group were completely deprotonated and then contributed to the loss of solubility of the chain segment.

It can be concluded that MCC has a higher swelling ratio in DI water and 0.1 N HCl pH 1.2, but lower swelling ratio in  phosphate buffer 7.4.

4.2.5.2 Swelling study of MCG

The swelling ratio of chitosan and MCG in $H_2O$, 0.1 N HCl pH 1.2 and phosphate buffer 7.4 are shown in Figure 4.13.

The swelling ratio of chitosan and MCC in $H_2O$ are shown in Figure 4.13 (a). The swelling ratio of chitosan and MCG 1 have been obtained at 1.5 and 3, respectively. MCG swelled in $H_2O$ rapidly because when grafting gluconolactone

onto chitosan, it separated chitosan backbones and drastically reduces its hydrogen bonding and crystallinity and increases the infiltration and water diffusion [52]. The swelling ratio increased with elapse of time and were constant around 2 minute after immersing in DI water. When increased ratio of gluconolactone, the swelling ratio increased.

The swelling ratio of chitosan and MCG in 0.1 N HCl pH 1.2 are shown in Figure 4.13(b). The swelling ratio of MCG 1 reached 3.2 and was greater than chitosan (1.5) and were constant around 2 minute after immersing in 0.1 N HCl pH 1.2. After grafting gluconolactone, the chemical stability of MCG in such acidic solution increased, as the crosslinking reaction creates covalent bridges between chitosan chains and give rise to the formation of a network structure [54].When increased ratio of gluconolactone, the swelling ratio increased.

The swelling ratio of chitosan and MCGs in phosphate buffer 7.4 are shown in Figure 4.13(c) The swelling ratio was measured at 1.5 and 2.8 in chitosan and MCG 1, respectively and were constant around 2 minute after immersing in phosphate buffer 7.4. In phosphate buffer 7.4, the amino group were completely deprotonated and then contributed to the loss of solubility of the chain segment. When increased ratio of gluconolactone, the swelling ratio increased.

It can be concluded that MCG has a higher swelling ratio in DI water and 0.1 N HCl pH 1.2, but lower swelling ratio in  phosphate buffer 7.4.
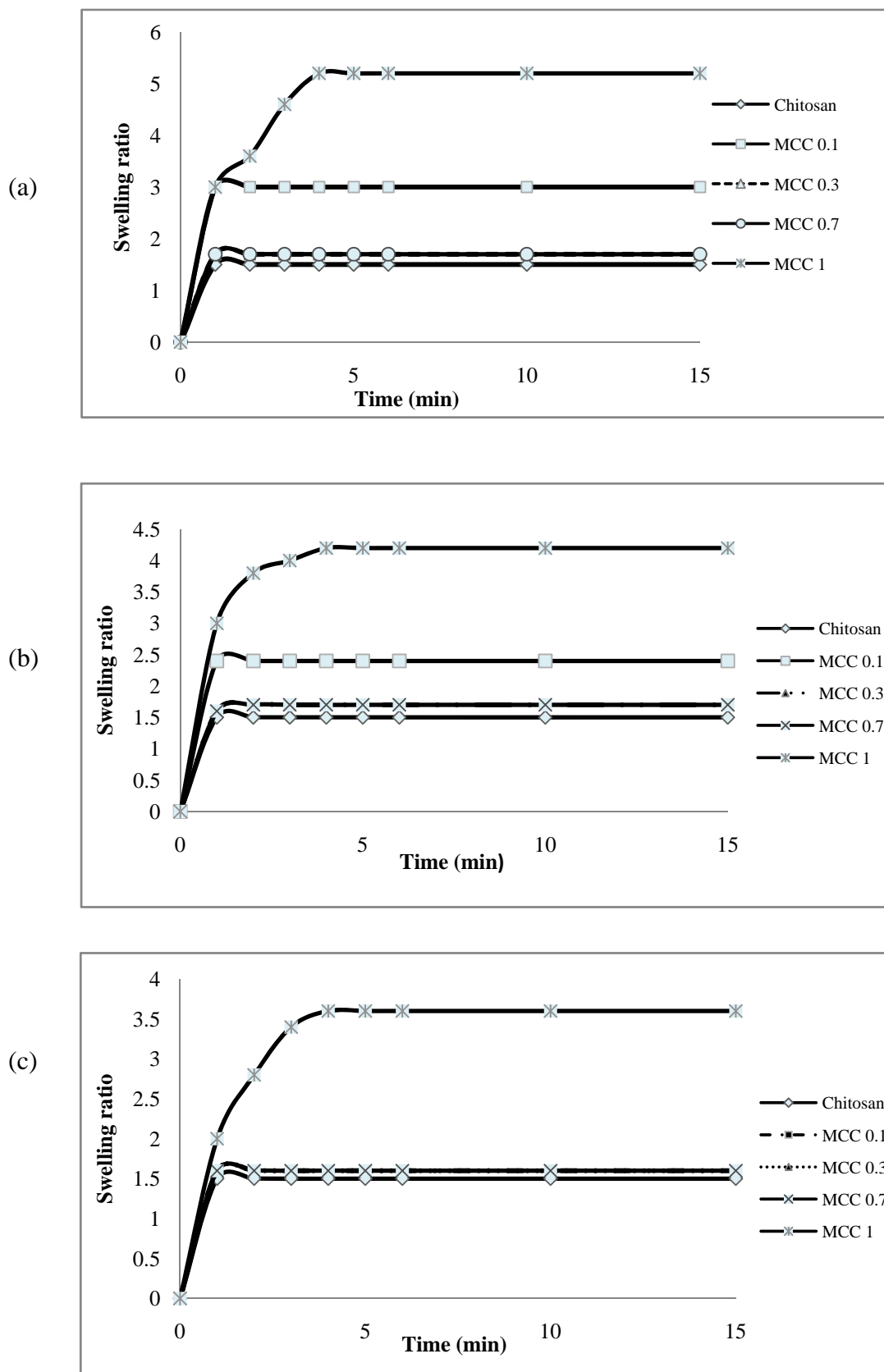
**Figure 4.12** The swelling chitosan and MCC (a) in $H_2O$, (b) in 0.1 N HCl pH 1.2, (c) in phosphate buffer pH 7.4.
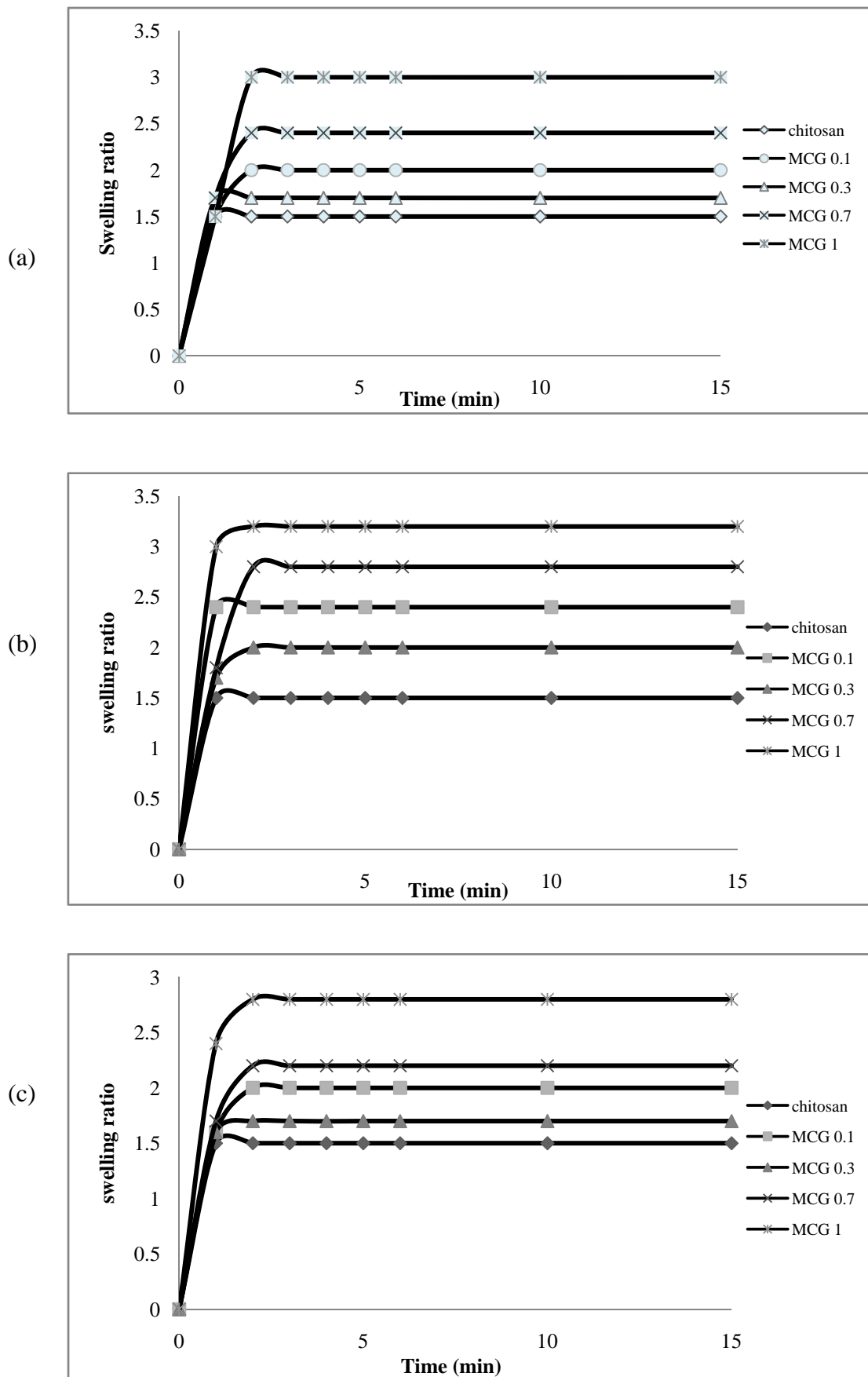
**Figure 4.13** The swelling chitosan and MCG (a) in H$_2$O, (b) in 0.1 N HCl pH 1.2, (c) in phosphate buffer pH 7.4.

4.2.6 Differential Scaning Calorimetry (DSC)

4.2.6.1 DSC thermogram of MCC

The DSC thermograms of MCCs prepared at four different caprolactone to chitosan ratios, 1:0.1, 1:0.3, 1:0.7, 1:1 are shown in Figure 4.14.

The thermogram of chitosan (Figure 4.14a) revealed the endothermic broad peak at 108.6 °C and exothermic peak at about 300°C. The two peaks represent the evaporation of water and the degradation of chitosan, respectively [55].

The thermogram of MCC 0.1 showed the first endothermic peak at 78.9°C were assigned to evaporation of water. The second endothermic of MCC occurred at temperature 188.1°C. This can be explained, due to caprolactone was grafted on chitosan backbone may result in the breaking of the in termolecular hydrogen bonds between chitosan chains. The exothermic peak at about 300°C corresponds to its thermal decomposition. The thermogram of MCC 0.3, MCC 0.7 and MCC 1 (Figure 4.14c to 4.14e) exhibit large endothermic peak around 150.4°C, 148.10°C and 151.8°C, respectively, the peak attributes to a degradation of polymer. A small endothermic peak at 125.8°C and 136.9°C of MCC 0.7 and MCC 1, respectively corresponded to the loss crystallization water strongly bound to the closely-packed polymeric structure.

The results indicated that the structure of chitosan chains has been changed due to the introduction of a hydroxyl group and the reduced ability of crystallization.

4.2.6.2 DSC thermogram of MCG

The DSC thermograms of chitosan and MCGs are shown in Figure 4.15.

The thermogram of chitosan (Figure 4.15a) revealed the endothermic broad peak at 108.6 °C and exothermic peak at about 300°C. The two peaks represent the evaporation of water and the degradation of chitosan, respectively.

The thermogram of MCG 0.1 (Figure 4.15b) was shown endothermic peak around 81.7°C and 188.2°C the fisrt thermal may be attributed to the evaporation of bound water that could not be remove completely. The second endothermic peak shifted to higher temperature from pure chitosan. This may resulted from the graft of gluconolactone on chitosan backbone causing in the decrease of chitosan crystallinity by loosening the hydrogen bonds. The exothermic peak at about 300°C corresponds to its thermal decomposition. The thermograms of MCG 0.3, MCG 0.7 and MCG 1 (Figure 4.15c to 4.15e) exhibit two peak, a smaller endothermic peak at 140.0°C, 137.1°C and 133.2°C corresponded to the loss crystallization water strongly bound to the closely-packed polymeric structure and larger endothermic peak around 160.1°C, 158.0°C and 147.5°C, respectively, the peak attributes to a degradation of polymer. The thermo-sensitive derivatives whose stability seem to decreased with the increasing hydrophilic character.
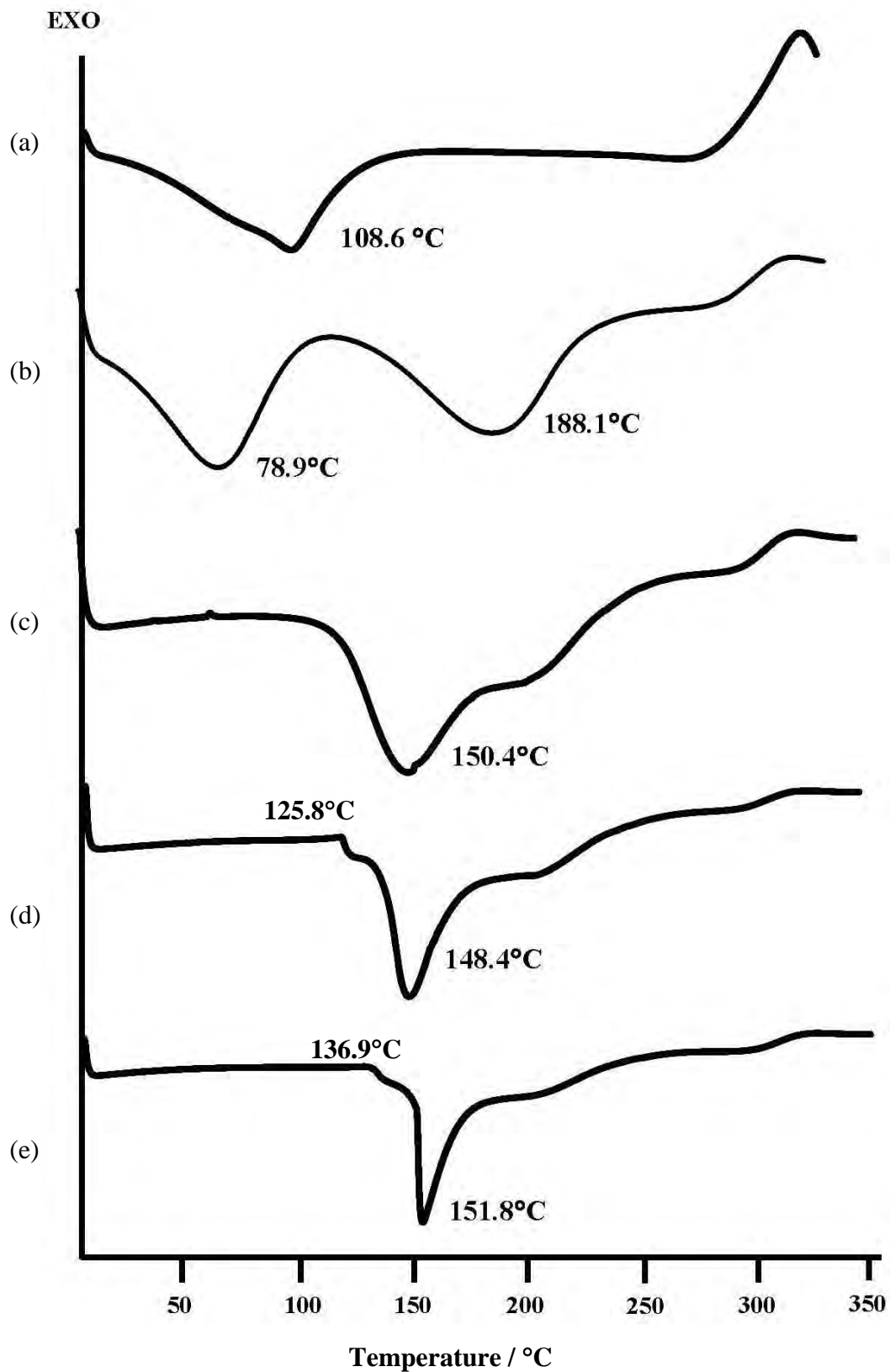
**Figure 4.14** The DSC thermograms of (a) chitosan, (b) MCC 0.1, (c) MCC 0.3, (d) MCC 0.7, (e) MCC 1
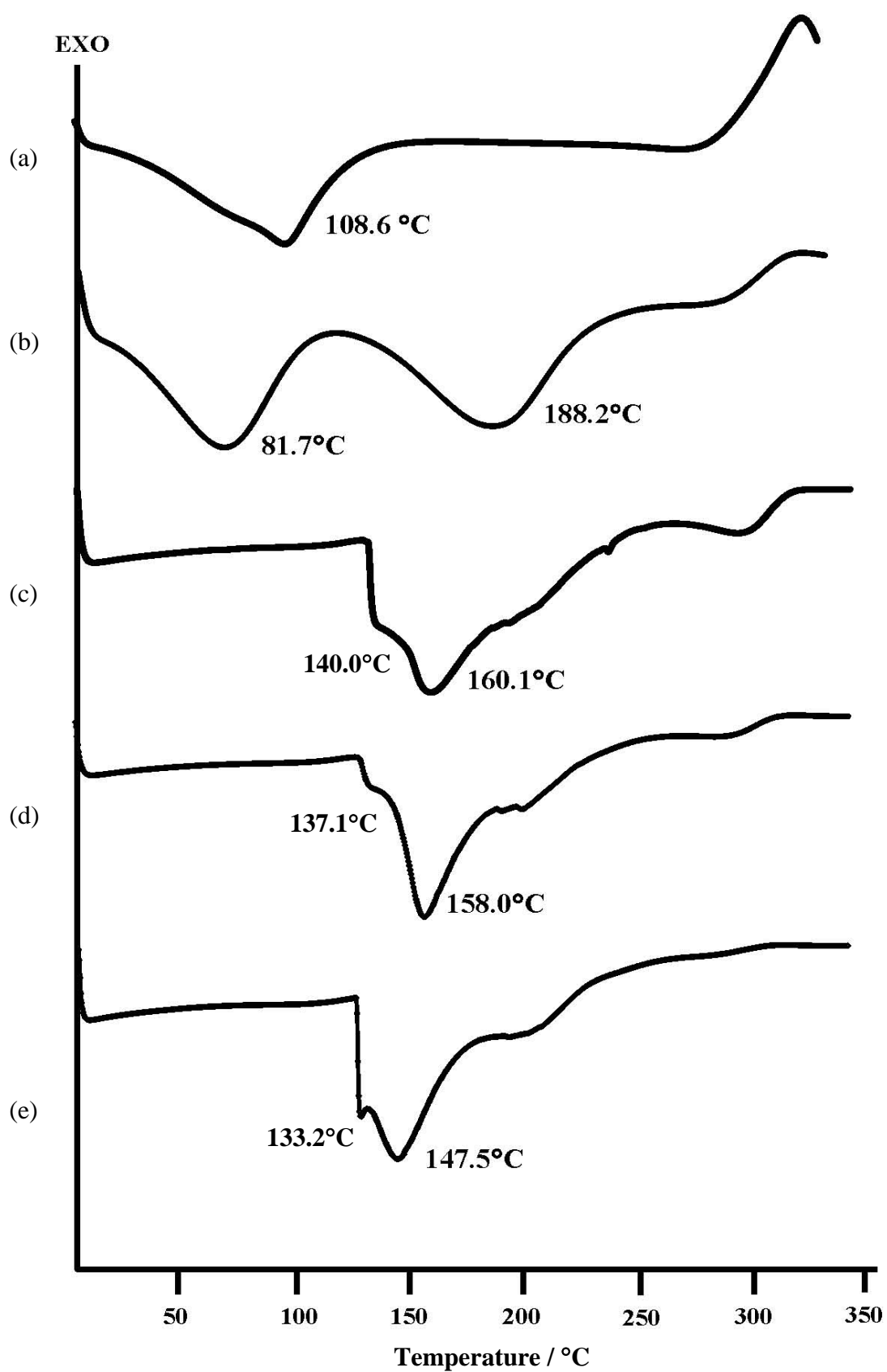
**Figure 4.15** The DSC thermograms of (a) chitosan, (b) MCG 0.1, (c) MCG 0.3, (d) MCG 0.7, (e) MCG 1

4.2.7 Cytotoxic activities of the chitosan, MCG and MCC

In this research, the cytotoxic activities of the chitosan, MCG 1 and MCC 1 were evaluated to investigate the cytotoxicity effects against the normal primate cell line (Vero cell).

**Table 4.6** The cytotoxic activity of  the chitosan, MCG and MCC against the Vero.

| Sample | Cytotoxicity |
|---|---|
| | Vero cell |
| Chitosan | Non-toxic |
| MCG 1 | Non-toxic |
| MCC 1 | Non-toxic |

The results showed that the chitosan, MCG 1 and MCC 1 were non-toxic to the Vero cell. Therefore the chitosan, MCG 1 and MCC 1 is biocompatible to human and may be applied to drug delivery system.

4.2.8 Inhibition of the chitosan, MCG and MCC against *E. coli* and *S. aureus* bacteria.

Inhibition of the chitosan, MCG and MCC against *E. coli* (Gram-negative) and *S. aureus* (Gram-positive) bacteria by agar diffusion method were shown in Figures 4.16 – 4.17.

Figures 4.16 – 4.17 show the antimicrobial activity of chitosan, MCG and MCC. The results showed that the antimicrobial activity of chitosan was higher than MCG, MCC and 1% lactic acid. The MCG and MCC itself had lower of its antimicrobial activity on *E. coli* and *S. aureus*.
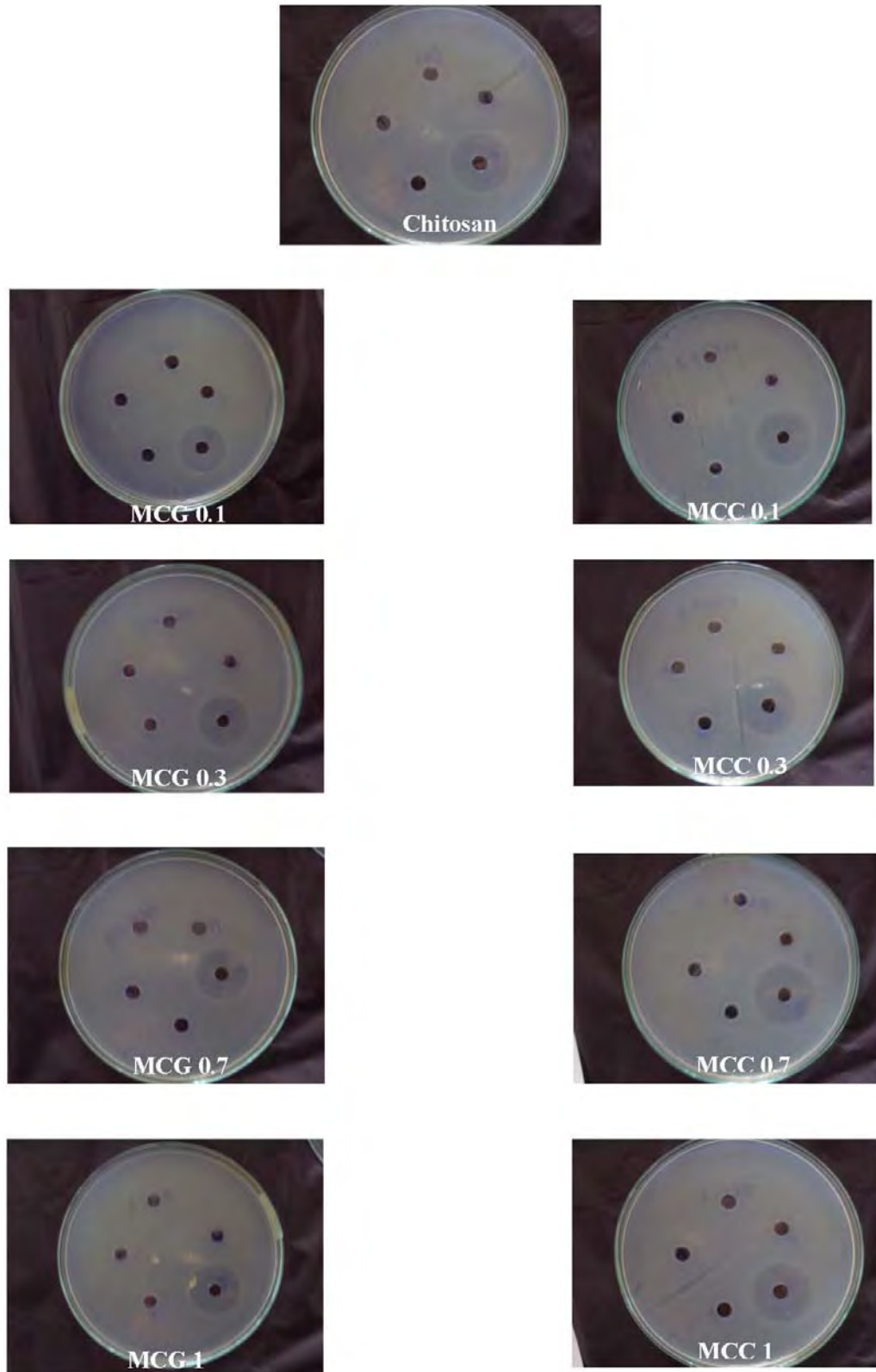
**Figure 4.16** Inhibition clear zones of chitosan, MCG and MCC against *E.coli*
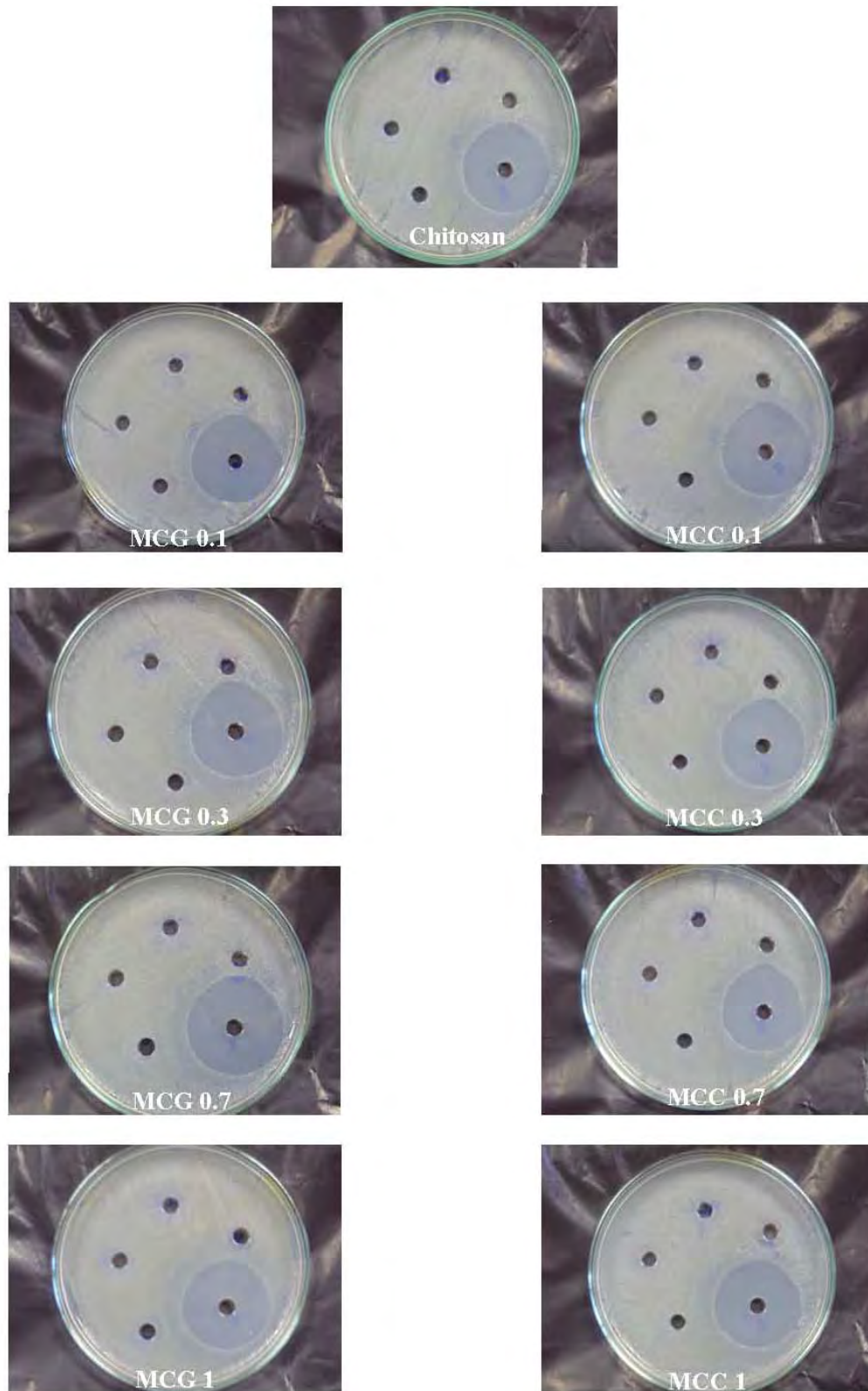
**Figure 4.17** Inhibition clear zones of chitosan, MCG and MCC against *S.aureus*

## 4.3 Pharmaceutical applications

In this research, pharmaceutical applications of modified chitosan as a gastrointestinal drug delivery system were also investigated. Two different model drugs; namely amoxicillin trihydrate (AMX) and sodium diclofenac (DFNa), were used as representative drugs for delivery at the stomach (pH 1.2) and the intestinal tract (pH 7.4), respectively. The drug delivery system was prepared in the form of beads. The beads were analyzed by SEM, FT-IR, DSC. Furthermore, the efficiency of the drug delivery system was determined by the encapsulation efficiency and release profiles of the model drugs in simulated gastric-intestine fluids were studied using HPLC for amoxicillin and UV-VIS spectroscopy for diclofenac sodium.

***Pharmaceutical applications of MCC + DFNa***

.

4.3.1 The encapsulation efficiency (%EE) of the DFNa – Alg/MCC beads

The percentages of encapsulation efficiency (%EE) of the DFNa -Alg/MCC beads prepared from various compositions are shown in Table 4.7.

For DFNa loaded pure alginate beads, the %EE is $55.50 \pm 0.15$, which is lower significant from the other formulation (ANOVA, $P = 0.00$)

The DFNa loaded pure MCC beads was not successfully fabricate, probably due to the MCC is high water solubility, therefore, it could not be formed the beads in the 4% NaOH coagulant. In this case, the polyelectrolyte complexes (PEC) of the MCC and alginate were prepared to facilate the beads formation.

Formulations C to E are the PEC complexes of Alg/MCC0.1 to Alg/MCC0.7 which showed high encapsulation efficiencies over 80%. Whereas, Formulation F consisted of Alg/MCC1 had significant lower %EE of $76.98 \pm 0.28$ compared to those formulations (ANOVA followed by LSD test, $P = 0.00$). The result point to the fact that MCC1 has the highest water solubility. Therefore, when the DFNa loaded Alg/MCC1 beads were immersed in the 4% aq. $CaCl_2$ solution for a long time, the beads were swollen continuously and graduately dissolved, resulting in the drug were diffused out from the beads.

**Table 4.7** The encapsulation efficiency (%EE) of the formulated chitosan beads with various compositions.

| Formulations | | Ratio of composition | | | % EE ± SD |
|---|---|---|---|---|---|
| | | DFNa | Alginate | Polymer | |
| A1 | Pure alginate | 1 | 1 | - | $55.50 \pm 0.15^b$ |
| A2 | Pure MCC | 1 | - | 1 | *ND |
| B | Chitosan | 1 | 1 | 0.5 | $80.98 \pm 0.16$ |
| C | MCC0.1 | 1 | 1 | 0.5 | $81.20 \pm 0.37^a$ |
| D | MCC0.3 | 1 | 1 | 0.5 | $80.24 \pm 0.28^a$ |
| E | MCC0.7 | 1 | 1 | 0.5 | $82.11 \pm 0.14^a$ |
| F | MCC1 | 1 | 1 | 0.5 | $76.98 \pm 0.28^a$ |

*ND: beads could not be prepared.

[a]: not significant different (ANOVA followed by LSD test, compared to Formulation B with $P > 0.05$)

[b]: significant different (ANOVA followed by LSD test, compared to Formulation B with $P < 0.05$)

### 4.3.2 Morphology of the DFNa – Alg/MCC beads

The surface topography, size and shape of the dried beads were observed by scanning electron microscopy (SEM). The effect of various of chitosan and the five different types of MCC on bead morphology were investigated and the SEM micrographs of the beads are presented in Figure 4.18.

For DFNa – Alg beads (Formulation A, without chitosan), the beads were in a spherical form with the particle size about 1 mm. The crystals of DFNa can be seen apparently cover the surface of the beads, because the pure alginate beads could not fully entrapped DFNa. The result was consistent with the %EE of DFNa – Alg beads ($55.50 \pm 0.15$).

The beads obtained from the polyeletrolyte complexes (PEC) of Alg/Chi and Alg/MCC were also in a spherical shape with the particle size about 1 mm. The surface for all formulations had rougher and more folded because of the network shrinking during dry.

From Figure 4.18, the cross-sections of all formulation beads showed the inner of the beads, the crystals of drug could be apparently seen inside the beads for all formulations. The cavities inside the all formulation beads were denser and tightly packed as the results of the ionic interactions between the $NH_3^+$ groups of chitosan or of the MCC and the $COO^-$ of Alg [56].

The particle sizes of the beads formed by Alg/Chi, Alg/MCC were larger than that of the beads formed by pure alginate.
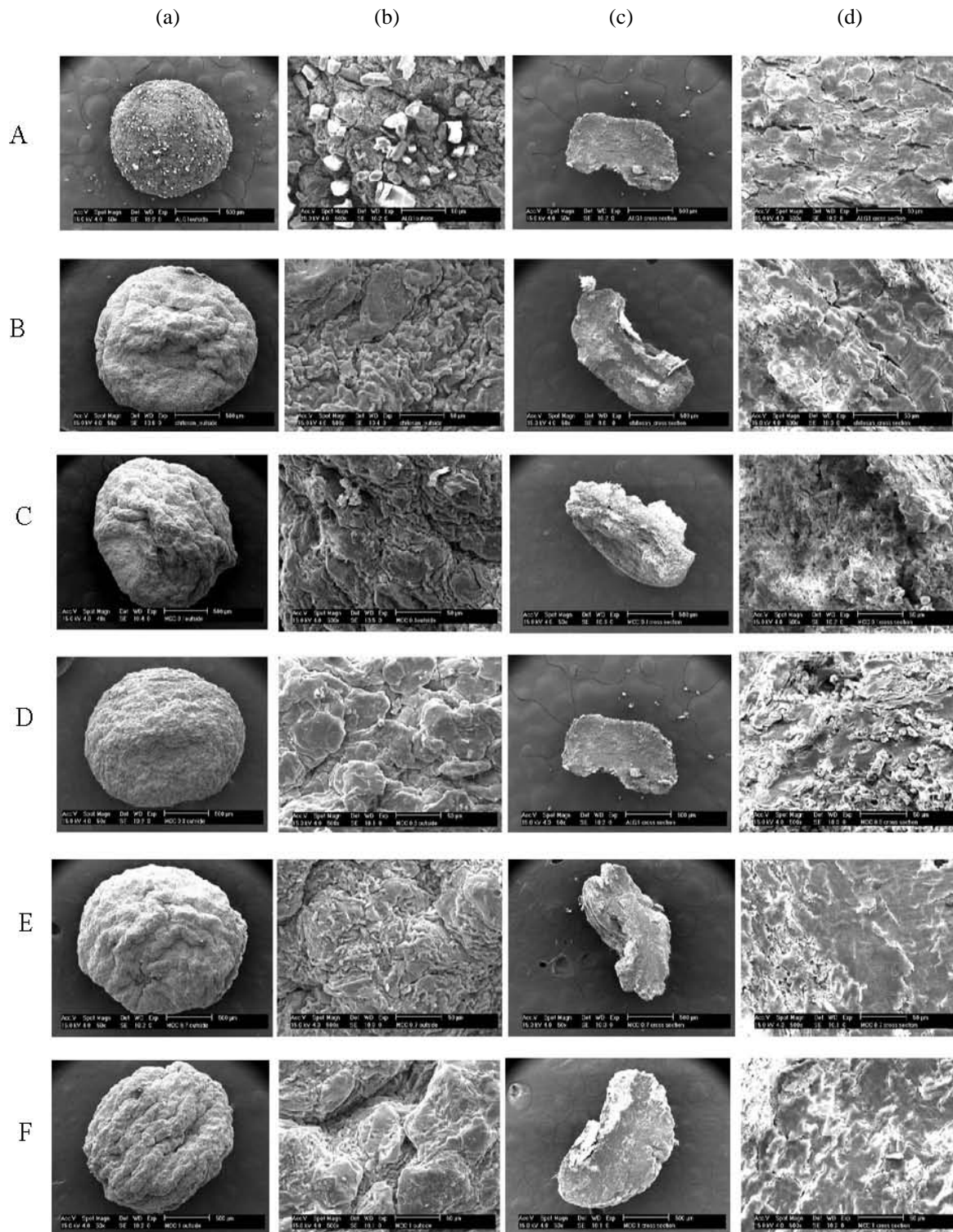
|  | (a) | (b) | (c) | (d) |
|---|---|---|---|---|
| A | | | | |
| B | | | | |
| C | | | | |
| D | | | | |
| E | | | | |
| F | | | | |



**Figure 4.18** Scanning electron photomicrographs of (a) the beads (x50), (b) surface (x500), (c) cross-section (x50) and (d) network inside bead (x500) of formulation A, B, C, D, E and F, respectively.

4.3.3 DSC thermograms of the DFNa – Alg, DFNa-Alg/MCC beads

The DSC thermograms of pure alginate, pure DFNa, pure chitosan and the representative of DFNa – Alg/MCC (DFNa – Alg/MCC 0.7) are shown in Figure 4.19. In this case, the DFNa – Alg/MCC 0.7 formulation was selected as a representative of DFNa loaded Alg/MCC beads because it  showed the highest encapsulation efficiency (%EE).

The thermogram of pure alginate (Figure 4.19a) showed the first endothermic range from 40°C to 133°C with the peak at 69°C was assigned to evaporation of water. The second small broad endothermic of alginate occurred at temperature 142.7°C was assigned to a dehydration process followed by decomposition of polymer and broad exothermic peak at 250.2°C attributes to the temperature of alginate degradation [57, 58].

The thermogram of pure DFNa (Figure 4.19b) showed the first small endothermic peak at 63°C and the second endothermic peak at 288°C, corresponding to the evaporation of water and decomposition of drug, respectively. The sharp exothermic peak at 296°C attributes to oxidation reaction between DFNa and oxygen in air environment fusion [59].

The thermogram of chitosan (Figure 4.19c) revealed the endothermic broad peak at 108.6 °C and exothermic peak at about 300°C. The two peaks represent the evaporation of water and the degradation of chitosan, respectively.

The thermogram of MCC 0.7 (Figure 4.19d) exhibited the endothermic peak around 148.10°C which attributes to a degradation of polymer.

The thermogram of DFNa – Alg/MCC 0.7 (Figure 4.19e) showed 3 endothermic peaks at 132.2°C, 175.5°C and 190.8°C attributes to the characteristic peak of Alg, MCC 0.7 and DFNa, respectively. These peaks were shifted from the original positions because of the interaction of polymer and drug.
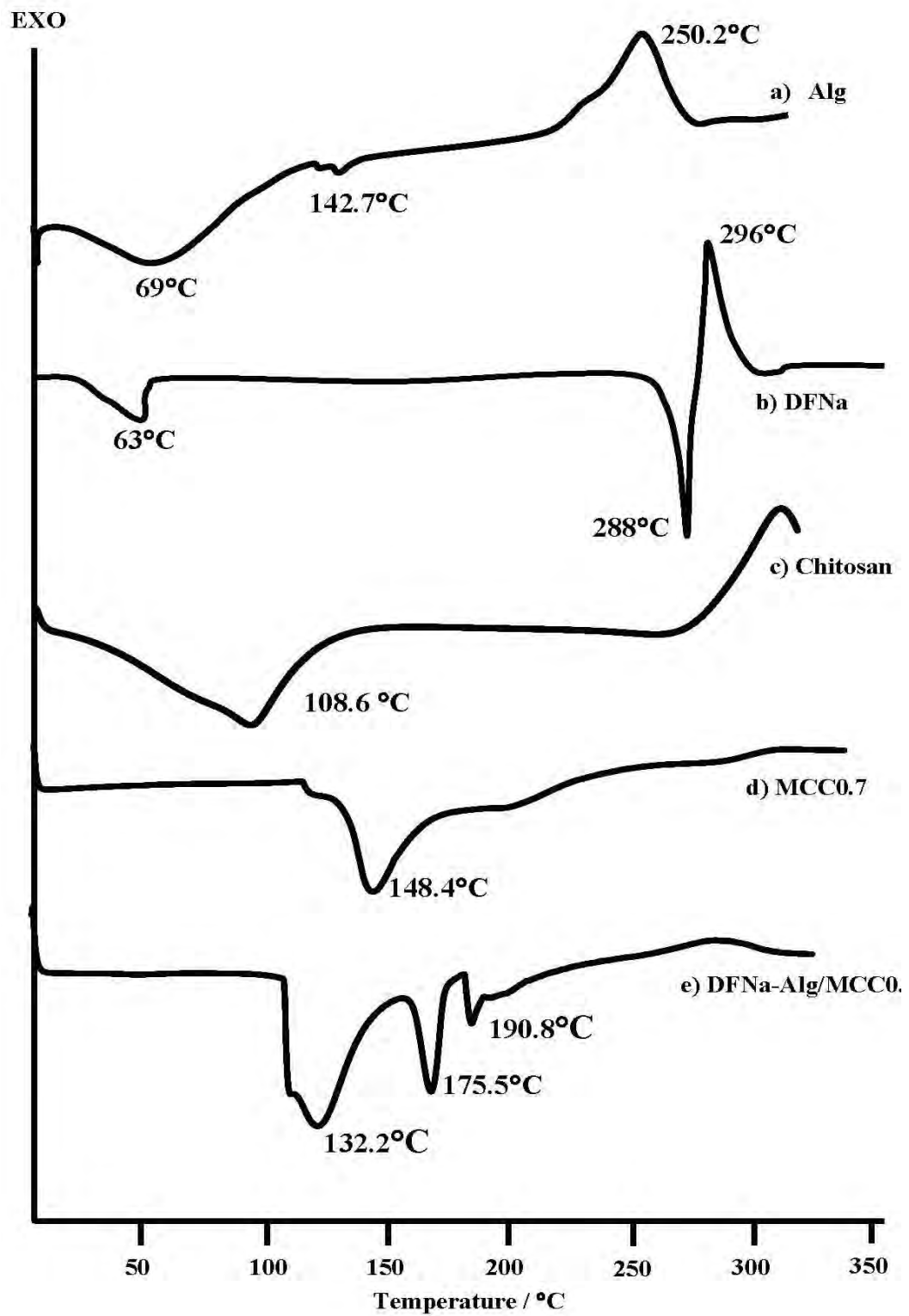
**Figure 4.19** The DSC thermograms of (a) alginate, (b) DFNa, (c) chitosan, (d) MCC 0.7, (e) DFNa - Alg/MCC 0.7

4.3.4 Fourier Transform Infrared Spectroscopy (FTIR) of the DFNa – Alg/MCC beads

FTIR spectroscopy was used to determine the chemical interactions of the samples as displayed in Figures 4.20 to 4.21.

The IR spectrum of pure alginate (Figure 4.20a) showed the characteristic absorption bands at 1618 $cm^{-1}$, 1419 $cm^{-1}$, 1030 $cm^{-1}$ attributed to the asymmetric stretching vibration of C=O, the –$CH_2$ bending and the stretching of C-O-C, respectively [58].

The IR spectrum of pure DFNa (Figure 4.20c) which showed the principle bands were observed at 743, 765, 1293, 1302 and 1573 $cm^{-1}$. The band at 743 and 765 $cm^{-1}$ resulted from C-H bending. The IR absorption bands at 1293 and 1302 $cm^{-1}$ resulted from C-N stretching and the band at 1573 $cm^{-1}$ resulted from C=C stretching combined with C=O stretching of carboxylate group, respectively.

Figure 4.20 (d) showed the IR spectrum of DFNa – Alg. The band at around 3399 $cm^{-1}$ attribute to O-H and N-H stretching vibration. The absorption band at 1607 $cm^{-1}$ assigned to C=O stretching of alginate. The bands at 1556 $cm^{-1}$ and 1505 $cm^{-1}$ resulted from C=O stretching of carboxylate group and C=C stretching of DFNa, respectively. The results confirm that there is no drug-polymer interactions.

Figure 4.20 (f) showed the IR spectrum of DFNa – Alg/Chi. The characteristic IR bands at 1694 $cm^{-1}$ and 1602 $cm^{-1}$ corresponded to the combination of C=O stretching and –$NH_2$ bending of chitosan and alginate, respectively, which are slightly shifted from the original positions of the native polymers. The band at 1507 $cm^{-1}$ resulted from the combination of C=O and C=C stretching of DFNa. The band at 1321 $cm^{-1}$ was due to C–N stretching vibration. The results suggest that there is the interaction between the alginate and chitosan.

**Figure 4.20** IR spectra of (a) alginate, (b) chitosan, (c) DFNa, (d) DFNa – Alg, (e) DFNa – Alg/Chi

Figures 4.21(a) to 4.21(d) showed the IR spectrum of DFNa – Alg/MCC 0.1 to DFNa – Alg/MCC 1, respectively. The broad absorption band around 3379 cm$^{-1}$ was assigned to the stretching vibration of N-H group bonded to –OH group. The new sharp bands at 1694 cm$^{-1}$ and 1579 cm$^{-1}$ were due to C=O stretching of MCC and C=O stretching of carboxylate group of DFNa, respectively. The results reveal that the alginate formed polyelectrolyte complex with MCC and/or participated intermolecular interactions with drug.

**Figure 4.21** IR spectra of (a) DFNa – Alg/MCC 0.1, (b) DFNa – Alg/MCC 0.3, (c) DFNa – Alg/MCC 0.7, (d) DFNa – Alg/MCC1

4.3.5 Swelling Analysis

4.3.5.1 Swelling Analysis in the Stimulated Gastric Fluid. (SGF, pH 1.2)

The swelling behaviors of the DFNa – Alg/MCC beads in this solution system (0.1 N HCl pH 1.2) were investigated in order to determine the pH-sensitive behavior. The mechanism of swelling in pH 1.2 are shown in Figure 4.23a. The results showed that the beads did not swell in the acidic condition. Chitosan is well known that it can swell in the acidic medium, because the protonation of the amino groups of chitosan take place at low pH. This causes the repulsion among polymer chains which allows more water into the gel network [54]. In case of MCC, some of the amino groups of chitosan were grafted with the hydrophobic carprolactone side chains, resulting in lower amino groups to be protonated. Hence, the repulsion force between cationic charge was reduced, less water could penetrate into the polymer network.

4.3.5.2 Swelling Analysis in the Stimulated Intestinal Fluid. (SIF, pH 7.4)

The swelling ratios of the beads with various compositions in SIF pH 7.4 are shown in Figure 4.22 and Table 4.8.

**Table 4.8** Swelling ratios of formulation A to F in SIF (pH 7.4)

| Time (h) | Formulation A | Formulation B | Formulation C | Formulation D | Formulation E | Formulation F |
|---|---|---|---|---|---|---|
|  | Pure alg | Pure Chi | MCC0.1 | MCC0.3 | MCC0.7 | MCC1 |
| 0 | 0 | 0 | 0 | 0 | 0 | 0 |
| 0.5 | 0 | 0 | 0 | 0 | 0 | 0 |
| 1 | 0 | 0.50 | 0.50 | 0.50 | 0.50 | 0.5 |
| 2 | 0.50 | 0.75 | 0.75 | 0.75 | 0.75 | 0.75 |
| 4 | 0.75 | 0.75 | 1.25 | 1 | 1.25 | 0.75 |
| 6 | 1 | 1 | 1.25 | 1 | 1.25 | 0.75 |
| 8 | 1 | 1 | 1.25 | 1 | 1.25 | 0.75 |
| 24 | 1 | 1 | 1.25 | 1 | 1.25 | 0.75 |

**Figure. 4.22** Swelling behavior of various polymer of the DFNa - Alg, DFNa – Alg/Chi, DFNa – Alg/MCC 0.1, DFNa – Alg/MCC 0.3, DFNa – Alg/MCC 0.7, DFNa – Alg/MCC1 in SIF

The swelling behaviors of the beads for all formulations in this dissolution system (phosphate buffer saline pH 7.4) showed that the Alg/MCC 0.1 and Alg/MCC 0.7 have the highest swelling ratio with near one fold compared to that of Alg beads and Alg/Chi beads. Figure 4.23b showed the mechanism of swelling in pH 7.4.

The DFNa – Alg/MCC beads, in this medium, the $Na^+$ ions of Alg in the external solution undergo ion-exchange process with $Ca^{2+}$ ions which were binding with $COO^-$ groups mainly in the DFNa. This phenomenon resulted in the electrostatic repulsion among negatively charged $COO^-$ groups which causes the chain relaxation and enhances the swelling properties [55].

**Figure 4.23** The swelling mechanism of Alg-MCC beads in buffer solution of different pH a) pH 1.2, b) pH 7.4

4.3.6 In Vitro Release Study

4.3.6.1 Sodium diclofenac release behavior from the beads in SGF

The dissolution profiles of DFNa can be described as graphs to explain and understand the drug released behavior from the beads.

The dissolution and release rate data of each formulation are given in Tables D1 - D2 (Appendix D). These dissolution profiles and release rate profiles are shown in Figure 4.24. In the acidic condition, the release rate was slow because of the low solubility of sodium diclofenac. Therefore, it did not dissolved out from the beads. The results suggest that the Alg/MCC system is a pH-sensitive system. This system can control the release of the drug from.



**Figure 4.24** The dissolution profiles of DFNa - Alg, DFNa – Alg/Chi, DFNa – Alg/MCC 0.1, DFNa – Alg/MCC 0.3, DFNa – Alg/MCC 0.7, DFNa – Alg/MCC1 in SIF

4.3.6.2 Sodium diclofenac release behaviors from the MCC beads in SIF

The dissolution and release rate data of each formulation are given in Tables D4 – D5 (Appendix D). These dissolution profiles and release rate profiles are shown in Figure 4.25, in the phosphate buffer pH 7.4. The beads without MCC exhibited the release rate faster than that of the one with MCC. The release rates for all formulations of Alg/MCC are similar. All Alg/MCC formulations can release almost DFNa (98.93%) over 24 hours, whereas Formulation A (without MCC) releases the lowest amount of drug only at 76.24% and rapid release. The slow release rate of drug molecules from the beads probably control by the polyelectrolyte complex between alginate and MCC



**Figure 4.25** The dissolution profiles of DFNa - Alg, DFNa – Alg/Chi, DFNa – Alg/MCC 0.1, DFNa – Alg/MCC 0.3, DFNa – Alg/MCC 0.7, DFNa – Alg/MCC1 in SIF

*Pharmaceutical applications of MCG + DFNa*

4.4.1 The encapsulation efficiency (%EE) of the DFNa – Alg/MCG beads

The percentages of encapsulation efficiency (%EE) of the DFNa -Alg/MCG beads prepared from various compositions are shown in Table 4.9.

The DFNa–Alg beads (pure alginate), the drug efficiencies was 55.50 ± 0.15%. The DFNa loaded pure MCG could not fabricate into the beads in 4% NaOH coagulant beads, because the MCG is high water solubility. The %EE of the Alg/Chi bead (Formulation B) is higher than that of pure Alg beads, because the effect of polyelectrolyte complex between the alginate and chitosan (ANOVA, $P$ = 0.00). When the beads consisted of MCG, the %EE are lower than that of the Alg/Chi, but higher than that of the Alg beads (ANOVA, $P$ = 0.00). For example, the encapsulation efficiencies of Formulation G and H (consisting of MCG 0.1 and MCG 0.3, respectively) are only 68.83%, compared to those formulations. This may be due to the MCG has high water solubility, so the drug can diffuse out from the beads into the aqueous medium during the coagulation process.

**Table 4.9** The encapsulation efficiency (%EE) of the formulated chitosan beads with various compositions.

| Formulations | | Ratio of composition | | | % EE ± SD |
|---|---|---|---|---|---|
| | | DFNa | Alginate | Polymer | |
| A1 | Pure alginate | 1 | 1 | - | 55.50 ± 0.15[b] |
| A2 | Pure MCC | 1 | - | 1 | *ND |
| B | Chitosan | 1 | 1 | 0.5 | 80.98 ± 0.16[a] |
| G | MCG 0.1 | 1 | 1 | 0.5 | 68.83 ± 0.51[b] |
| H | MCG 0.3 | 1 | 1 | 0.5 | 77.35 ± 0.45[b] |
| I | MCG 0.7 | 1 | 1 | 0.5 | 83.31 ± 0.07[b] |
| J | MCG 1 | 1 | 1 | 0.5 | 80.43 ± 0.34[b] |

*ND: beads could not be prepared.

[a]: not significant different (ANOVA followed by LSD test, compared to Formulation B with $P > 0.05$)

[b]: significant different (ANOVA followed by LSD test, compared to Formulation B with $P < 0.05$)

### 4.4.2 Morphology of the DFNa – Alg/MCG beads

The surface topography, size and shape of the dried beads were observed by scanning electron microscopy (SEM). The effect of various of chitosan and the five different types of MCG on bead morphology were investigated. The SEM micrographs of the beads are presented in Figure 4.26.

The SEM of Formulation A (DFNa – Alg beads) the beads were well form spherical shape with the particle size of 1 mm. The crystals of DFNa precipitated on the particle surface. Crystals of DFNa attached on the surface is the cause of a burst effect and were consistent with the lower %EE of DFNa – Alg beads ($55.50 \pm 0.15$).

The beads prepared from the polyelectrolyte complex with alginate and either chitosan or MCG did not show any crystals of DFNa precipitated at the surface of the beads. The cross-sections of all formulation beads (Figure 4.26d) are dense and tightly packed interior. The crystal of drugs could be apparently seen inside the beads The particle sizes of the beads formed by Alg/Chi, Alg/MCG were larger than that of the beads formed by pure alginate.

**Figure 4.26** Scanning electron photomicrographs of (a) the beads (x50), (b) surface (x500), (c) cross-section (x50) and (d) network inside bead (x500) of formulation A, B, G, H, I and J, respectively.

### 4.4.3 DSC thermograms of the DFNa – Alg, DFNa-Alg/MCG beads

The DSC thermograms of pure alginate, pure DFNa, pure chitosan and the representative of DFNa – Alg/MCG (DFNa – Alg/MCG 1) are shown in Figure 4.27. In this case, the DFNa – Alg/MCG 1 formulation was selected as a representative of DFNa loaded Alg/MCG beads because it showed the highest encapsulation efficiency (%EE).

The DSC thermogram of pure alginate, DFNa, chitosan (Figures 4.27a to 4.27c, respectively) were similar described in section above.

The thermogram of MCG 1 (Figure 4.27d) exhibited the endothermic peak around 147.5°C, the peak attributes to a degradation of polymer.

The thermogram of DFNa – Alg/MCG 1 showed 3 endothermic peaks (Figure 4.27e) at 121.6°C, 176.3°C and 208.4°C attributes to the characteristic peak of Alg, MCG 1 and DFNa, respectively. These peaks were shifted from the original positions because of the interaction of polymer and drug.

**Figure 4.27** The DSC thermograms of (a) alginate, (b) DFNa, (c) chitosan, (d) MCG 1, (e) DFNa - Alg/MCG 1

4.4.4 Infrared Spectroscopy (FT-IR) of the DFNa – Alg/MCG beads

FTIR spectroscopy was used to determine the chemical interaction of the samples as displayed in Figures 4.28 to 4.29.

The IR spectrum of pure alginate, DFNa, chitosan, DFNa-Alg and DFNa-Alg/Chi (Figures 4.28a to 4.28e, respectively) were already described in section above (data not shown in this section).
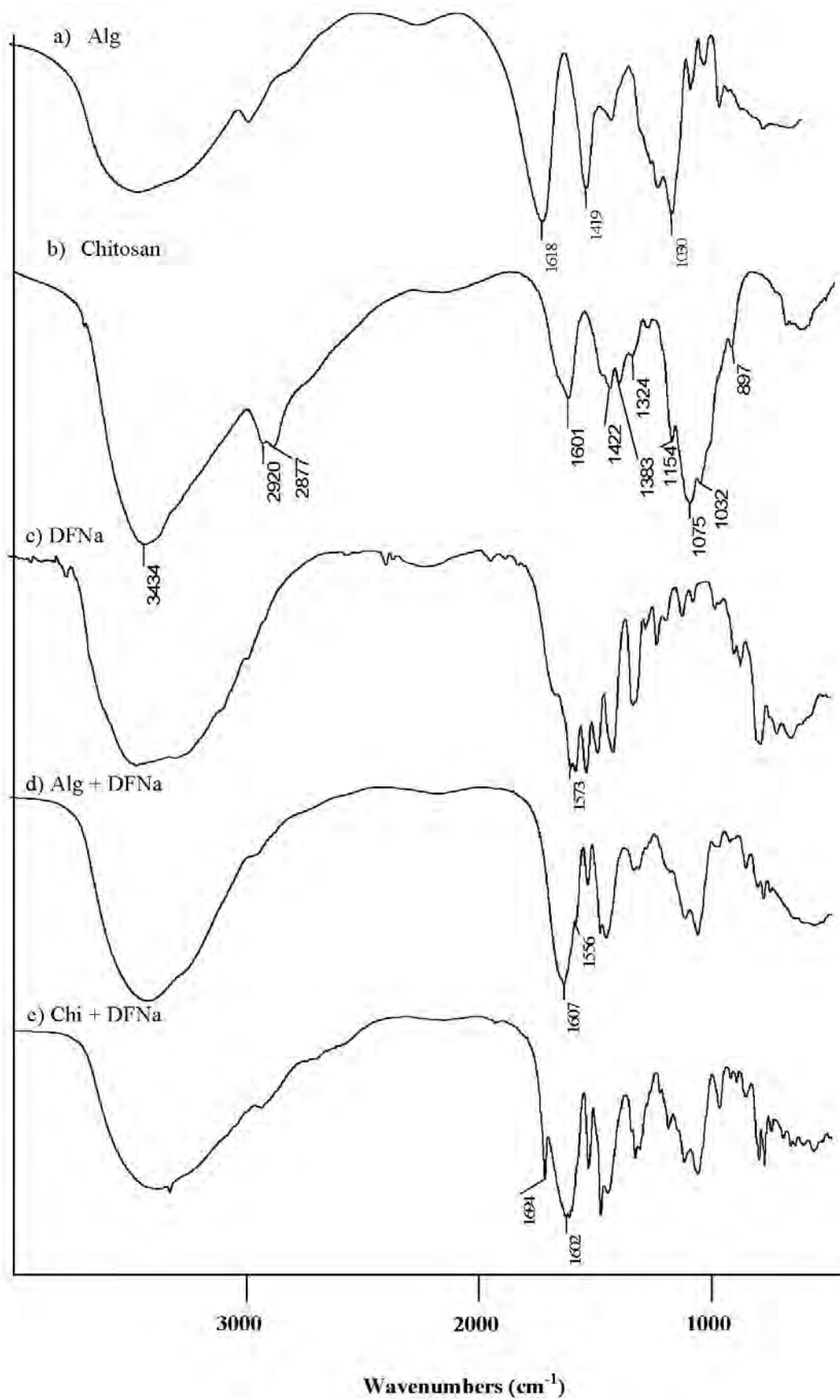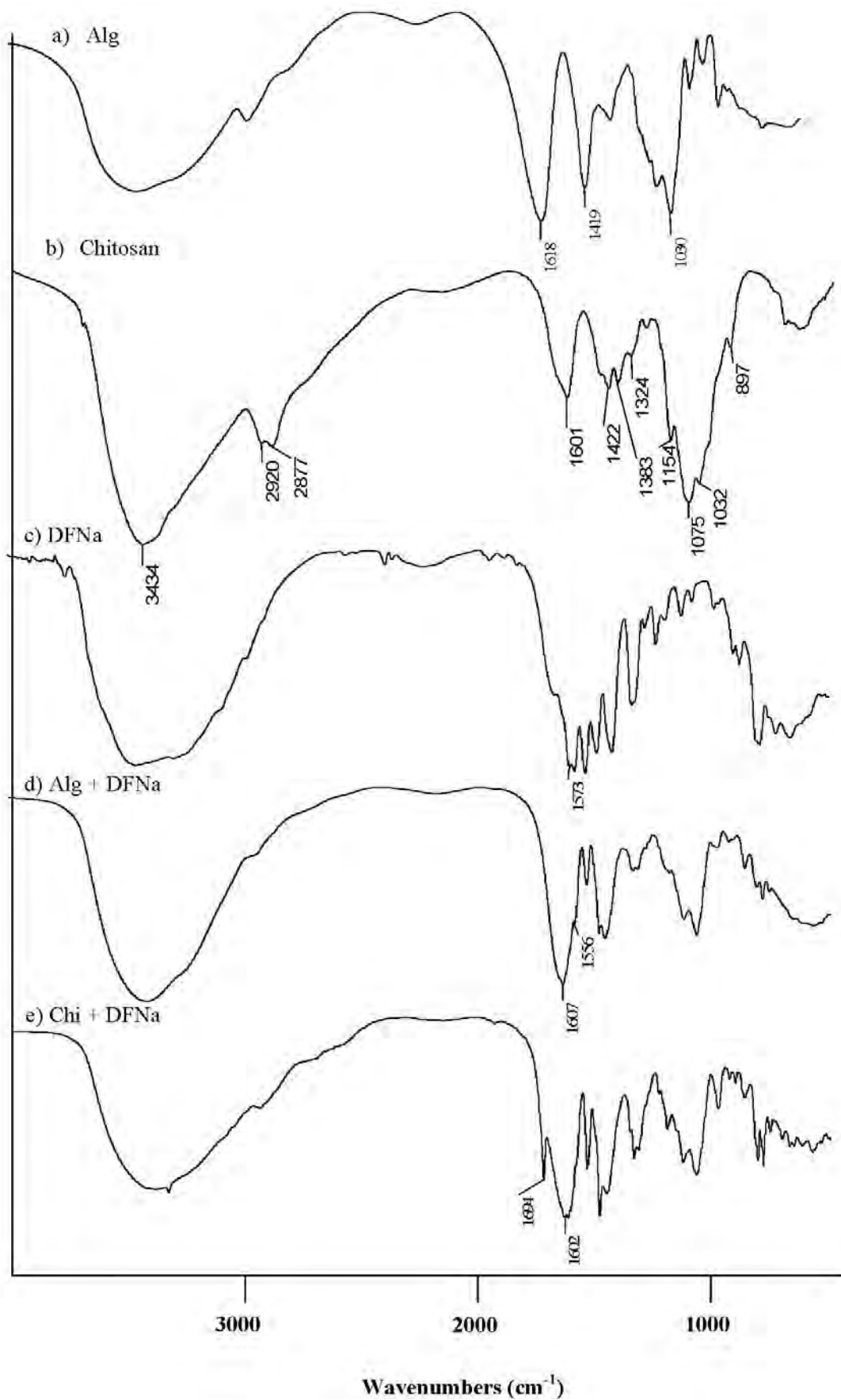
**Figure 4.28** IR spectra of (a) alginate, (b) chitosan, (c) DFNa, (d) DFNa – Alg, (e) DFNa – Alg/Chi

Figure 4.29(a) shows the IR spectrum of DFNa – Alg/MCG 0.1. The wide absorption band at 3354 cm$^{-1}$, due to the stretching vibration of N-H group bonded to O-H group of DFNa. The band at 1694 cm$^{-1}$ and 1578 cm$^{-1}$ assigned to C=O stretching of MCG 0.1 and C=O stretching of carboxylate group of DFNa, respectively. The band at 1508 cm$^{-1}$ resulted from C=C stretching The band at 1605 cm$^{-1}$ and 1321 cm$^{-1}$ were assigned to amide II and amide III (–NH$_2$ bending and C–N stretching), respectively. The absorption band at 1160 cm$^{-1}$ attributed to C-O-C stretching. The IR spectrum of DFNa – Alg/MCG 0.3 to DFNa – Alg/MCG 1 are similar to that of DFNa – Alg/MCG 0.1.
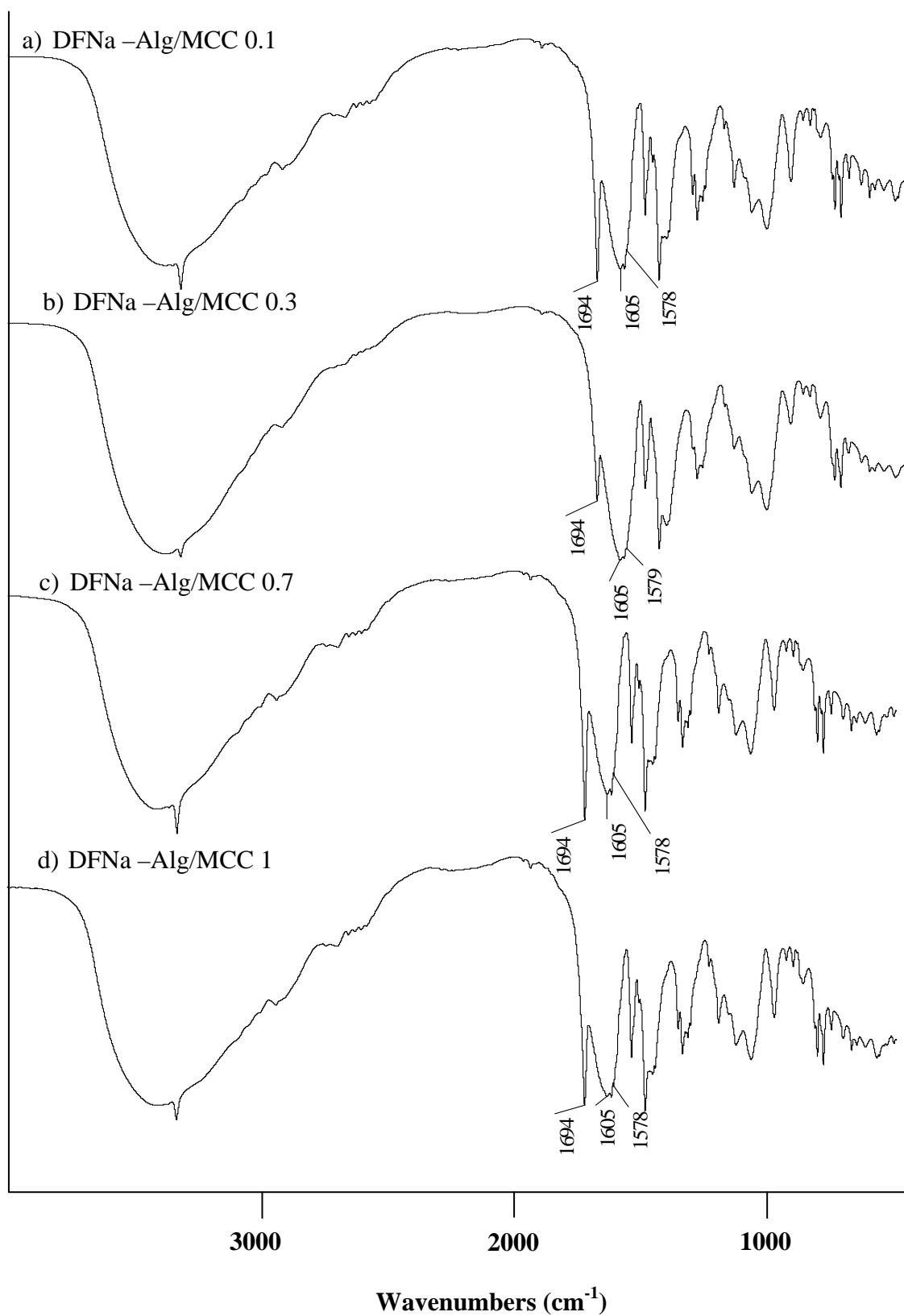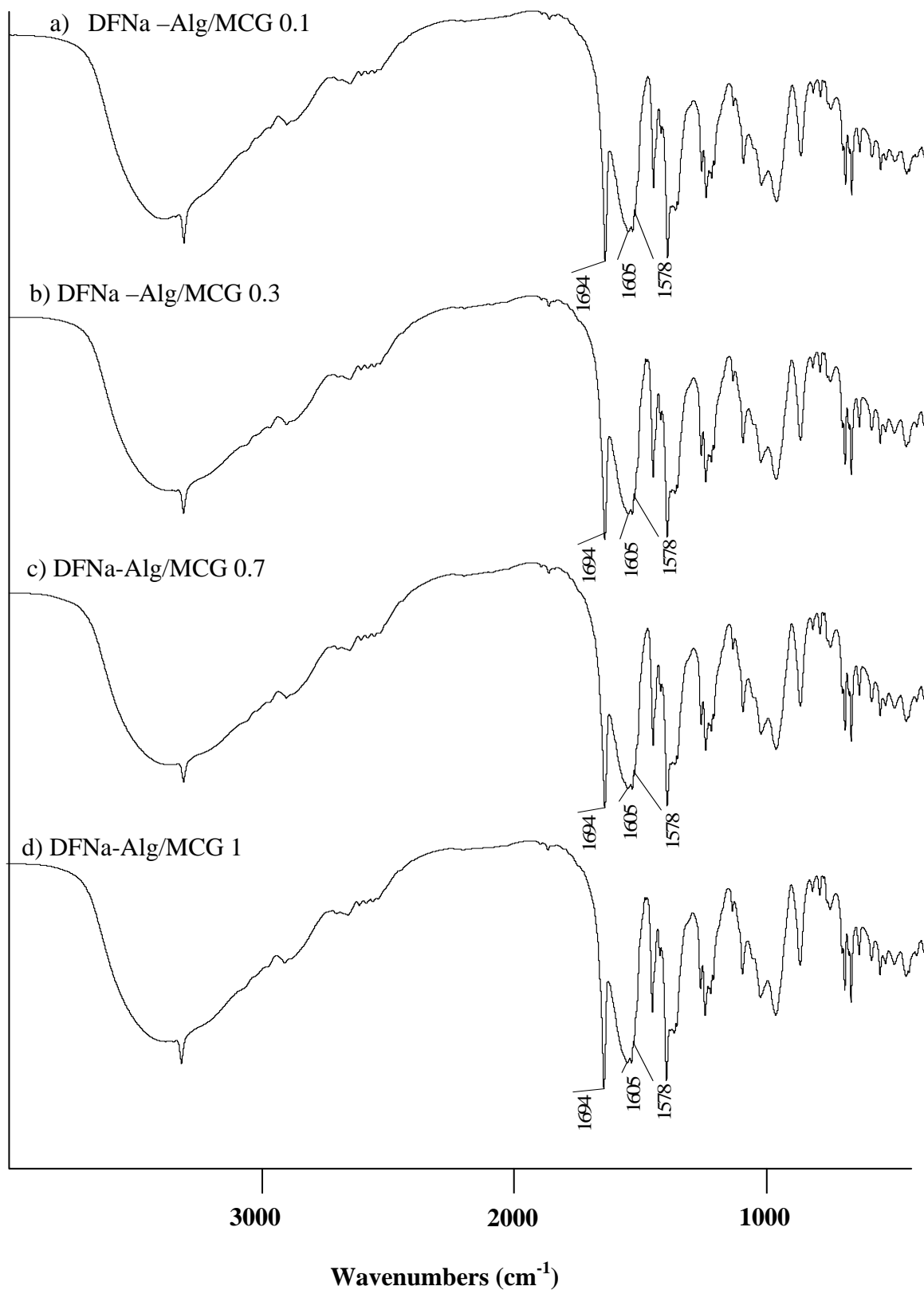
**Figure 4.29** IR spectra of (a) DFNa – Alg/MCG 0.1, (b) DFNa – Alg/MCG 0.3, (c) DFNa – Alg/MCG 0.7, (d) DFNa – Alg/MCG 1

4.4.5 Swelling Analysis

4.4.5.1 Swelling Analysis in the Stimulated Gastric Fluid. (SGF, pH 1.2)

The mechanism of swelling in pH 1.2 are shown in Figure 4.31a. At the pH 1.2, $-NH_2$ unit on chitosan due to conversion into $NH_3^+$. A number of $NH_3^+$ could generate the ionic repulsion and resulted in swelling behavior. But in the case of MCC the reason are similar to as mentioned above 4.3.5.1, the amino group of MCC was lower to be protonated. This causes the less ionic repulsion occurring between $NH_3^+$ groups themselves which reduce the result in swelling ratio

4.4.5.2 Swelling Analysis in the Stimulated Intestinal Fluid. (SIF, pH 7.4)

Figure 4.30 and Table 4.10 are shown the swelling ratios of the beads with various types of MCG in SIF pH 7.4. The mechanism of swelling in pH 7.4 are shown in Figure 4.31b. The beads can swell in pH 7.4 because the $Ca^{2+}$ ions present in polymannuronate units are exchanged with $Na^+$ ions, thus causing the beads to swell along with uptake of water. The swelling behaviors of the beads for all formulations in this dissolution system (phosphate buffer saline pH 7.4) had higher swelling ratio than that of Alg/MCG0.1.

**Table 4.10** Selling ratio of formulation A – B, G – J beads in SIF (pH 7.4)

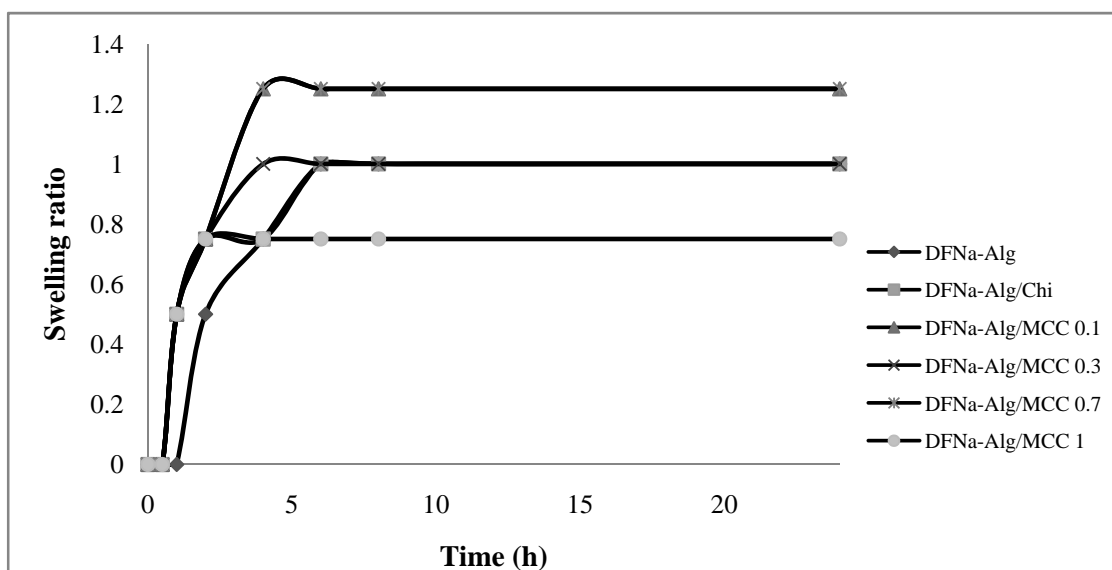| Time (h) | Formulation A | Formulation B | Formulation G | Formulation H | Formulation I | Formulation J |
|---|---|---|---|---|---|---|
| | Pure alg | Pure Chi | MCG0.1 | MCG0.3 | MCG0.7 | MCG1 |
| 0 | 0 | 0 | 0 | 0 | 0 | 0 |
| 0.5 | 0 | 0 | 0 | 0 | 0 | 0 |
| 1 | 0 | 0.50 | 0.25 | 0.25 | 0.25 | 0.25 |
| 2 | 0.50 | 0.75 | 0.50 | 0.50 | 0.50 | 0.75 |
| 4 | 0.75 | 0.75 | 0.50 | 1 | 1 | 1 |
| 6 | 1 | 1 | 0.75 | 1 | 1 | 1 |
| 8 | 1 | 1 | 0.75 | 1 | 1 | 1 |
| 24 | 1 | 1 | 0.75 | 1 | 1 | 1 |
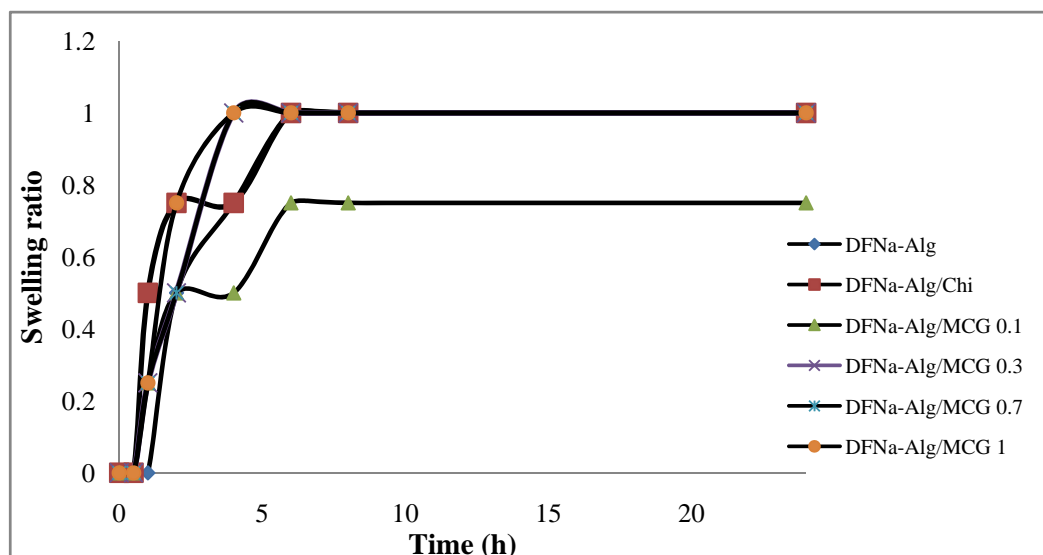
**Figure 4.30** Swelling behavior of various polymer of the DFNa - Alg, DFNa – Alg/Chi, DFNa – Alg/MCG 0.1, DFNa – Alg/MCG 0.3, DFNa – Alg/MCG 0.7, DFNa – Alg/MCG1 in SIF
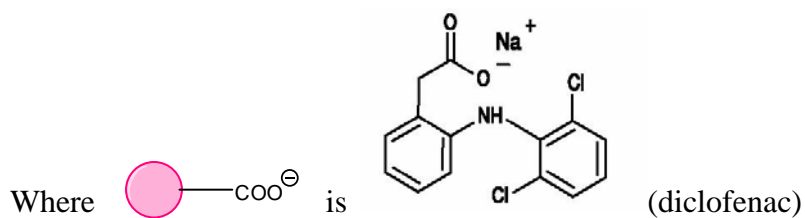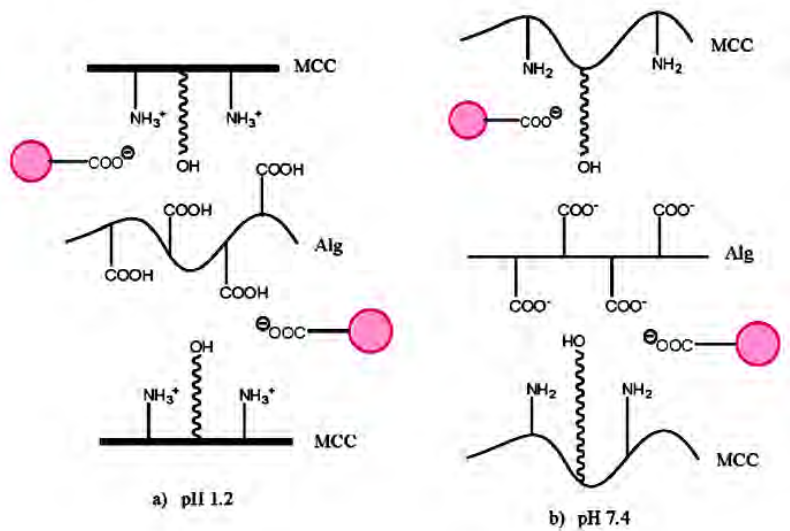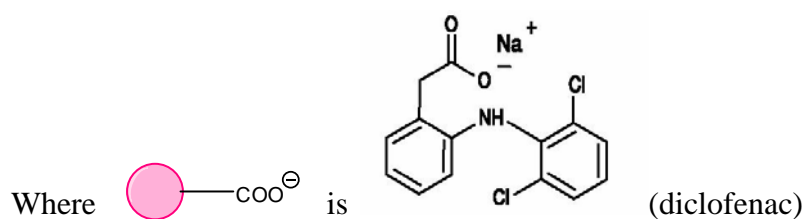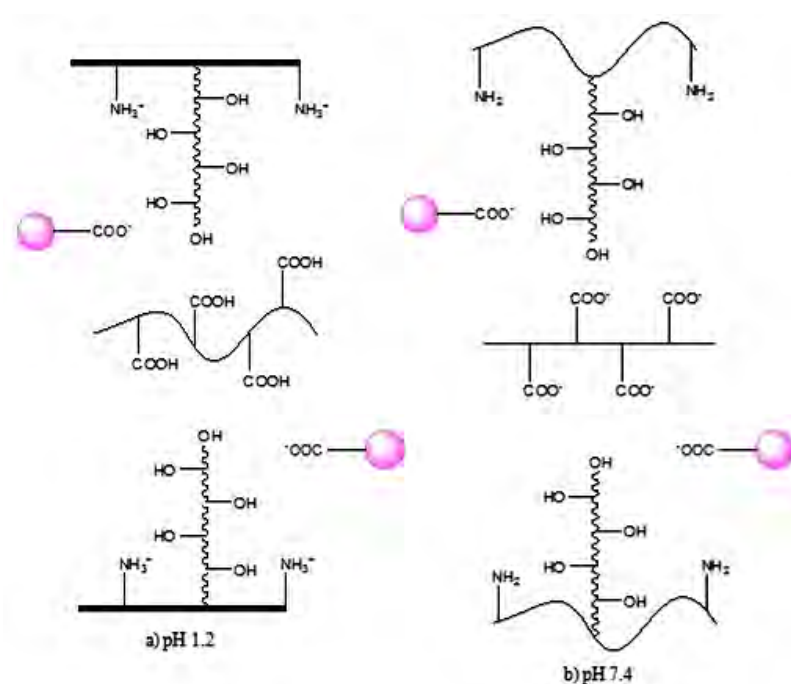


**Figure 4.31** The swelling mechanism of Alg-MCG beads in buffer solution of different pH  a) pH 1.2, b) pH 7.4

4.4.6 In Vitro Release Study

4.4.6.1 Sodium diclofenac release behavior from the beads in SGF

The dissolution and release rates of each formulation are given in Tables D2 – D3 (Appendix D) and Figure 4.32.  The dissolution profiles and release rate profiles are clearly showed that lower 1% of the drug could release from the beads in the acidic condition  within 24 hours. The release profiles in SGF were similar to that of Alg/MCC beads. The results suggest that the Alg/MCG is a pH-sensitive system.
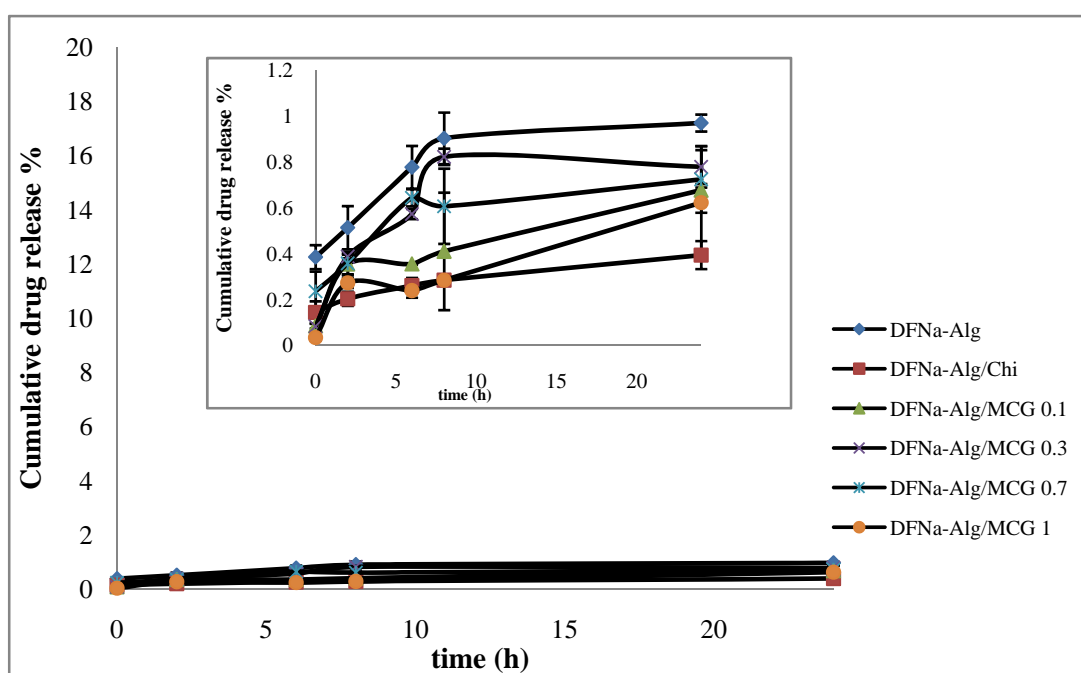


**Figure 4.32** The dissolution profiles of DFNa - Alg, DFNa – Alg/Chi, DFNa – Alg/MCG 0.1, DFNa – Alg/MCG 0.3, DFNa – Alg/MCG 0.7, DFNa – Alg/MCG 1 in SGF

4.4.6.2 Sodium diclofenac release behaviors from the MCG beads in SIF

The dissolution and release rates of each formulation are given in Tables D5 – D6 (Appendix D). Figure 4.33 shows the DFNa release profiles in the phosphate buffer pH 7.4. The release pattern of DFNa from Alg/MCG 0.3 showed the similar trend to that from the pure Alg and Alg/Chi beads. The drug release pattern of formulation Alg/MCC 0.7 was slowest compared to the other formulations. Only 40% of drug can be released from the beads at the 8th hour and then continuously released up to nearly 90% within 24 hours. The release rate of DFNa from Alg/MCG beads depend on the types of MCG.

It can be concluded that the Alg/MCG bead is a pH-sensitive drug delivery system, because this system could effectively control release of drug in the gastrointestinal track. This can be implied that when the beads arrive the stomach, the drug could not be released. When the drug passed the stomach to the intestinal track (pH 7.4). the drug slow and sustained released from the bead within 24 hours.
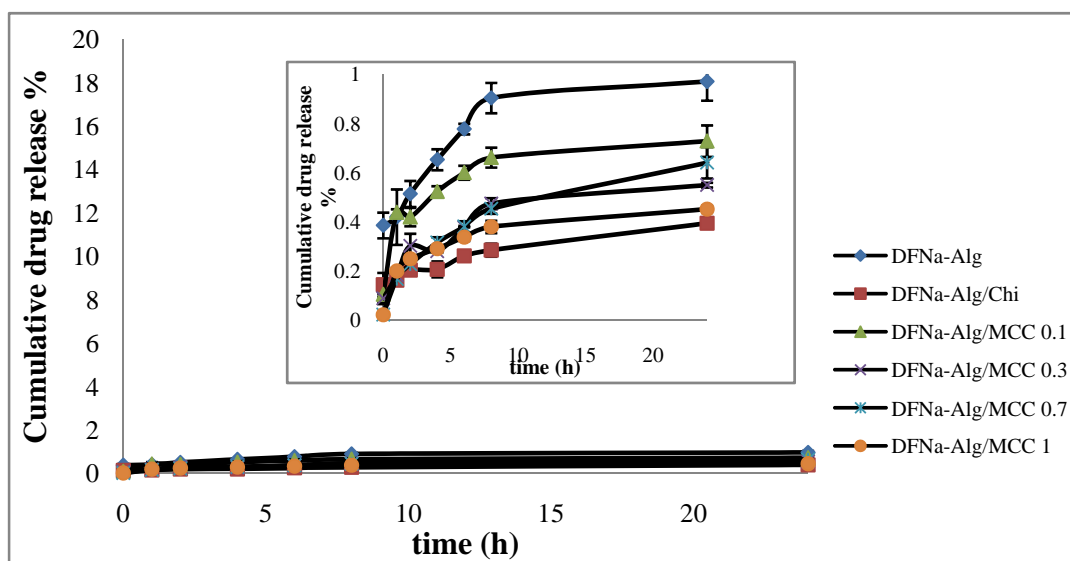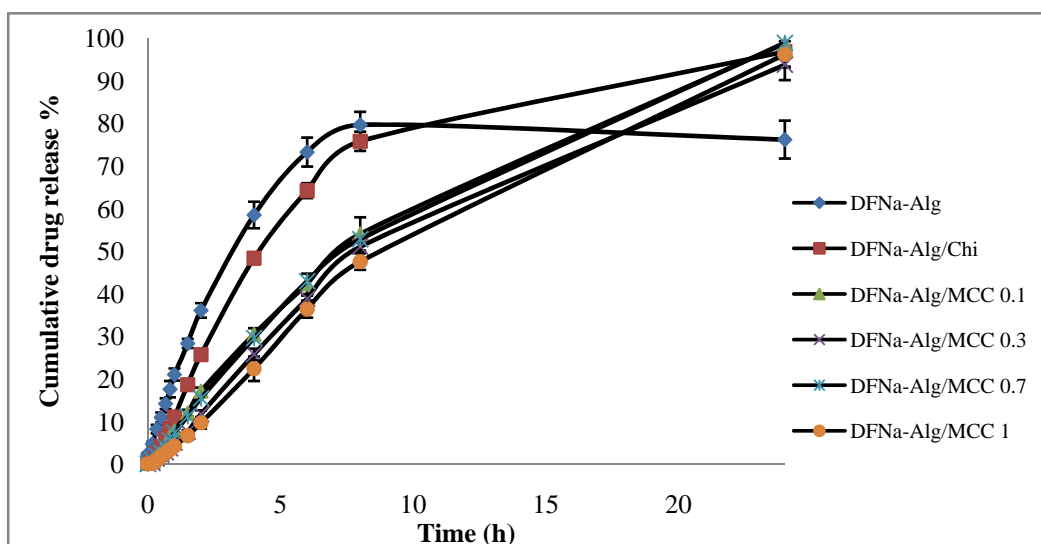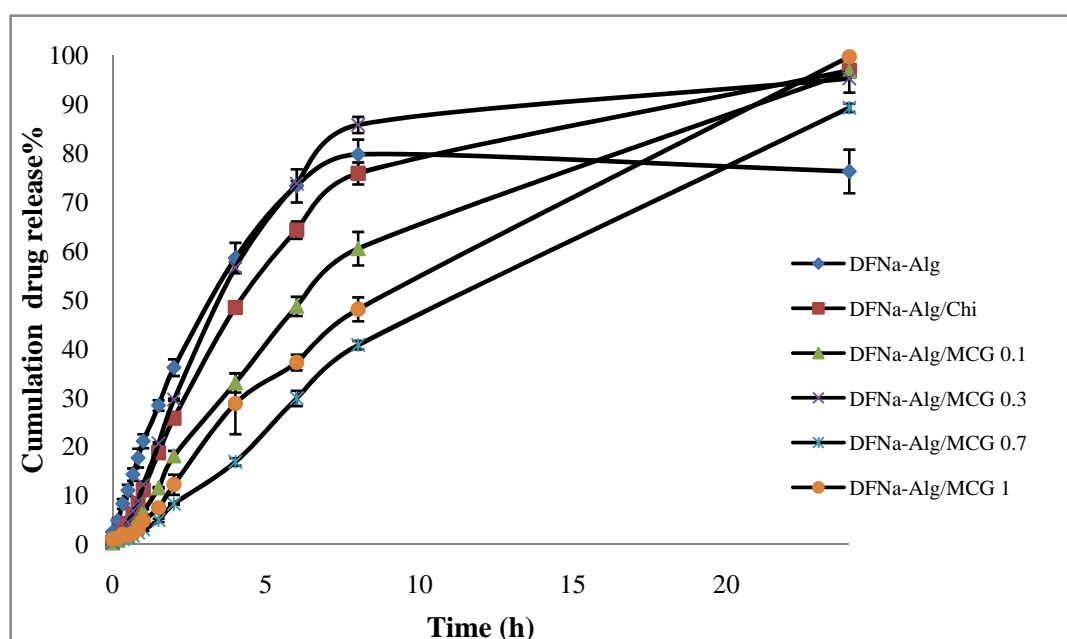


**Figure 4.33** The dissolution profiles of DFNa - Alg, DFNa – Alg/Chi, DFNa – Alg/MCG 0.1, DFNa – Alg/MCG 0.3, DFNa – Alg/MCG 0.7, DFNa – Alg/MCG 1 in SIF

*Pharmaceutical applications of MCC + AMX*

4.5.1 The encapsulation efficiency (%EE) of the AMX – Alg/MCC beads

The percentages of encapsulation efficiency (%EE) of the AMX -Alg/MCC beads prepared from various compositions are shown in Table 4.11.

For AMX loaded pure alginate beads, the %EE is 56.38 ± 0.22. The AMX loaded pure MCC beads was did not form the beads in 4% NaOH coagulant, probably due to the MCC is high water solubility. The Formulation P (MCC 1) gave the lowest %EE at 63.98 ± 3.16% compared to those formulations. Formulation N to O (MCC 0.3 to MCC 0.7) gave the highest encapsulation efficiency over 80%. The reason for the lowest %EE of Formulation P (MCC 1) are similar to as mentioned above 4.3.1, the MCC 1 has the highest water solubility. This result due to AMX loaded MCC 1 beads, the beads were dissolved and drug diffused out from the beads.

**Table 4.11** The encapsulation efficiency (%EE) of the formulated chitosan beads with various compositions.

| Formulations | | Ratio of composition | | | % EE ± SD |
|---|---|---|---|---|---|
| | | DFNa | Alginate | Polymer | |
| K1 | Pure alginate | 1 | 1 | - | 56.38 ± 0.22 |
| K2 | Pure MCC | 1 | - | 1 | *ND |
| L | Chitosan | 1 | 1 | 0.5 | 69.46 ± 1.88 |
| M | MCC0.1 | 1 | 1 | 0.5 | 67.20 ± 6.51 |
| N | MCC0.3 | 1 | 1 | 0.5 | 82.33 ± 0.31 |
| O | MCC0.7 | 1 | 1 | 0.5 | 84.31 ± 0.56 |
| P | MCC1 | 1 | 1 | 0.5 | 63.98 ± 3.16 |

*ND: beads could not be prepared.

4.5.2 Morphology of the AMX – polymer beads

4.5.2.1 Morphology of the AMX – MCC based beads

The surface topography, size and shape of the dried beads were observed by scanning electron microscopy (SEM). The effect of various of chitosan and the five different types of MCC on bead morphology were investigated. The SEM micrographs of the beads are presented in Figure 4.34.

Formulation K (AMX - Alg beads), the surface structure reveals cracks by partial collapsing of the polymer network during dehydration and the shape of all formulations appeared as spherical with the particle size of 1 mm. All formulation had rough exterior and folded inside due to the shrinking after drying process.

The cross-sections, from Figure 4.34 could be used to confirm the homogenicity of AMX and polymer matrix of all formulation beads. In addition, the crystal of drugs could be apparently seen inside the beads for all formulations and can not find crystal of drug outside the beads. The all formulation beads were very dense network inside and tightly packed. Because the ionic interaction between $COO^-$ alginate can from a polyeletrolyte cpx (PEC) with the $NH_3^+$ cationic chitosan or modified chitosan.

The particle sizes of the beads formed by Alg/Chi, Alg/m-Chi were larger than that of the beads formed by pure alginate.
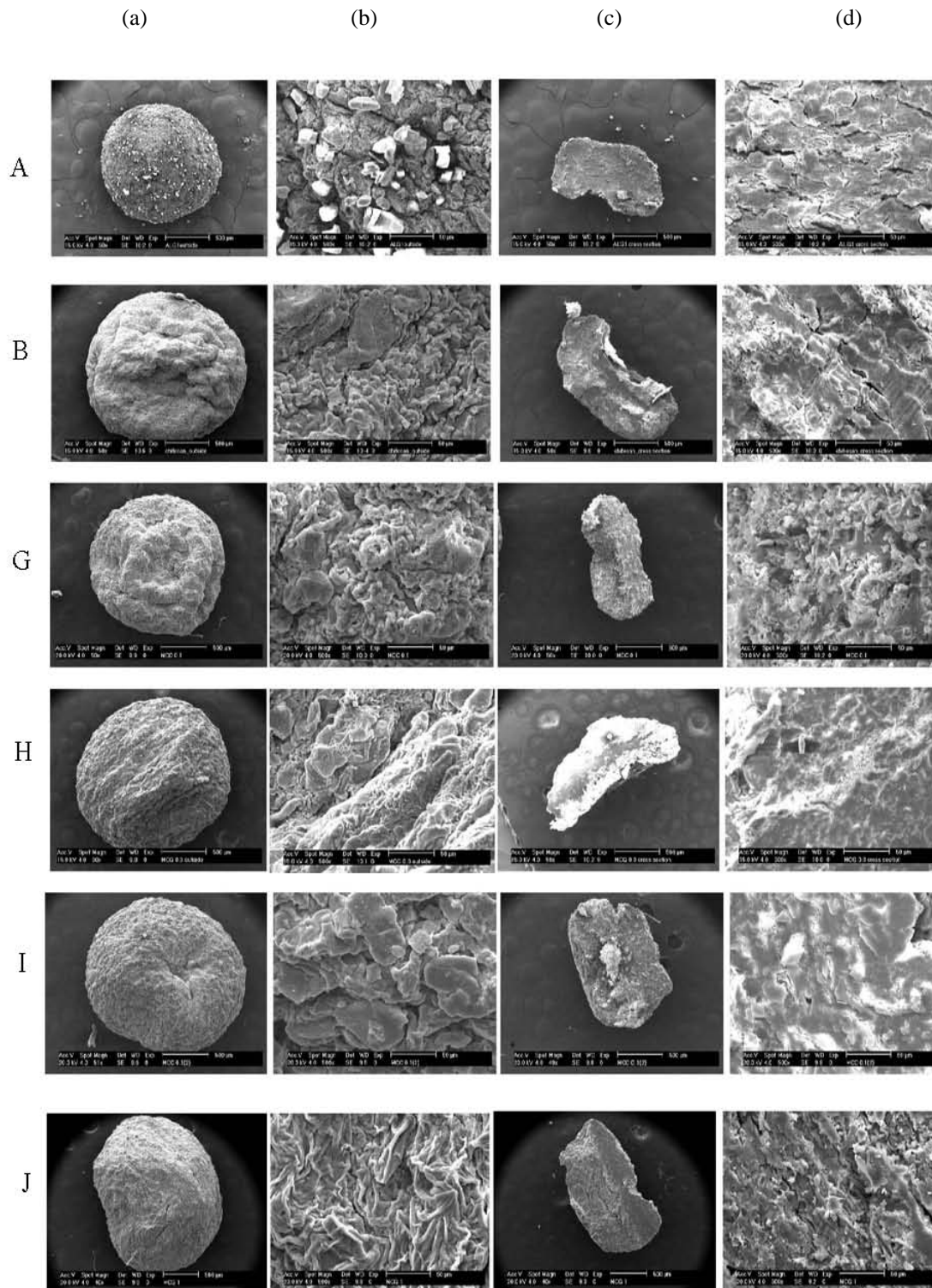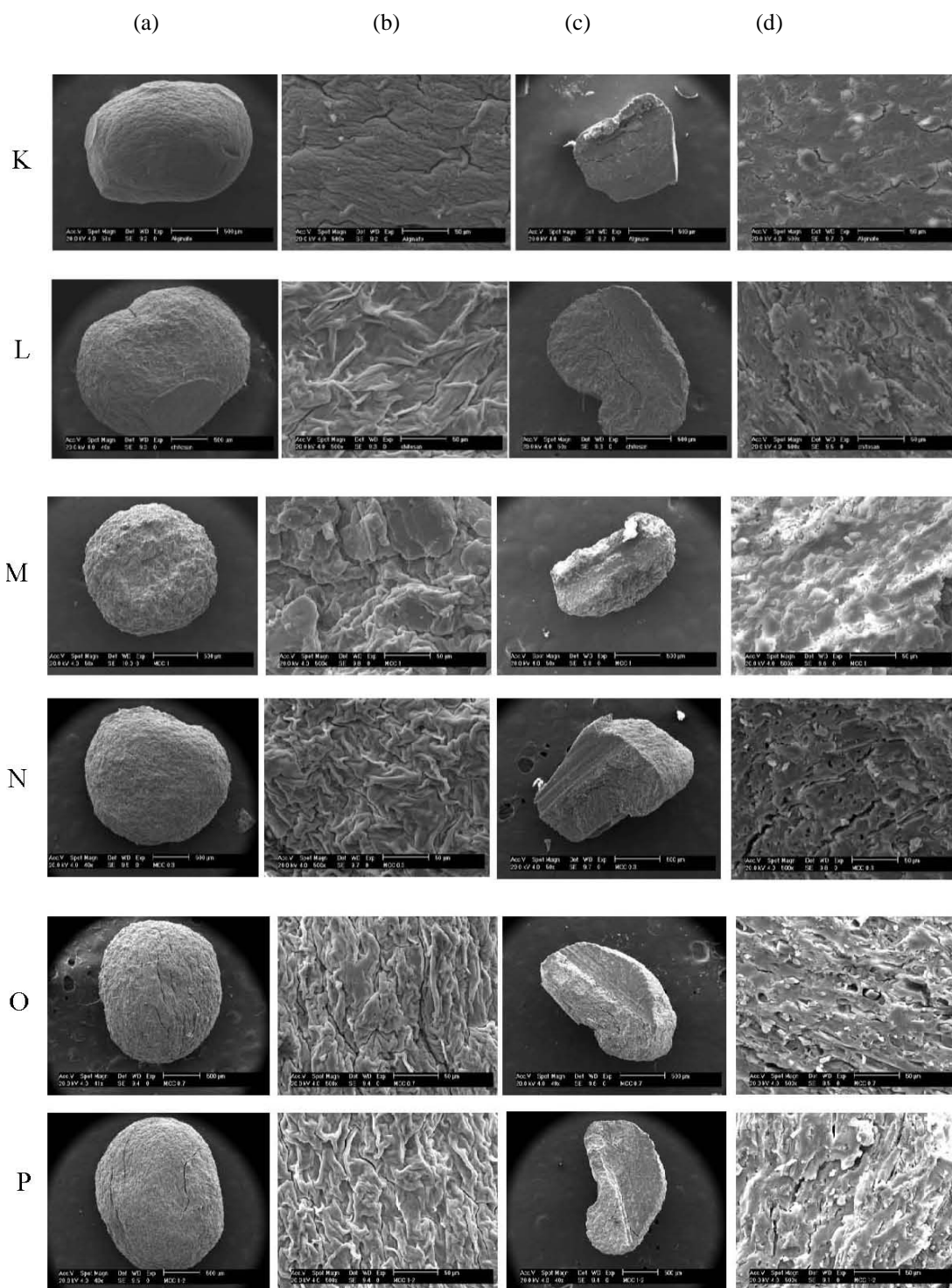
**Figure 4.34** Scanning electron photomicrographs of (a) the beads (x50), (b) surface (x500), (c) cross-section (x50) and (d) network inside bead (x500) of formulation K, L, M, N, O and P, respectively.

4.5.3 DSC thermograms of the AMX – Alg, AMX - Alg/MCC 0.7beads

The DSC thermograms of pure alginate, pure AMX, pure chitosan, the representative of AMX – Alg/MCC 0.7 are shown in Figure 4.35. Because AMX – Alg/MCC 0.7 showed high encapsulation efficiency (%EE).

The thermogram of pure alginate (Figure 4.35a) showed the first endothermic rang from 40°C to 133°C with the peak at 69°C was assigned to evaporation of water. The second small broad endothermic of alginate occurred at temperature 142.7°C was assigned to a dehydration process followed by decomposition of polymer and broad exothermic peak at 250.2°C attributes to the temperature of alginate degradation.

The thermogram of pure AMX (Figure 4.35b) showed the first endothermic peak at 136.2°C was assigned to evaporation of water. The exothermic peak at 176.8°C the fusion of the solvated crystals and degradation of AMX.

The thermogram of chitosan (Figure 4.35c) revealed the endothermic broad peak at 108.6 °C and exothermic peak at about 300°C. The two peaks represent the evaporation of water and the degradation of chitosan, respectively.

The thermogram of MCC 0.7 (Figure 4.35d) exhibited the endothermic peak around 148.10°C, the peak attributes to a degradation of polymer.

The thermogram of AMX – Alg/MCC 0.7 (Figure 4.35e) showed 3 endothermic peaks at 127°C, 166.3°C and 186.2°C attributes to the characteristic peak of Alg, MCC 0.7 and AMX, respectively. These peaks were shifted from the original positions because of the interaction of polymer and drug.
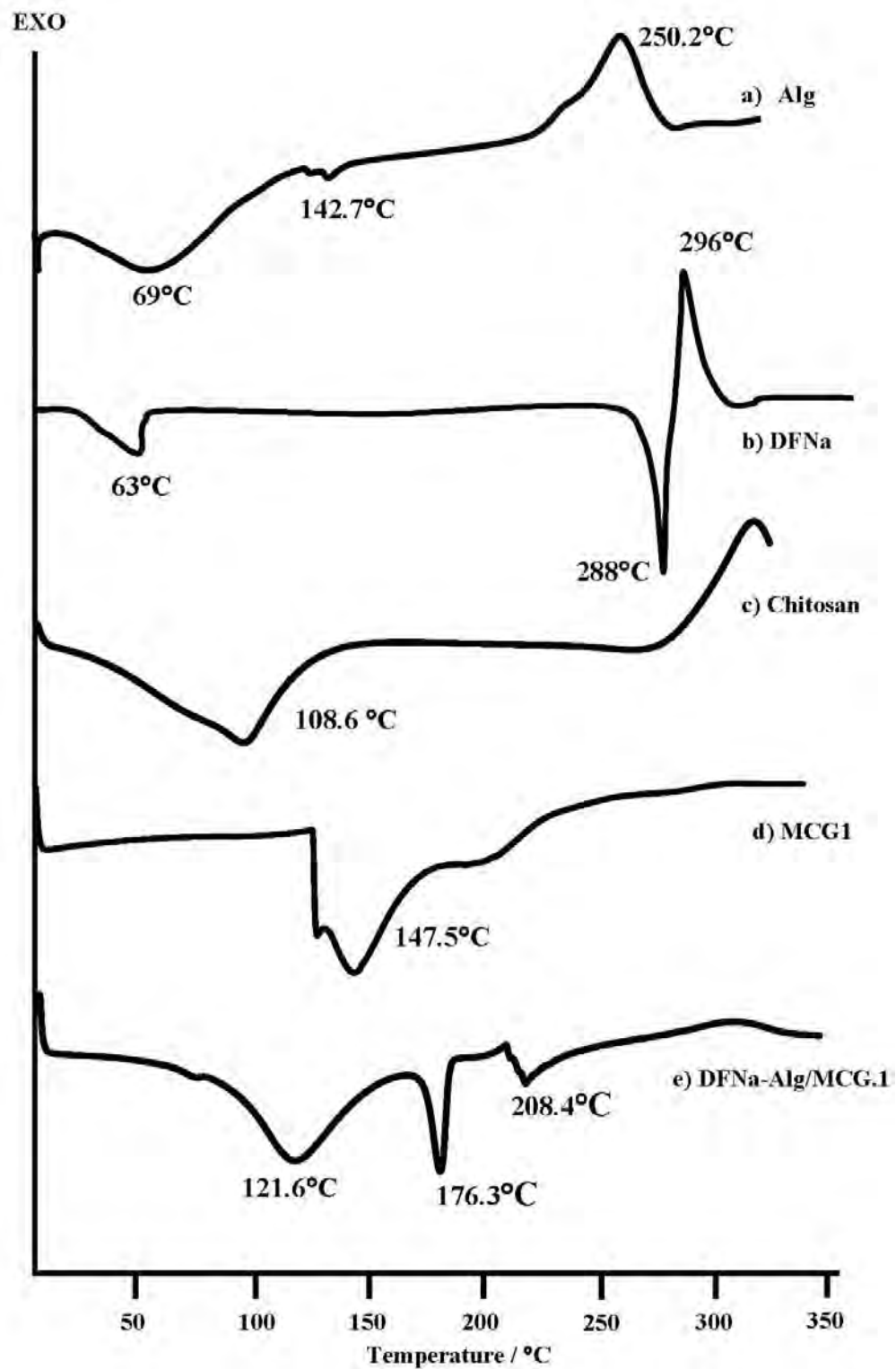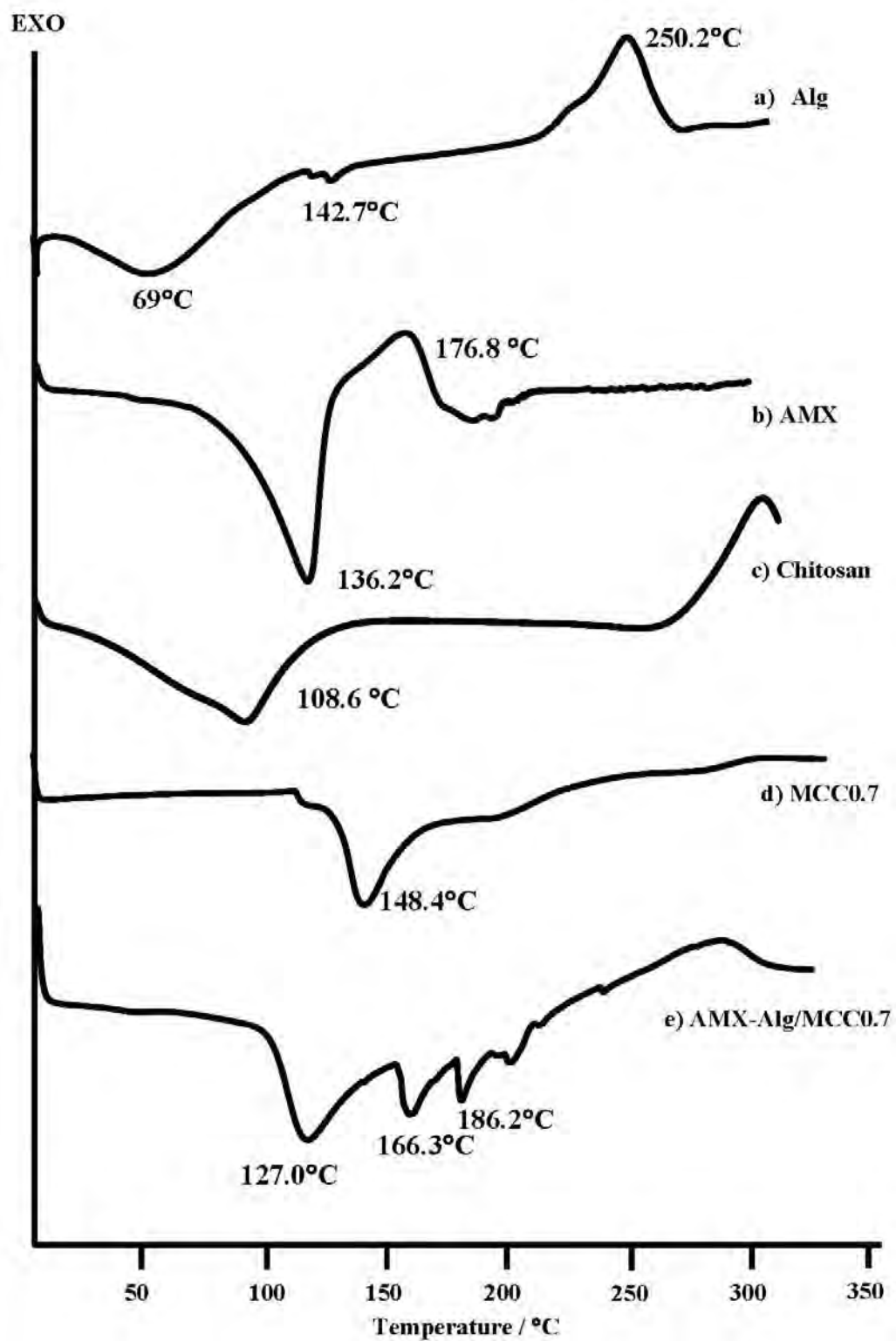
**Figure 4.35** The DSC thermograms of (a) alginate, (b) AMX, (c) chitosan, (d) MCC 0.7, (e) AMX- Alg/MCC 0.7

4.5.4 Infrared Spectroscopy (FT-IR) of the AMX– Alg/MCC beads

FTIR spectroscopy was used to determine the chemical interaction of the samples as displayed in Figures 4.36 to 4.37.

The IR spectrum of pure alginate (Figure 4.36a) showed the characteristic absorption bands at 1618 $cm^{-1}$, 1419 $cm^{-1}$, 1030 $cm^{-1}$ attributed to the asymmetric stretching vibration of C=O, the –$CH_2$ bending and the stretching of C-O-C, respectively.

The IR spectrum of pure AMX (Figure 4.36b) showed the principle bands were observed at 1769, 1678 and 1582 $cm^{-1}$. The band at around 3000 $cm^{-1}$ attribute to O-H, -COOH and N-H stretching vibration. The band at 1775 and 1678 $cm^{-1}$ resulted from C=O stretching of carboxylate group. The IR absorption bands at 1582 $cm^{-1}$ resulted from C=C stretching.

Figure 4.36 (c) showed the IR spectrum of AMX – Alg. The band at around 3418 $cm^{-1}$ attribute to O-H and N-H stretching vibration. The absorption band at 1611 $cm^{-1}$ assigned to the combination peaks from both polymer and drug, while the major peaks of them were not shifted from the original position and there were no new adsorption peaks of drug-loaded alginate beads. Therefore, it could indicate that there were no chemical interactions between the polymer and the drug used.

Figure 4.36 (d) showed the IR spectrum of AMX – Alg/Chi. The characteristic IR bands at 1775 and 1684 $cm^{-1}$ resulted from C=O stretching of carboxylate group. The principle peaks of both polymers and drug were also presented at the same positions and there were no new absorption bands of drug-loaded beads.
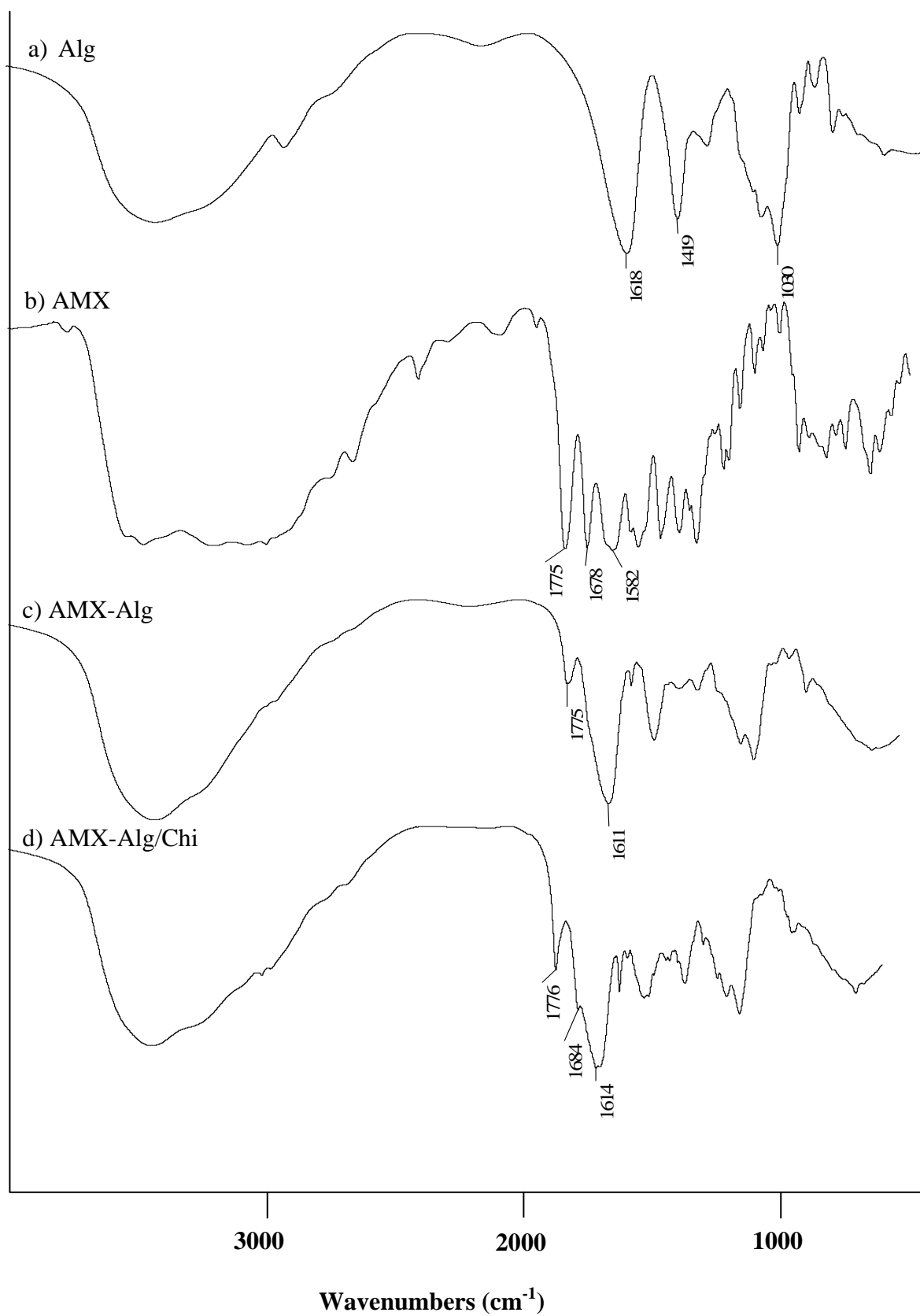
**Figure 4.36** IR spectra of (a) alginate, (b) AMX, (c) AMX – Alg, (d) AMX – Alg/Chi

Figure 4.37 (a) shows the IR spectrum of AMX – Alg/MCC 0.1. The wide absorption band at 3383 cm$^{-1}$, due to the O-H, -COOH and N-H stretching vibration. The band at 1775 cm$^{-1}$ resulted from C=O stretching of carboxylate group. The absorption band at 1613 cm$^{-1}$ assigned to the combination peaks from both polymer and drug. The band at 1416 cm$^{-1}$ assigned to C-O stretching. The absorption band at 1178 cm$^{-1}$ attributed to C-O-C stretching.

Figures 4.37 (b) to 4.37(d) shows the IR spectrum of AMX – Alg/MCC 0.3, AMX – Alg/MCC 0.7 and AMX – Alg/MCC 1, respectively. The wide absorption band around 3400 cm$^{-1}$ was assigned to the stretching vibration of N-H group bonded to –OH group. The band at 1775 and 1687 cm$^{-1}$ resulted from C=O stretching of carboxylate group. The absorption band at 1597 cm$^{-1}$ and 1328 cm$^{-1}$ were assigned to -NH$_2$ bending and C–N stretching vibration of amide group.
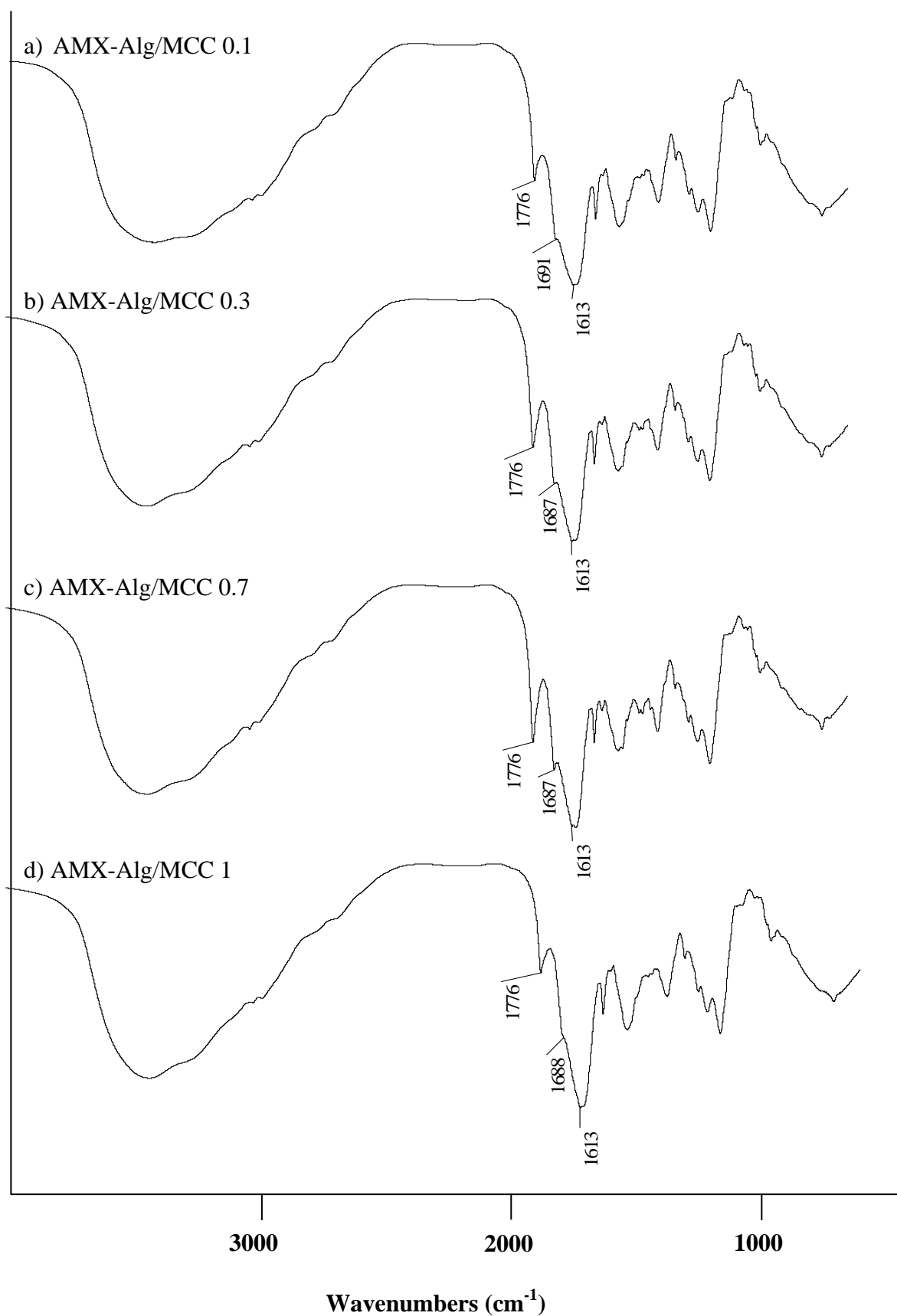
**Figure 4.37** IR spectra of (a) AMX– Alg/MCC 0.1, (b) AMX – Alg/MCC 0.3, (c) AMX – Alg/MCC 0.7, (d) AMX – Alg/MCC1

4.5.5 Swelling Analysis

4.5.5.1 Swelling Analysis in the Stimulated Gastric Fluid. (SGF, pH 1.2)

The swelling behaviors of the AMX – pure Alg beads in this solution system (0.1 N HCl pH 1.2) did not swell. It is due to the complete deletion of calcium from alginate matrices, which are converted to the insoluble alginic acid [46].

The swelling behaviors at the pH 1.2 the beads coated with chitosan and MCCs. The mechanism of swelling involves the protonation of the amino groups on chitosan are shown in Figure 4.40. This protonation leads to chain repulsion, diffusion of proton and counter ions together with water inside the gel.

Figure 4.38 and Table 4.12 are shown the swelling ratios of the beads with various compositions in SGF pH 1.2. The swelling behaviors of the beads for all formulations in this dissolution system (0.1 N HCl pH 1.2) MCC 0.3 showed the highest swelling ratio.

**Table 4.12** Swelling ratio of formulation K - P beads in SGF (pH 1.2)

| Time (h) | Formulation K | Formulation L | Formulation M | Formulation N | Formulation O | Formulation P |
|---|---|---|---|---|---|---|
| | Pure alg | Pure Chi | MCC0.1 | MCC0.3 | MCC0.7 | MCC1 |
| 0 | 0 | 0 | 0 | 0 | 0 | 0 |
| 1 | 0 | 0.20 | 0.50 | 0.33 | 0.00 | 0.25 |
| 1 | 0 | 0.20 | 0.50 | 0.67 | 0.25 | 0.50 |
| 2 | 0 | 0.20 | 0.50 | 0.67 | 0.25 | 0.50 |
| 4 | 0 | 0.20 | 0.50 | 0.67 | 0.25 | 0.50 |
| 6 | 0 | 0.20 | 0.50 | 0.67 | 0.25 | 0.50 |
| 8 | 0 | 0.20 | 0.50 | 1.00 | 0.25 | 0.50 |
| 24 | 0 | 0.20 | 0.50 | 1.00 | 0.25 | 0.50 |
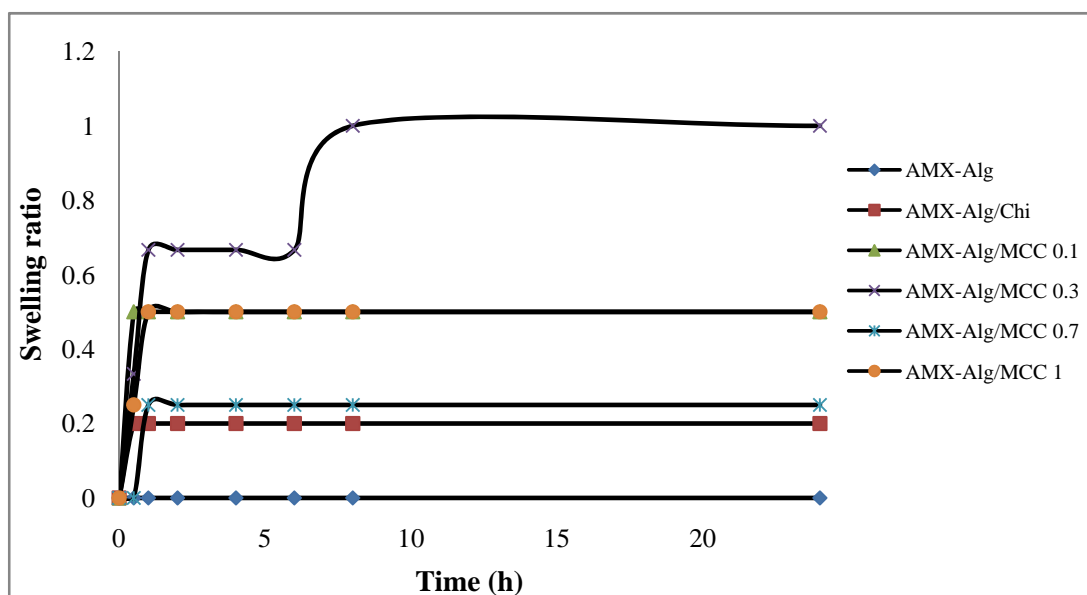
**Figure.4.38** Swelling behavior of various polymer of the AMX - Alg, AMX – Alg/Chi, AMX – Alg/MCC 0.1, AMX – Alg/MCC 0.3, AMX – Alg/MCC 0.7, AMX – Alg/MCC1 in SGF

4.5.5.2 Swelling Analysis in the Stimulated Intestinal Fluid. (SIF, pH 7.4)

The mechanism in this pH 7.4 (Figure 4.40), -COOH group changes into –COO$^-$ group and the hydrogen bonding among –NH$_2$ is little dissociated. Thus, the electrostatic repulsion within the hydrogel beads makes the hydrogel dramatically swell.

Figure 4.39 and Table 4.13 are shown the swelling ratios of the beads with various compositions in SIF pH 7.4. The swelling behaviors of the beads for all formulations in this dissolution system (phosphate buffer saline pH 7.4) MCC 0.3 showed the highest swelling ratio.

**Table 4.13** Swelling ratio of formulation K - P beads in SIF (pH 7.4)

| Time (h) | Formulation K | Formulation L | Formulation M | Formulation N | Formulation O | Formulation P |
|---|---|---|---|---|---|---|
| | Pure alg | Pure Chi | MCC0.1 | MCC0.3 | MCC0.7 | MCC1 |
| 0 | 0 | 0 | 0 | 0 | 0 | 0 |
| 1 | 0.25 | 0.20 | 0.50 | 0.33 | 0 | 0.25 |
| 1 | 0.50 | 0.40 | 1.00 | 0.33 | 0.50 | 0.50 |
| 2 | 1.00 | 1.00 | 1.50 | 0.67 | 1.00 | 1.25 |
| 4 | 1.50 | 1.20 | 1.75 | 1.67 | 1.00 | 1.50 |
| 6 | 1.75 | 1.40 | 1.75 | 2.33 | 1.50 | 1.50 |
| 8 | 1.75 | 1.40 | 1.75 | 2.33 | 1.50 | 1.50 |
| 24 | 1.75 | 1.40 | 2.00 | 2.33 | 1.50 | 1.50 |
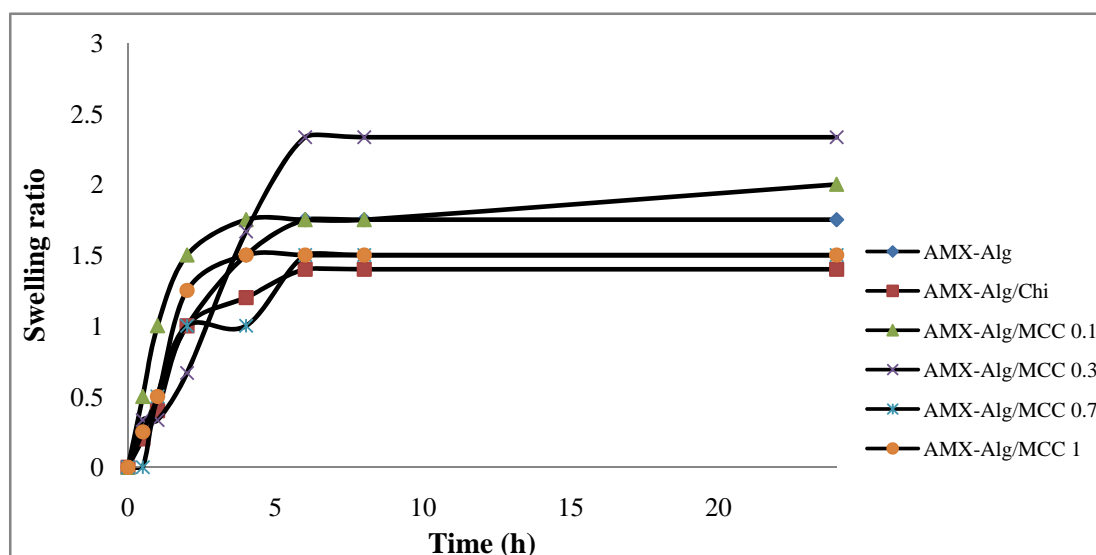


**Figure 4.39** Swelling behavior of various polymer of the AMX - Alg, AMX – Alg/Chi, AMX – Alg/MCC 0.1, AMX – Alg/MCC 0.3, AMX – Alg/MCC 0.7, AMX – Alg/MCC1 in SIF
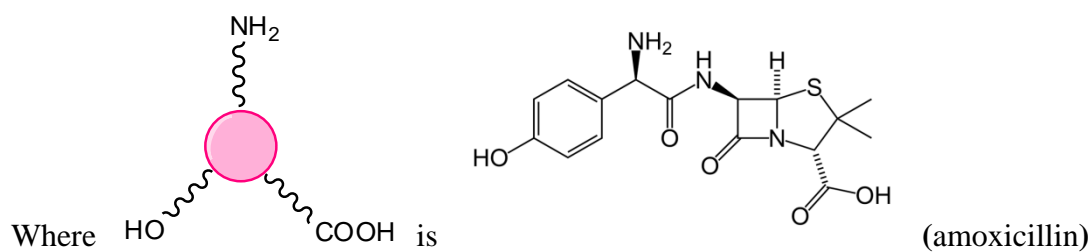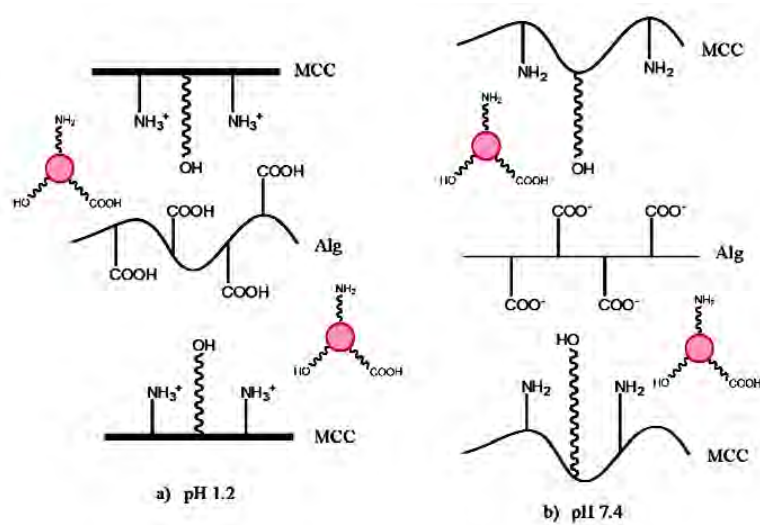
**Figure 4.40** The swelling mechanism of Alg-MCC beads in buffer solution of different pH a) pH 1.2, b) pH 7.4

4.5.6 Inhibition of the AMX – Alg/MCC beads against *E. coli* and *S. aureus* bacteria.

Inhibition of the AMX – Alg/MCC beads against *E. coli* (Gram-negative) and *S. aureus* (Gram-positive) bacteria by agar diffusion method were shown in Figures 4.41 – 4.42 and Table 4.14.
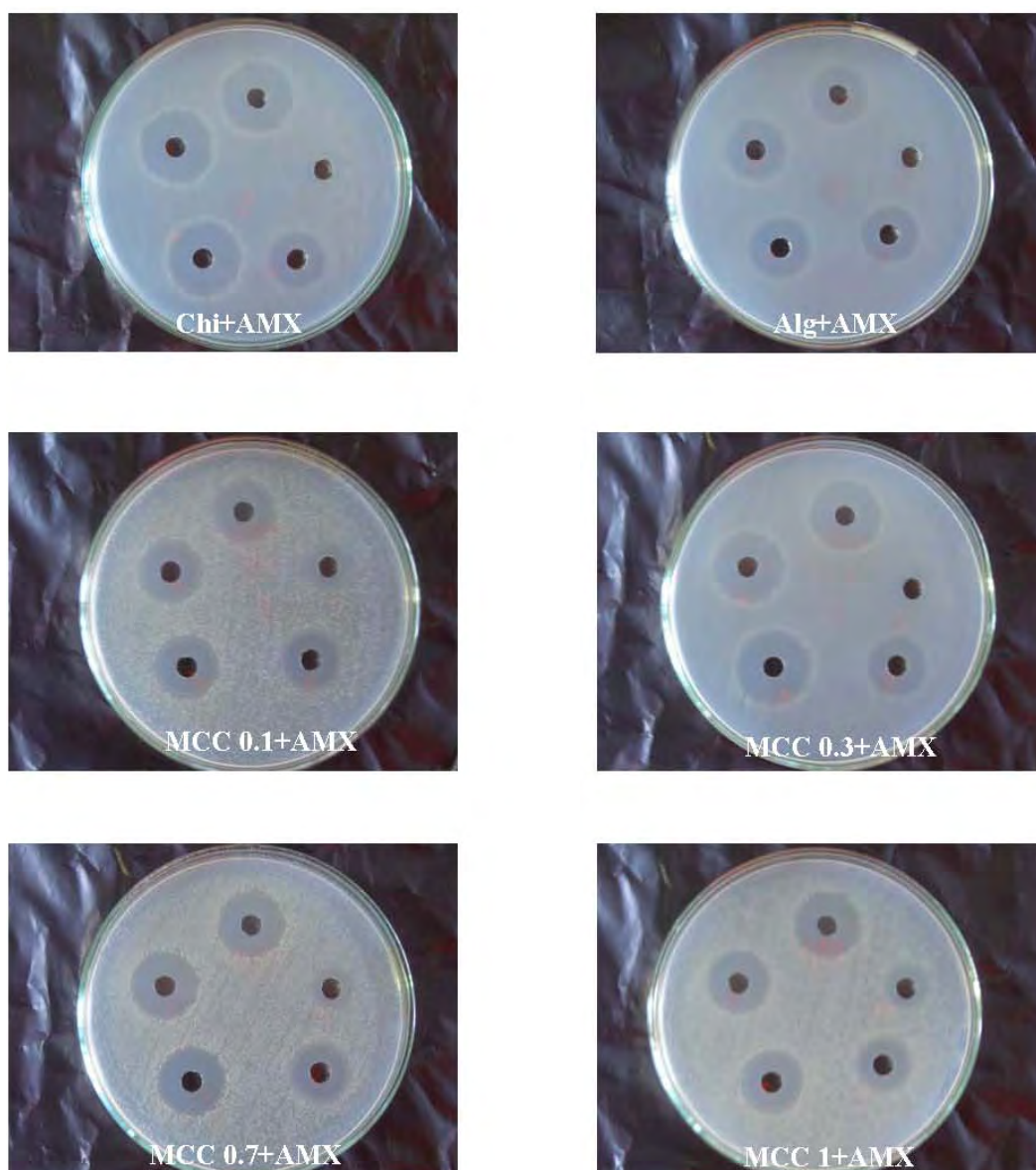


**Figure 4.41** Inhibition clear zones of amoxicillin release from the AMX – Alg/MCC beads at 2 hour against *E. coli*
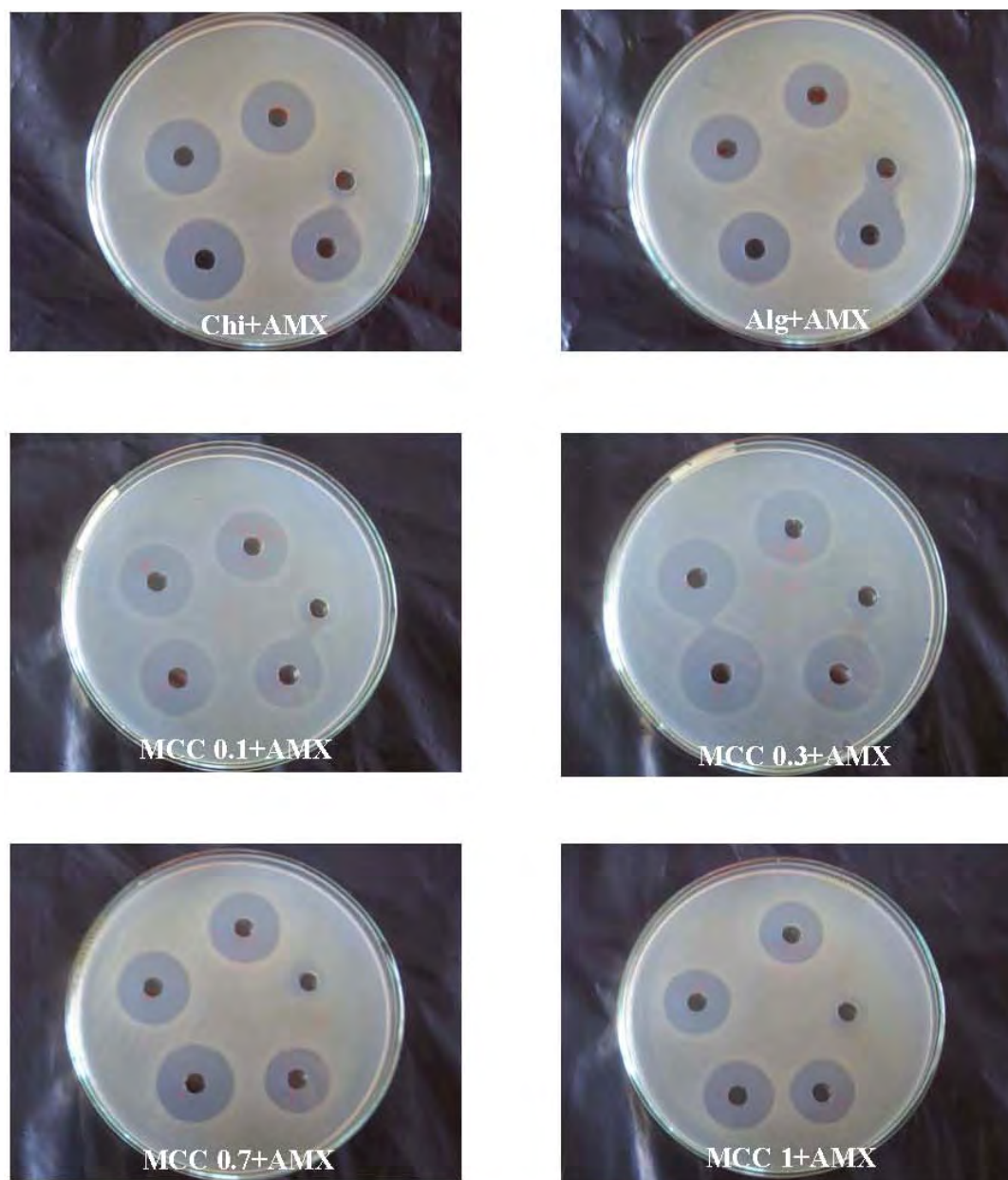
**Figure 4.42** Inhibition clear zones of amoxicillin release from the AMX – Alg/MCC beads at 2 hour against *S. aureus*

**Table 4.14** Diameters of the wall from the inhibition of the AMX-Alg/MCC beads against bacteria

| Formulation | *E .coli* | % Inhibition | *S. aureus* | % Inhibition |
|---|---|---|---|---|
| Control (AMX 50 ppm) | $1.50 \pm 0.00$ | - | $1.90 \pm 0.00$ | - |
| Control (1% lactic acid) | $1.00 \pm 0.00$ | - | $1.00 \pm 0.00$ | - |
| AMX-Alg | $1.70 \pm 0.00$ | 13.33 | $1.87 \pm 0.06$ | 0 |
| AMX-Alg/Chi | $2.10 \pm 0.00$ | 40.00 | $2.08 \pm 0.03$ | 9.65 |
| AMX-Alg/MCC 0.1 | $1.77 \pm 0.06$ | 17.78 | $2.10 \pm 0.00$ | 10.53 |
| AMX-Alg/MCC 0.3 | $2.03 \pm 0.06$ | 35.56 | $2.30 \pm 0.10$ | 21.05 |
| AMX-Alg/MCC 0.7 | $1.90 \pm 0.00$ | 26.67 | $2.13 \pm 0.06$ | 12.28 |
| AMX-Alg/MCC 1 | $1.87 \pm 0.06$ | 24.44 | $2.00 \pm 0.00$ | 5.26 |

1% Lactic acid as a control can not inhibit both *E. coli* and *S. aureus*. The AMX-Alg/Chi can inhibit both *E. coli* and *S .aureus* with the inhibition zone of 2.10 and 2.08 cm, respectively. Therefore, the AMX-Alg/Chi showed the stronger inhibition against *E. coli* than that of the AMX-Alg/MCC and the AMX-Alg/MCC 0.3 showed the stronger inhibition against *S. aureus* than that of the AMX-Alg/Chi.

4.5.7 In Vitro Release Study

4.5.7.1 Amoxicillin trihydrate release behavior from the beads in SGF

The dissolution profiles of AMX can be described as graphs to explain and understand the drug released behavior from the beads.

In SGF, the dissolution and release rate data of each formulation are given in Tables D7 – D8 (Appendix D). These dissolution profiles and release rate profiles are shown in Figure 4.43. In the acidic condition, the release rate was significantly reduce by 70% in 4 hour. It is because the chitosan layer could moderately prevent the drug to leak out. The percentage of AMX release within 24 hours of Formulation L showed significant higher release 100% and Formulation M – P had no significant effect on the drug release (89.72%, 91.59%, 94.43% and 90.38%, respectively).
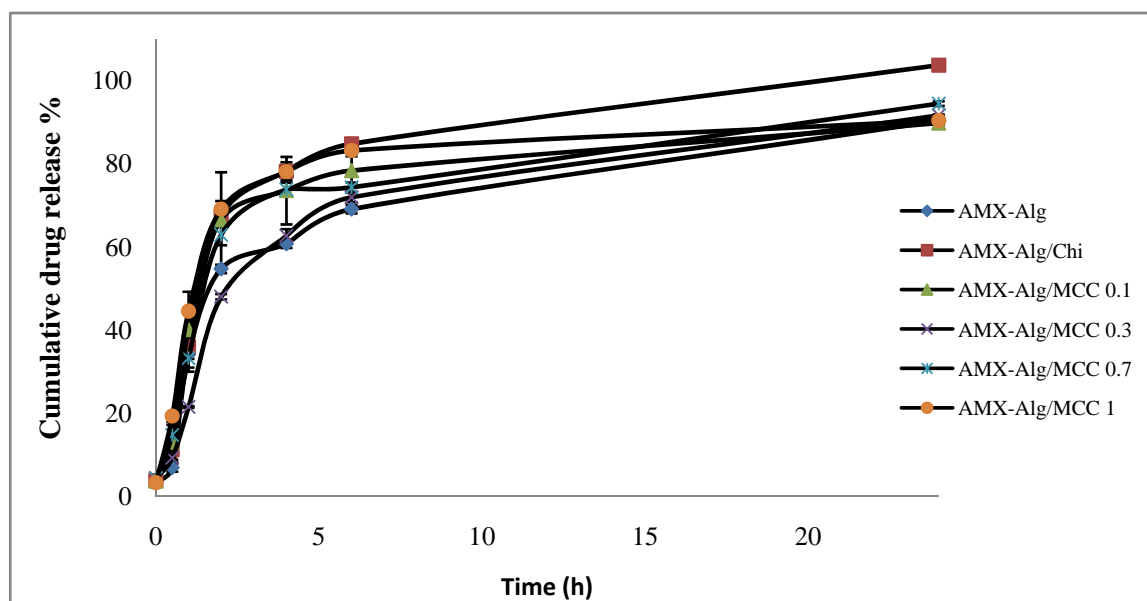


**Figure 4.43** The dissolution profiles of AMX - Alg, AMX – Alg/Chi, AMX – Alg/MCC 0.1, AMX – Alg/MCC 0.3, AMX – Alg/MCC 0.7, AMX – Alg/MCC1 in SGF

4.5.7.2 Amoxicillin trihydrate release behavior from the beads in SIF

The dissolution and release rate data of each formulation are given in Tables D10 – D11 (Appendix D). These dissolution profiles and release rate profiles are shown in Figure 4.44, in the phosphate buffer pH 7.4, the amounts of AMX released increased as compared to those released at pH 1.2. This fact can be attributed to that the swelling of the hydrogel network increased considerably due to ionization of carboxylic groups in the beads at neutral pH. The results showed that there was no significant difference among those formulations. At the interval of 6 hour, 99.67% of AMX from the AMX – Alg beads were released, while the release from AMX – Alg/Chi, AMX – Alg/MCC 0.1, AMX – Alg/MCC 0.3, AMX – Alg/MCC 0.7 and AMX – Alg/MCC 1 were 99.03%, 94.89%, 99.75%, 99.99% and 99.20%, respectively.
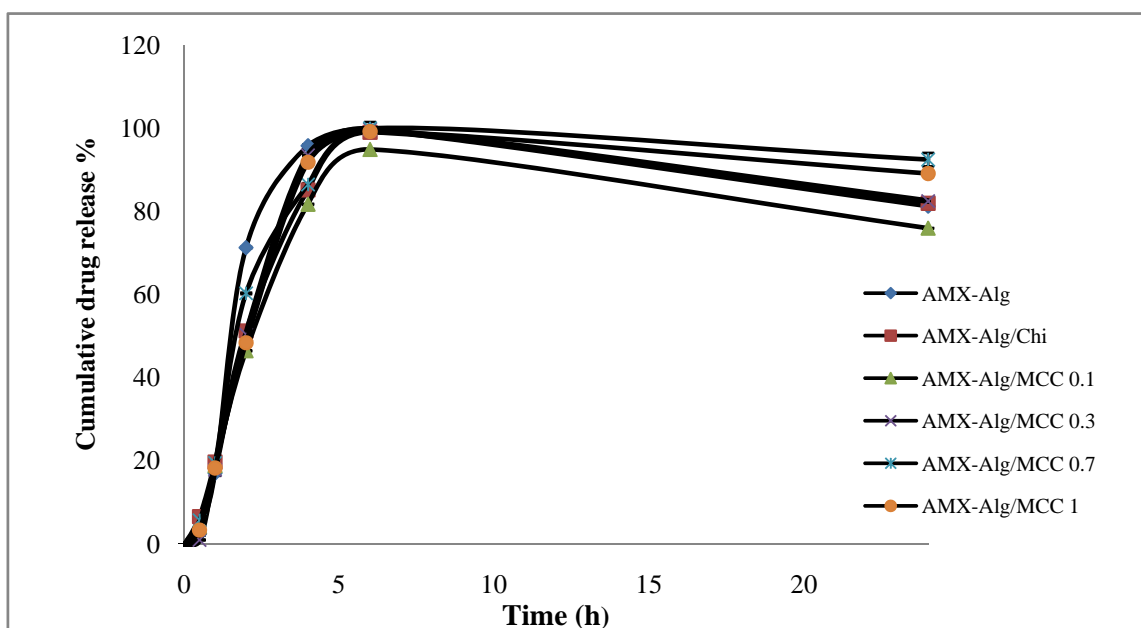


**Figure 4.44** The dissolution profiles of AMX - Alg, AMX – Alg/Chi, AMX – Alg/MCC 0.1, AMX – Alg/MCC 0.3, AMX – Alg/MCC 0.7, AMX – Alg/MCC1 in SIF

*Pharmaceutical applications of MCG + AMX*

4.6.1 The encapsulation efficiency (%EE) of the AMX – Alg/MCG beads

The percentages of encapsulation efficiency (%EE) of the AMX -Alg/MCG beads prepared from various compositions are shown in Table 4.15.

The Formulation K (AMX-Alg), showed the %EE is $56.38 \pm 0.22$. The AMX loaded pure MCG beads was not successfully fabricate, probably due to the MCG is high water solubility. It could not form the beads in 4% NaOH coagulant. Formulation Q, R and T (MCG 0.1, MCG 0.3 and MCG 1) showed high encapsulation efficiency over 80%. This is caused by ionic interactions between carboxylate groups in the alginate and the protonated amine groups in the MCG.

**Table 4.15** The encapsulation efficiency (%EE) of the formulated chitosan beads with various compositions.

| Formulations | | Ratio of composition | | | % EE $\pm$ SD |
|---|---|---|---|---|---|
| | | DFNa | Alginate | Polymer | |
| K1 | Pure alginate | 1 | 1 | - | $56.38 \pm 0.22$ |
| K2 | Pure MCC | 1 | - | 1 | *ND |
| L | Chitosan | 1 | 1 | 0.5 | $69.46 \pm 1.88$ |
| Q | MCG0.1 | 1 | 1 | 0.5 | $81.08 \pm 2.89$ |
| R | MCG0.3 | 1 | 1 | 0.5 | $86.35 \pm 1.23$ |
| S | MCG0.7 | 1 | 1 | 0.5 | $64.84 \pm 1.69$ |
| T | MCG1 | 1 | 1 | 0.5 | $84.53 \pm 0.55$ |

*ND: beads could not be prepared.

4.6.2 Morphology of the AMX – Alg/MCG beads

The surface topography, size and shape of the dried beads were observed by scanning electron microscopy (SEM). The effect of various of chitosan and the five different types of MCG on bead morphology were investigated. The SEM micrographs of the beads are presented in Figure 4.45.

The shape of all formulations appeared as spherical with the particle size of 1 mm. The surface for all formulations had leading to corrugation because of the dehydration of the chitosan membrane surrounding the beads.

Figure 4.45d are shown the cross-sections of all formulation beads, at the inner of the beads the crystal of drugs could be apparently seen inside and presented the dense, strong network and tightly packed. As the results, $COO^-$ of Alg could form the electrolyte complex with the $NH_3^+$ of chitosan or modified chitosan.

The particle sizes of the beads formed by Alg/Chi, Ag/m-Chi were larger than that of the beads formed by pure alginate.
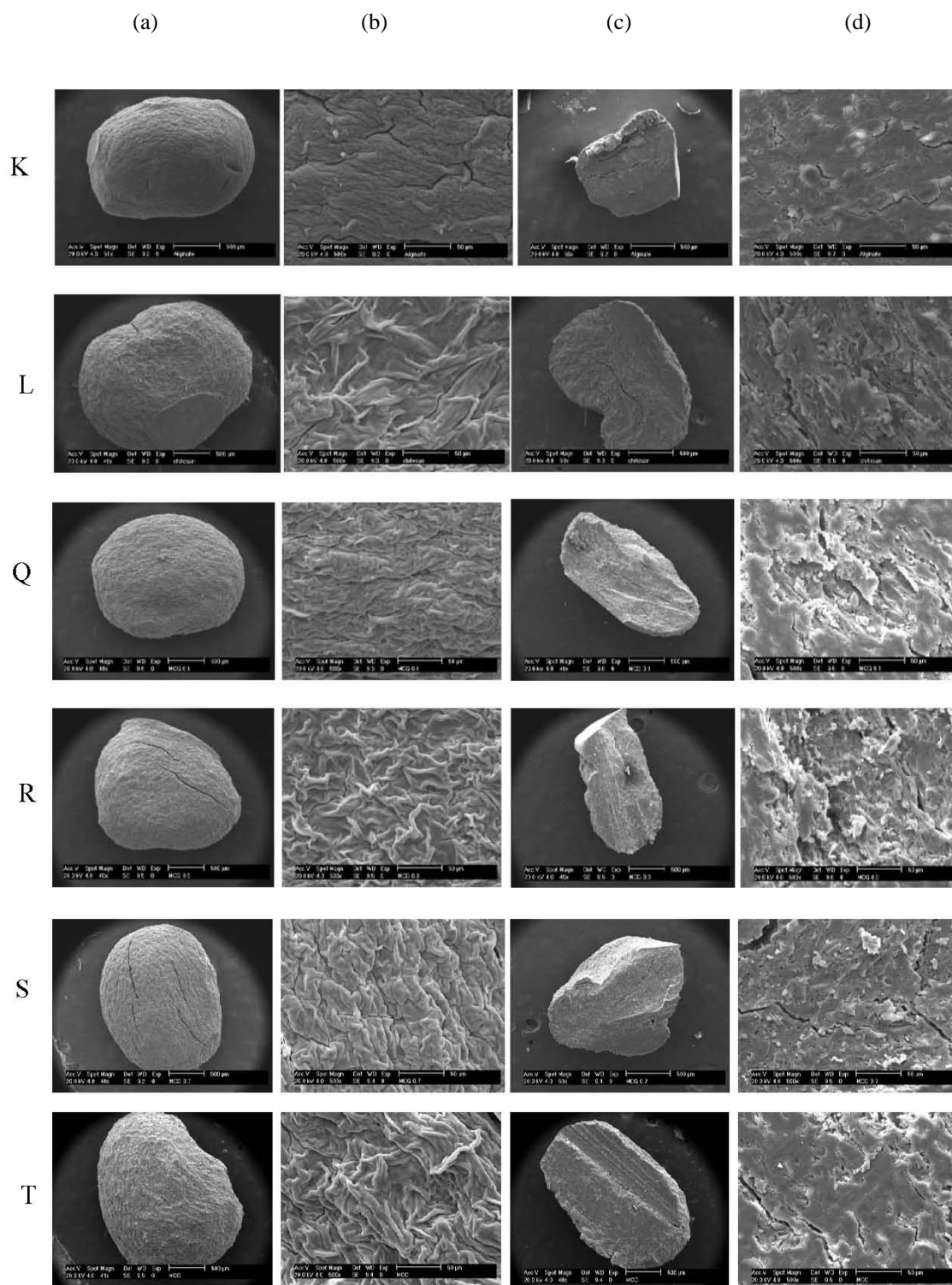
**Figure 4.45** Scanning electron photomicrographs of (a) the beads (x50), (b) surface (x500), (c) cross-section (x50) and (d) network inside bead (x500) of formulation K, L, Q, R, S and T, respectively.

4.6.3 DSC thermograms of the AMX – Alg, AMX - Alg/MCG 0.3beads

The DSC thermograms of pure alginate, pure AMX, pure chitosan and the representative of AMX – Alg/MCG (AMX – Alg/MCG 0.3) are shown in Figure 4.46. In this case, the AMX – Alg/MCG 0.3 formulation was selected as a representative of AMX loaded Alg/MCG beads because it showed the highest encapsulation efficiency (%EE).

The DSC thermogram of pure alginate, DFNa, chitosan (Figures 4.46a to 4.46c, respectively) were similar described in section above 4.5.3.

The thermogram of MCG 0.3 (Figure 4.46d) exhibited the endothermic peak around 160.1°C, the peak attributes to a degradation of polymer.

The thermogram of AMX – Alg/MCG 0.3 showed 3 endothermic peaks (Figure 4.46e) at 124.7°C, 169.4°C and 209.7°C attributes to the characteristic peak of Alg, MCG 0.3 and AMX, respectively. These peaks were shifted from the original positions because of the interaction of polymer and drug.
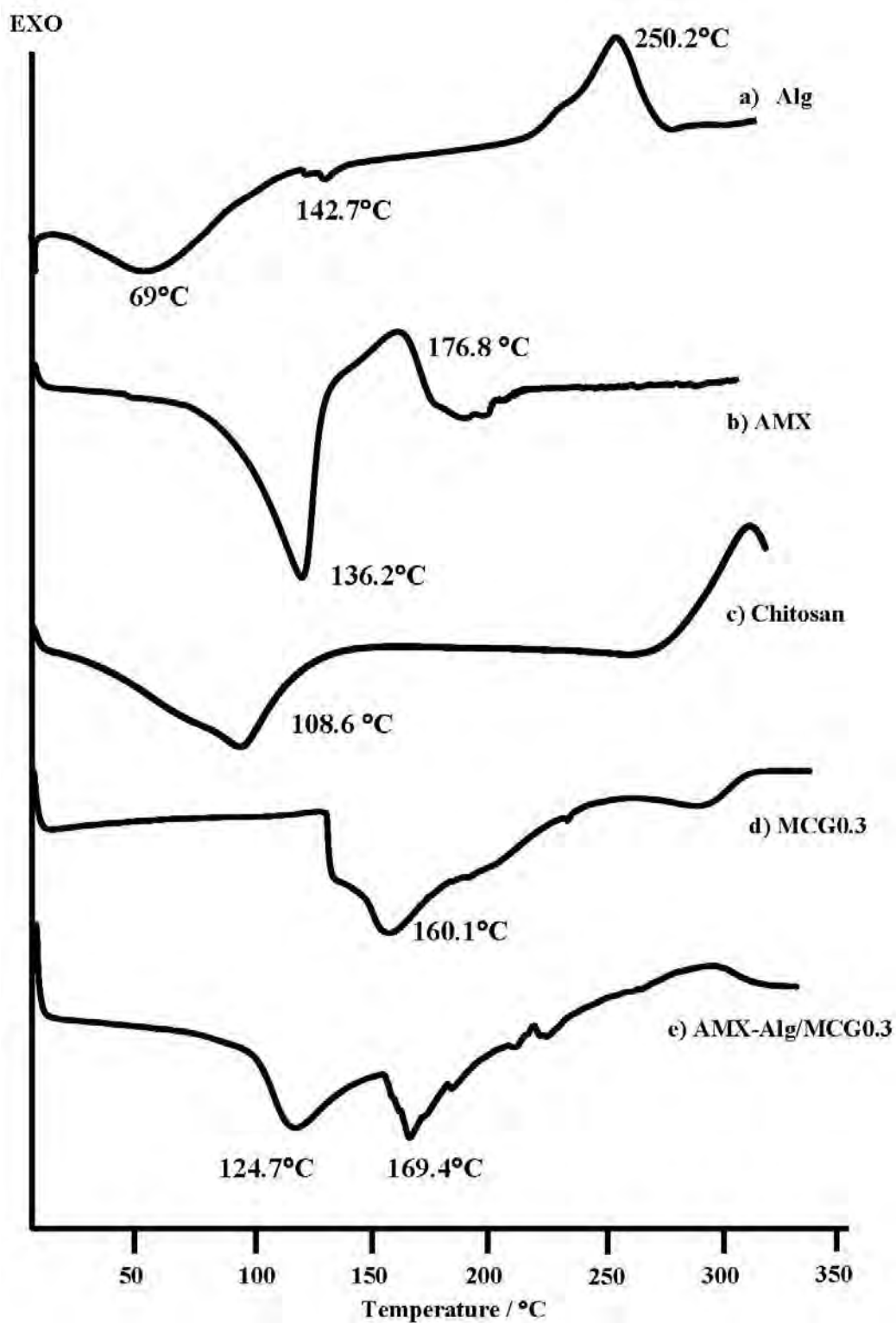
**Figure 4.46** The DSC thermograms of (a) alginate, (b) AMX, (c) chitosan, (d) MCG 0.3, (e) AMX- Alg/MCG 0.3

4.6.**4** Infrared Spectroscopy (FT-IR) of the AMX – Alg/MCG beads

FTIR spectroscopy was used to determine the chemical interaction of the samples as displayed in Figures 4.47 to 4.48.

The IR spectrum of pure alginate (Figure 4.47a) showed the characteristic absorption bands at 1618 $cm^{-1}$, 1419 $cm^{-1}$, 1030 $cm^{-1}$ attributed to the asymmetric stretching vibration of C=O, the –$CH_2$ bending and the stretching of C-O-C, respectively.

The IR spectrum of pure AMX (Figure 4.47b) showed the principle bands were observed at 1769, 1678 and 1582 $cm^{-1}$. The band at around 3000 $cm^{-1}$ attribute to O-H, -COOH and N-H stretching vibration. The band at 1775 and 1678 $cm^{-1}$ resulted from C=O stretching of carboxylate group. The IR absorption bands at 1582 $cm^{-1}$ resulted from C=C stretching.

Figure 4.47 (c) showed the IR spectrum of AMX – Alg. The band at around 3418 $cm^{-1}$ attribute to O-H and N-H stretching vibration. The absorption band at 1611 $cm^{-1}$ assigned to the combination peaks from both polymer and drug, while the major peaks of them were not shifted from the original position and there were no new adsorption peaks of drug-loaded alginate beads. Therefore, it could indicate that there were no chemical interactions between the polymer and the drug used.

Figure 4.47 (d) showed the IR spectrum of AMX – Alg/Chi. The characteristic IR bands at 1775 and 1684 $cm^{-1}$ resulted from C=O stretching of carboxylate group. The principle peaks of both polymers and drug were also presented at the same positions and there were no new absorption bands of drug-loaded beads.
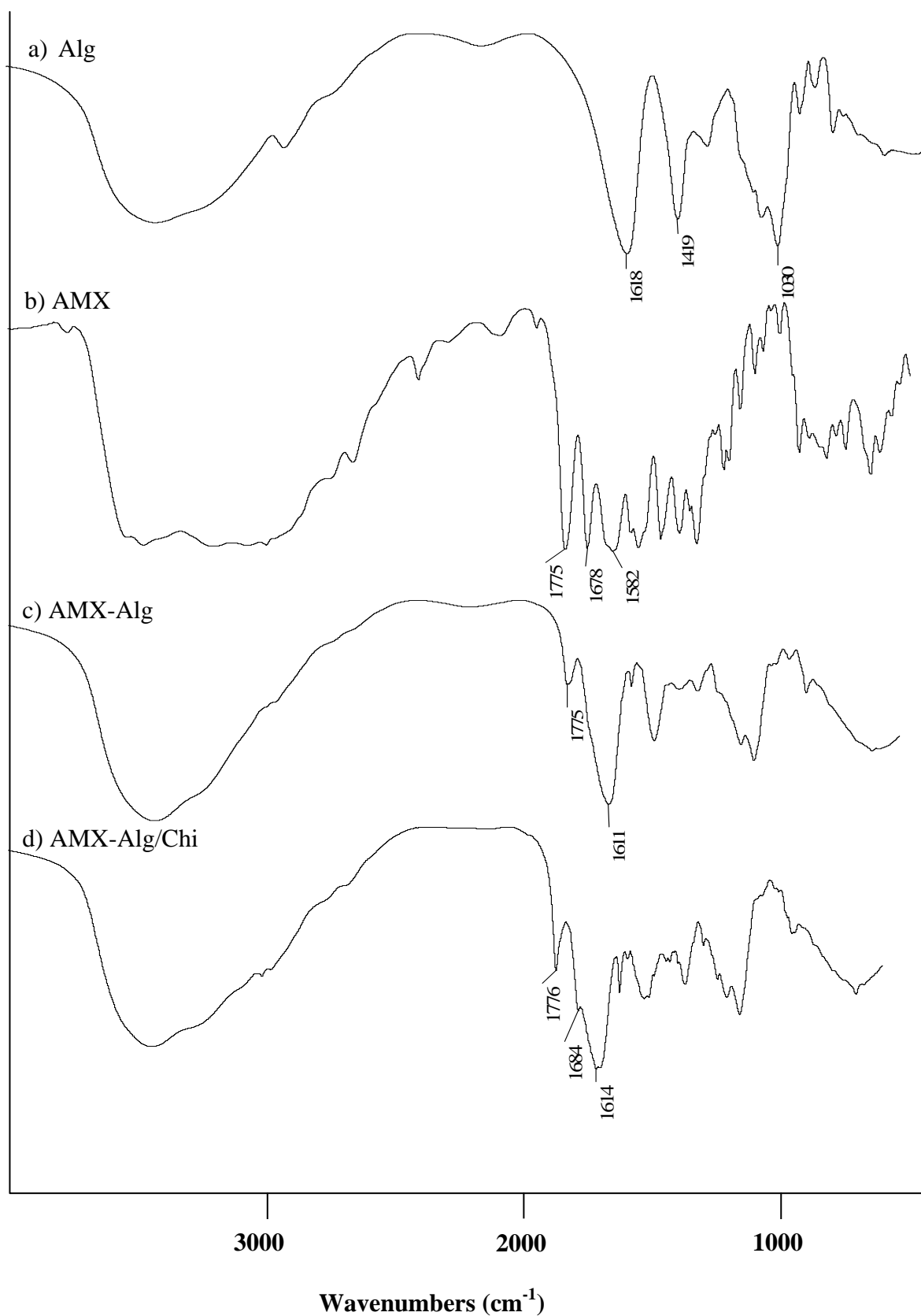
**Figure 4.47** IR spectra of (a) alginate, (b) AMX, (c) AMX – Alg, (d) AMX – Alg/Chi

Figure 4.48 (a) shows the IR spectrum of AMX – Alg/MCG 0.1. The wide absorption band at 3411 cm$^{-1}$, due to the O-H, -COOH and N-H stretching vibration. The band at 1776 cm$^{-1}$ resulted from C=O stretching of carboxylate group. The absorption band at 1613 cm$^{-1}$ assigned to the combination peaks from both polymer and drug. The band at 1418 cm$^{-1}$ assigned to C-O stretching. The absorption band at 1178 cm$^{-1}$ attributed to C-O-C stretching.

Figures 4.48 (b) to 4.48(d) shows the IR spectrum of AMX – Alg/MCG 0.3, AMX – Alg/MCG 0.7 and AMX – Alg/MCG 1, respectively. The wide absorption band around 3419 cm$^{-1}$ was assigned to the stretching vibration of N-H group bonded to –OH group. The band at 1776 and 1686 cm$^{-1}$ resulted from C=O stretching of carboxylate group. The absorption band at 1597 cm$^{-1}$ and 1328 cm$^{-1}$ were assigned to -NH$_2$ bending and C–N stretching vibration of amide group.

a) AMX-Alg/MCG 0.1

1776
1688
1613

b) AMX-Alg/MCG 0.3

1776
1686
1613

c) AMX-Alg/MCG 0.7

1776
1685
1612

d) AMX-Alg/MCG 1

1775
1686
1613

3000          2000          1000

**Wavenumbers (cm$^{-1}$)**
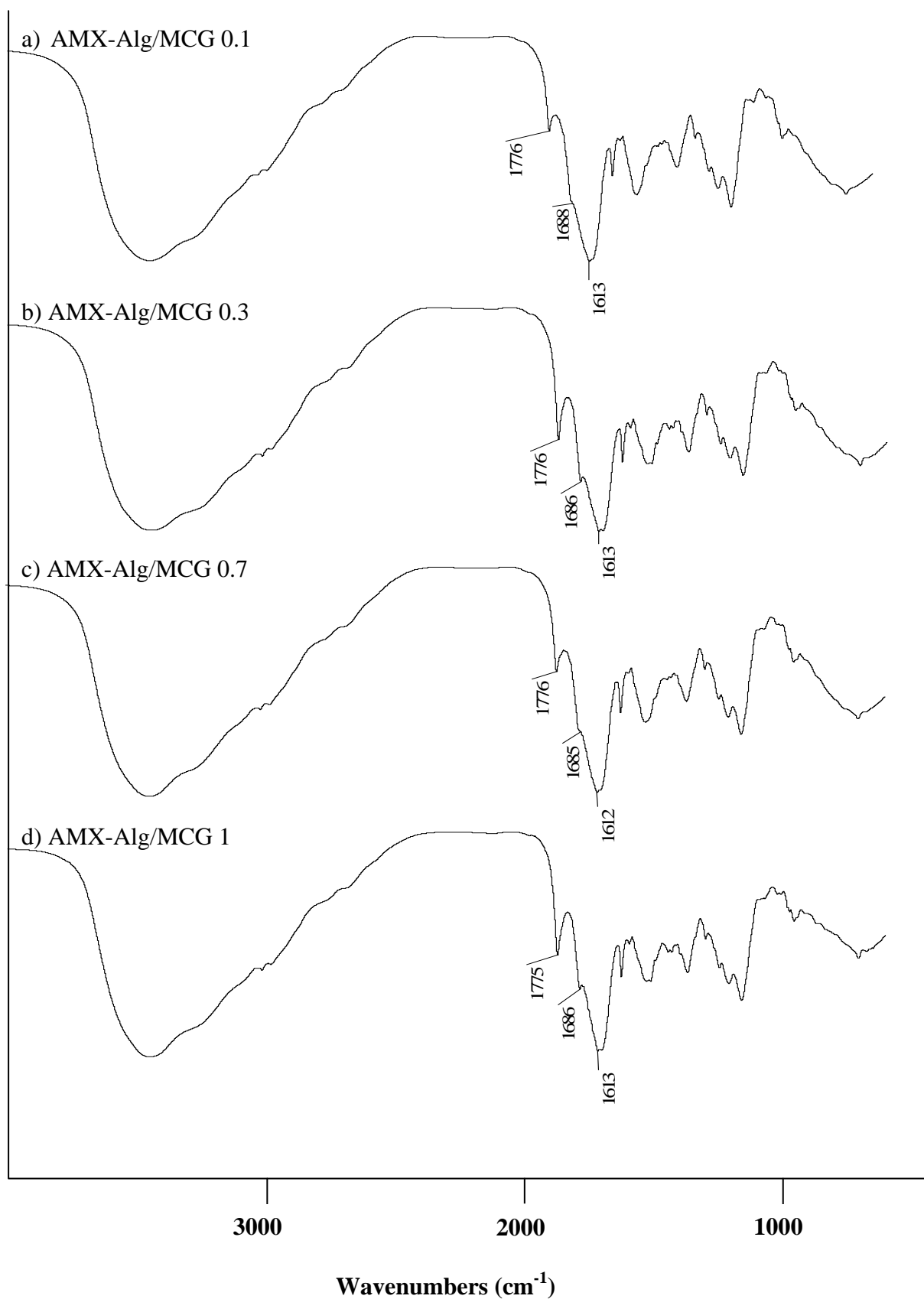
**Figure 4.48** IR spectra of (a) AMX– Alg/MCG 0.1, (b) AMX – Alg/MCG 0.3, (c) AMX – Alg/MCG 0.7, (d) AMX – Alg/MCG1

4.6.5 Swelling Analysis

4.6.5.1 Swelling Analysis in the Stimulated Gastric Fluid. (SGF, pH 1.2)

At the pH 1.2, the swelling behaviors of the AMX – pure Alg beads did not swell. Because the calcium ions from alginate matrices are deleted and converted in an insoluble alginic acid [46].

In SGF, the beads coated with chitosan and MCGs, the mechanism of swelling are shown in Figure 4.51. Chitosan is highly soluble and cationic charged in SGF due to conversion of amine units into soluble from $-NH_3^+$, $-COO^-$ can convert to $-COOH$ groups, and the hydrogen bonding can be formed $-OH$ in the acid solution. Which is responsible for the swelling [60].

The swelling ratios of the beads with various compositions in SGF pH 1.2 are shown in Figure 4.49 and Table 4.16. The swelling behaviors of the beads for all formulations in this dissolution system (0.1 N HCl pH 1.2) MCG 0.1 and MCG 0.3 were showed the highest swelling ratio.

**Table 4.16** Swelling ratio of formulation K – L, Q – T beads in SGF (pH 1.2)

| Time (h) | Formulation K | Formulation L | Formulation Q | Formulation R | Formulation S | Formulation T |
|---|---|---|---|---|---|---|
| | Pure alg | Pure Chi | MCG0.1 | MCG0.3 | MCG0.7 | MCG1 |
| 0 | 0 | 0 | 0.00 | 0.00 | 0.00 | 0.00 |
| 1 | 0 | 0.20 | 0.33 | 0.33 | 0.00 | 0.33 |
| 1 | 0 | 0.20 | 0.67 | 0.67 | 0.25 | 0.33 |
| 2 | 0 | 0.20 | 0.67 | 0.67 | 0.25 | 0.67 |
| 4 | 0 | 0.20 | 0.67 | 0.67 | 0.25 | 0.67 |
| 6 | 0 | 0.20 | 0.67 | 1.00 | 0.25 | 0.67 |
| 8 | 0 | 0.20 | 1.00 | 1.00 | 0.50 | 0.67 |
| 24 | 0 | 0.20 | 1.00 | 1.00 | 0.50 | 0.67 |
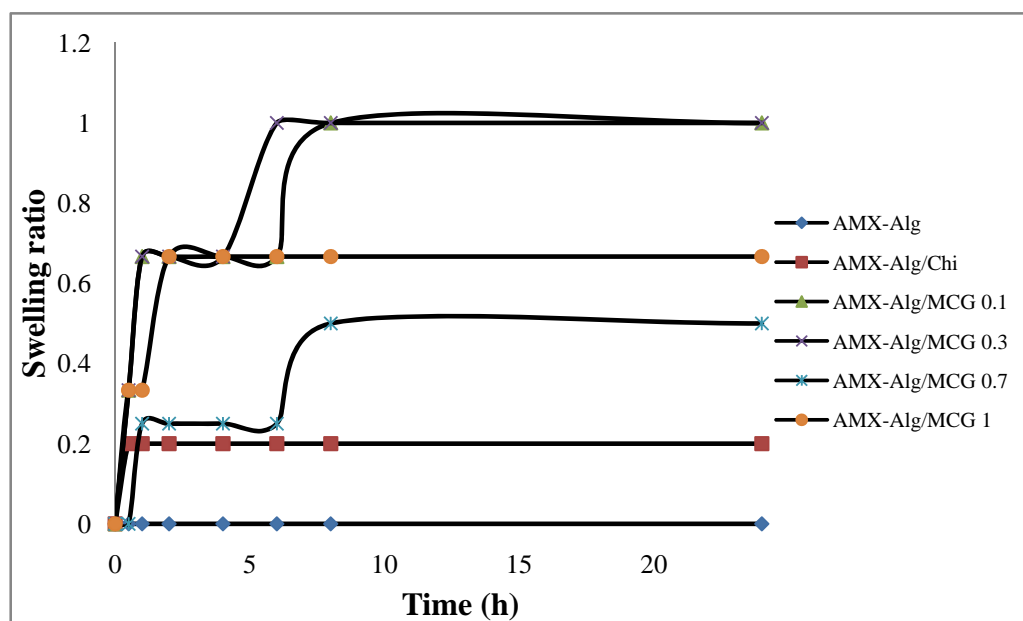
**Figure 4.49** Swelling behavior of various polymer of the AMX - Alg, AMX – Alg/Chi, AMX – Alg/MCG 0.1, AMX – Alg/MCG 0.3, AMX – Alg/MCG 0.7, AMX – Alg/MCG1 in SGF

4.6.5.2 Swelling Analysis in the Stimulated Intestinal Fluid. (SIF, pH 7.4)

The AMX – Alg/MCG beads, the mechanism of swelling at the pH 7.4 are shown in Figure 4.51, amino units on chitosan are deprotonated and the –COOH groups changed into –COO⁻. Therefore, the electrostatic repulsion between the identical –COO⁻ groups in alginate cause the swelling of hydrogel network.

The swelling ratios of the beads with various compositions in SIF pH 7.4 are shown in Figure 4.50 and Table 4.17. The swelling behaviors of the beads for all formulations in this dissolution system (phosphate buffer saline pH 7.4) MCC 0.3 showed the highest swelling ratio.

**Table 4.17** Swelling ratio of formulation K – L, Q – P beads in SIF (pH 7.4)

| Time (h) | Formulation K | Formulation L | Formulation Q | Formulation R | Formulation S | Formulation T |
|---|---|---|---|---|---|---|
| | Pure alg | Pure Chi | MCG0.1 | MCG0.3 | MCG0.7 | MCG1 |
| 0 | 0 | 0 | 0.00 | 0.00 | 0.00 | 0.00 |
| 1 | 0.25 | 0.20 | 0.67 | 0.67 | 0.25 | 0.33 |
| 1 | 0.50 | 0.40 | 0.67 | 0.67 | 0.25 | 0.67 |
| 2 | 1.00 | 1.00 | 1.33 | 1.00 | 0.50 | 1.33 |
| 4 | 1.50 | 1.20 | 2.00 | 1.67 | 1.25 | 2.00 |
| 6 | 1.75 | 1.40 | 2.00 | 1.67 | 1.25 | 2.33 |
| 8 | 1.75 | 1.40 | 2.00 | 1.67 | 1.50 | 2.33 |
| 24 | 1.75 | 1.40 | 2.00 | 1.67 | 1.50 | 2.33 |
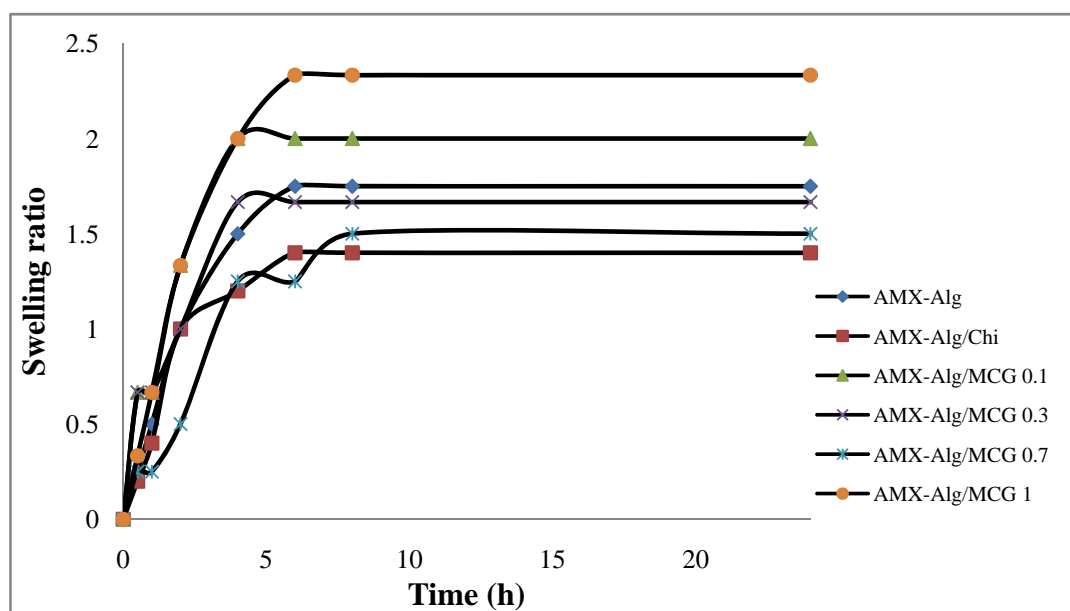


**Figure 4.50** Swelling behavior of various polymer of the AMX - Alg, AMX – Alg/Chi, AMX – Alg/MCG 0.1, AMX – Alg/MCG 0.3, AMX – Alg/MCG 0.7, AMX – Alg/MCG 1 in SIF
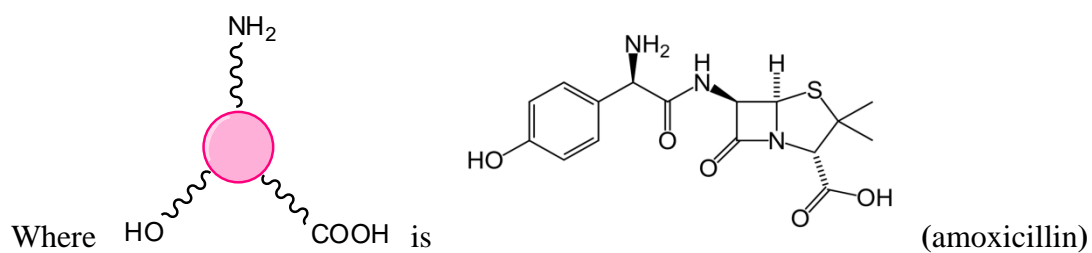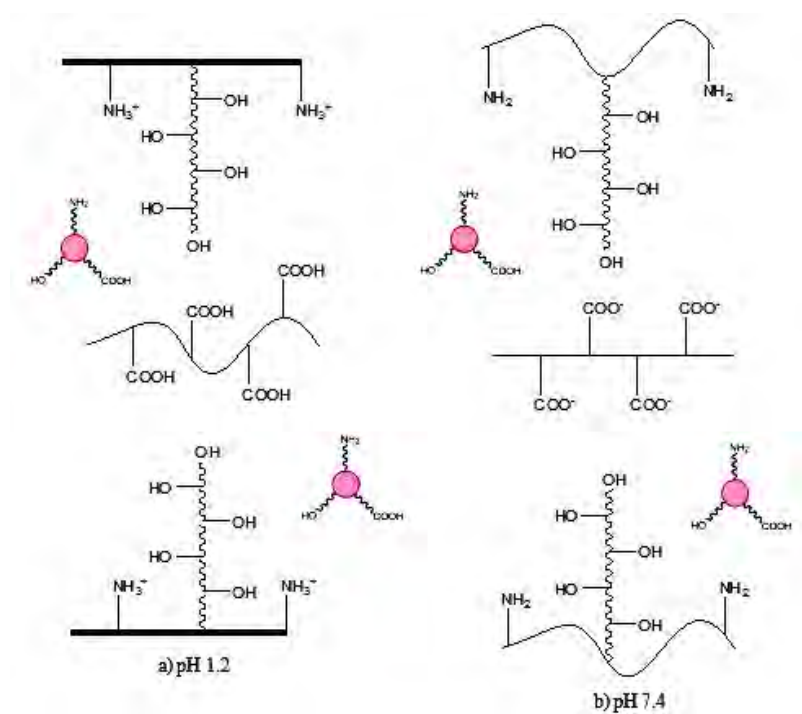
**Figure 4.51** The swelling mechanism of Alg-MCG beads in buffer solution of different pH a) pH 1.2, b) pH 7.4

4.6.6 Inhibition of the AMX – Alg/MCG beads against *E. coli* and *S. aureus* bacteria.

Inhibition of the AMX – Alg/MCG beads against *E. coli* (Gram-negative) and *S. aureus* (Gram-positive) bacteria by agar diffusion method were shown in Figures 4.52 – 4.53 and Table 4.18.
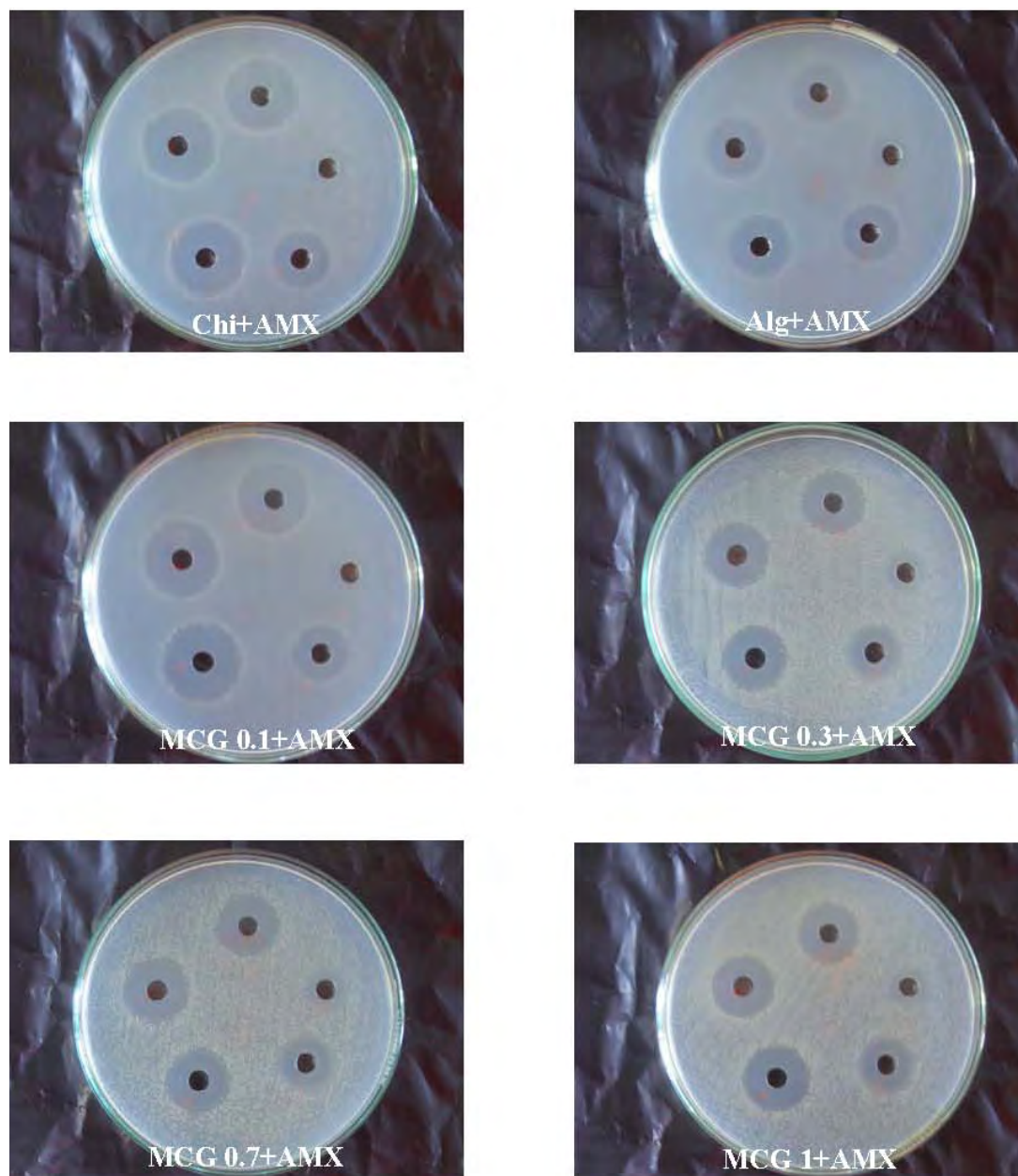


**Figure 4.52** Inhibition clear zones of amoxicillin release from the AMX – Alg/MCG beads at 2 hour against *E. coli*
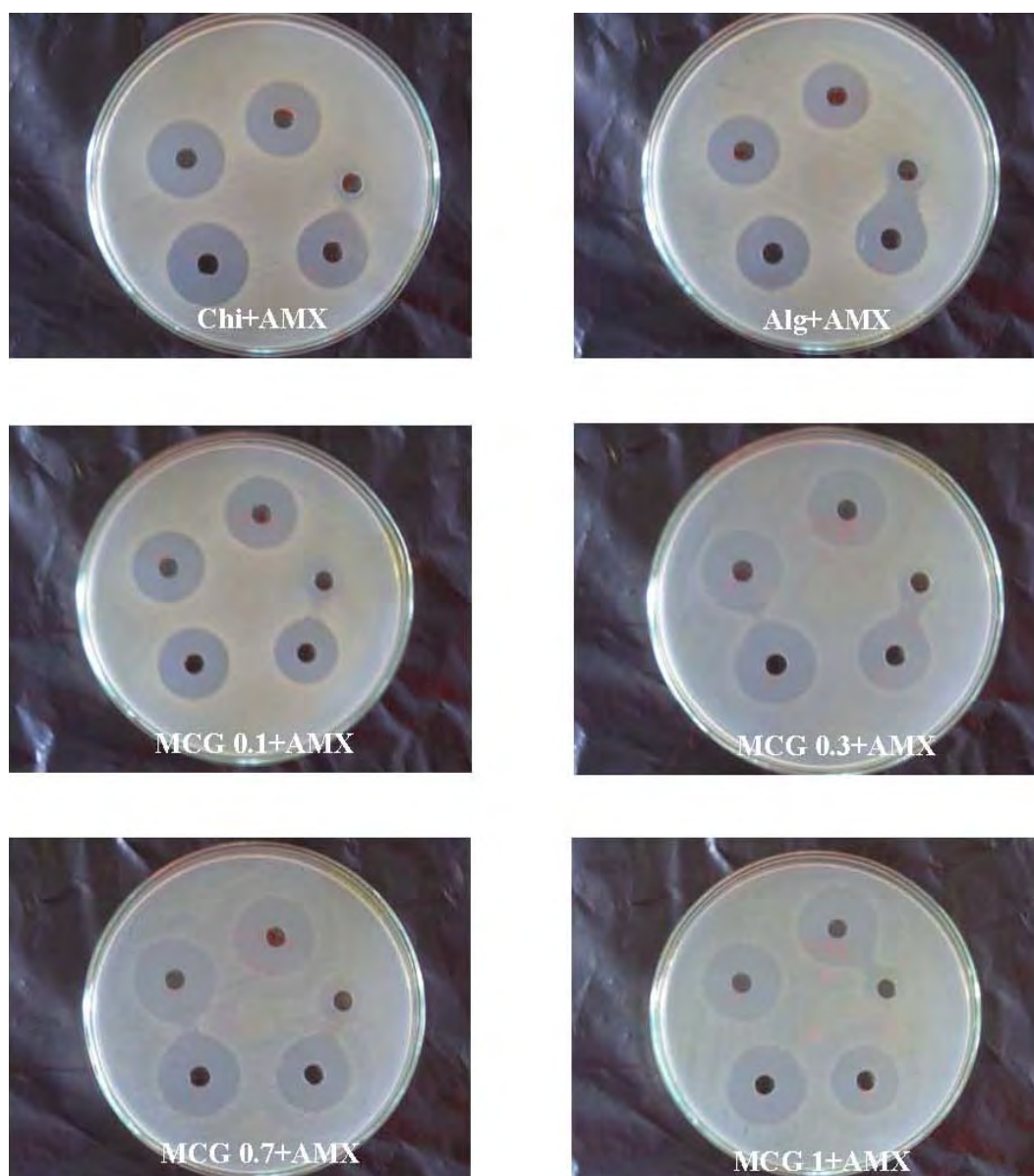
**Figure 4.53** Inhibition clear zones of amoxicillin release from the AMX – Alg/MCG beads at 2 hour against *S. aureus*

**Table 4.18** Diameters of the wall from the inhibition of the AMX-Alg/MCG beads against bacteria

| Formulation | *E. coli* | % Inhibition | *S. aureus* | % Inhibition |
|---|---|---|---|---|
| Control (AMX 50 ppm) | $1.50 \pm 0.00$ | - | $1.90 \pm 0.00$ | - |
| Control (1% lactic acid) | $1.00 \pm 0.00$ | - | $1.00 \pm 0.00$ | - |
| AMX-Alg | $1.70 \pm 0.00$ | 13.33 | $1.87 \pm 0.06$ | 0 |
| AMX-Alg/Chi | $2.10 \pm 0.00$ | 40.00 | $2.08 \pm 0.03$ | 9.65 |
| AMX-Alg/MCG 0.1 | $2.03 \pm 0.06$ | 35.56 | $2.10 \pm 0.00$ | 10.53 |
| AMX-Alg/MCG 0.3 | $1.80 \pm 0.00$ | 20.00 | $2.20 \pm 0.00$ | 15.79 |
| AMX-Alg/MCG 0.7 | $1.80 \pm 0.00$ | 20.00 | $2.30 \pm 0.10$ | 21.05 |
| AMX-Alg/MCG 1 | $1.90 \pm 0.10$ | 26.67 | $2.37 \pm 0.06$ | 24.56 |

1% Lactic acid as a control can not inhibit both *E. coli* and *S. aureus*. The AMX-Alg/Chi can inhibit both *E. coli* and *S. aureus* with diameter of well 2.10 and 2.08 cm, respectively. Therefore, the AMX-Alg/Chi showed the stronger inhibition against *E. coli* than that of the AMX-Alg/MCG and the AMX-Alg/MCG 1 showed the stronger inhibition against *S. aureus* than that of the AMX-Alg/Chi.

4.6.7 In Vitro Release Study

4.6.7.1 Amoxicillin trihydrate release behavior from the beads in SGF

The dissolution profiles of AMX can be described as graphs to explain and understand the drug released behavior from the beads.

The dissolution and release rate data of each formulation are given in Tables D8 – D9 (Appendix D). Figure 4.54 showed the release profiles of AMX from the beads. In SGF, the release rate reached to 50% in 2 hour. Because the chitosan layer were important to retard the release of drug. After 24 hours, the Formulation L showed percentage of drug release higher the drug release 100% and Formulation K, Q – T the release maintained at approximately 90 - 95%.
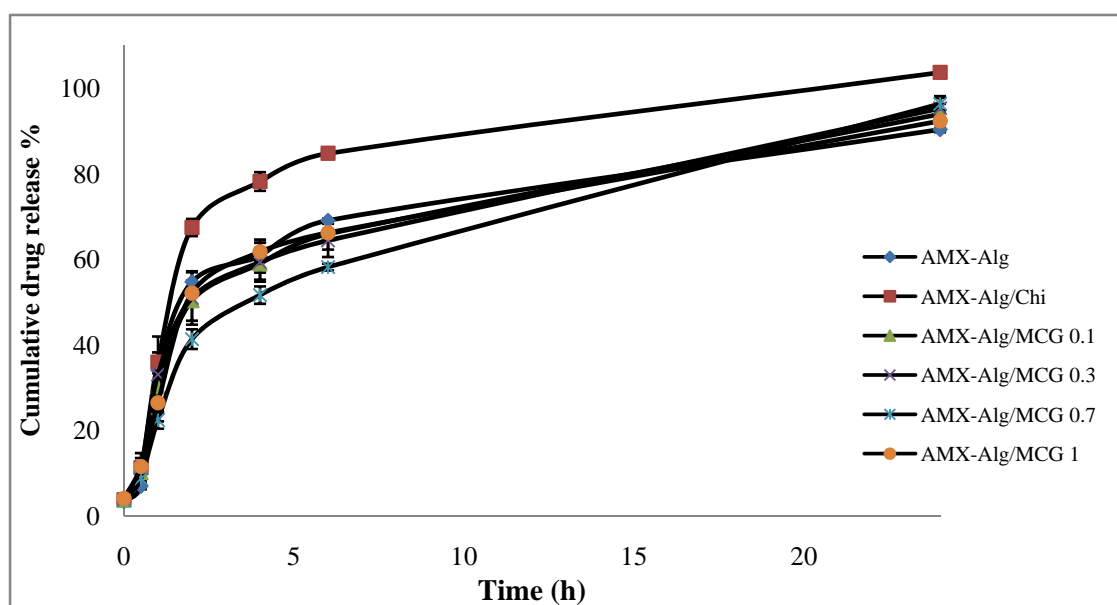


**Figure 4.54** The dissolution profiles of AMX - Alg, AMX – Alg/Chi, AMX – Alg/MCG 0.1, AMX – Alg/MCG 0.3, AMX – Alg/MCG 0.7, AMX – Alg/MCG 1 in SGF

4.6.7.2 Amoxicillin trihydrate release behavior from the beads in SIF

Swelling behavior is very important property for a drug delivery because they have great influences on controlled drug delivery. The release rate of AMX from the beads based on alginate was directly depended on the swelling behaviors of alginate in phosphate buffer. The rapid swelling behaviors of the beads in SIF may possibly accelerate the initial stage of the drug release. The release profile of AMX in SIF are shown in Figure 4.55. The dissolution and release rate data of each formulation are given in Tables D11 – D12 (Appendix D). The results showed that all Formulations were no significant difference percentage of drug release. At the 6 hour, all Formulations gave the high percentage of drug release over 90%. The dissolution percentage of the Formulation AMX – Alg, AMX – Alg/Chi, AMX – Alg/MCG 0.1, AMX – Alg/MCG 0.3, AMX – Alg/MCG 0.7 and AMX – Alg/MCG 1 were 99.67%, 99.03%, 90.03%, 92.72%, 78.22% and 98.90%, respectively.
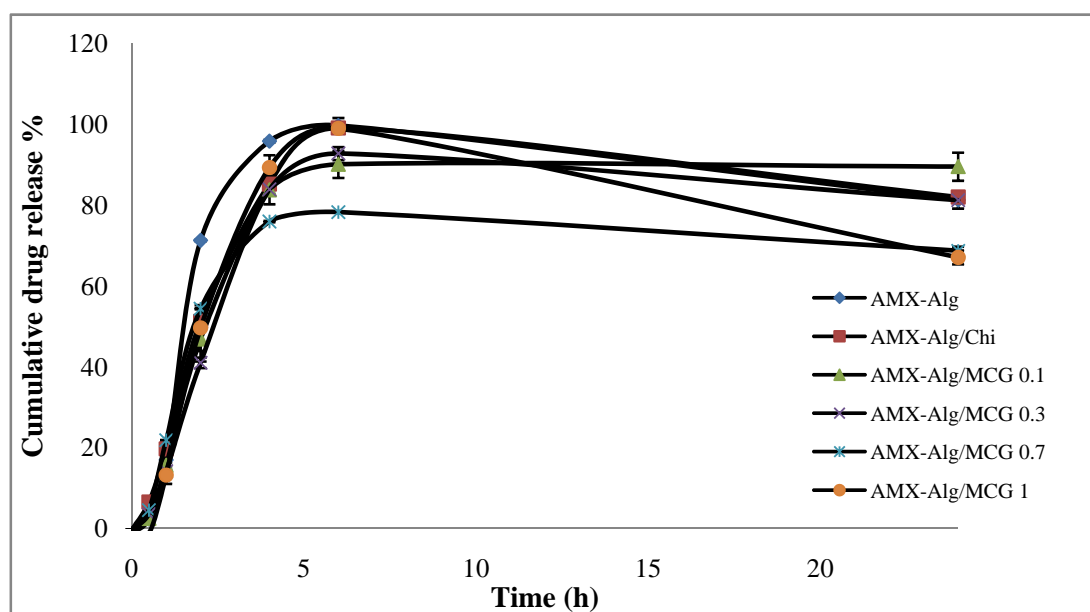


**Figure 4.55** The dissolution profiles of AMX - Alg, AMX – Alg/Chi, AMX – Alg/MCG 0.1, AMX – Alg/MCG 0.3, AMX – Alg/MCG 0.7, AMX – Alg/MCG 1  in SIF

# CHAPTER V

# CONCLUSION

## 5.1 Conclusion

In this work, the MCCs and MCGs were successfully synthesized using a simple method with gluconolactone and caprolactone to improve mucoadhesive property of chitosan. The obtained MCCs and MCGs, had large amount of free hydroxyl groups, hydrophobic and hydrophilic side chain, high molecular weight, chain flexibility. The modified chitosan showed excellent mucoadhesive properties over chitosan, has good solubility, swelling property and non-toxic to Vero cell.

The modified chitosan were synthesized for drug controlled release application in a gastrointestinal drug delivery system, using amoxicillin trihydrate (AMX) and sodium diclofenac (DFNa) as model drugs for delivery in the simulated stomach (pH 1.2) and the intestinal tract (pH 7.4), respectively.

The controlled release of sodium diclofenac loaded aliginate beads prepared by solution method and coated with polymer offered an excellent encapsulation, up to 80% of drug entrapment efficiency. The dissolution profile of DFNa from DFNa-Alg/MCG 0.3 beads exhibited a good slow release profile, achieving from 6 to 24 hour and each MCC, MCG had no significant effect on the drug release The drug prolonged release was far more superior upon further cross-linking the hydrogel with polymer.

The sodium diclofenac loaded aliginate beads were able to provide the best delayed release in the gastric simulated fluid (pH 1.2). The remaining drug content was gradually released within 24 hours in the intestinal simulated fluid (pH 7.4). In all, the chitosan, MCC and MCG, had been proven very useful as a novel alternative for gastrointestinal drug release system.

The controlled release of amoxicillin trihydrate loaded aliginate beads in the gastric simulated fluid (pH 1.2) had an excellent encapsulation, up to 70% of drug

entrapment efficiency. The dissolution profile of AMX from AMX-Alg/MCG 0.7 beads exhibited that a good slow release profile was achieved from the 6 hour to 24 hour and each MCC, MCG had no significant effect on the drug release The drug prolonged release was far more superior upon further cross-linking the hydrogel with polymer.

## 5.2 Suggestion for the future work

In the present study, the controlled release profile of sodium diclofenac and amoxicillin trihydrate in a gastrointestinal drug delivery system, we suggest that the combinations of sodium diclofenac and amoxicillin trihydrate and other drugs and other polymers should be further studied.

# REFERENCES

[1] Bernkop-Schnurch, A. Thiomers: A new generation of mucoadhesive polymers. Advanced Drug Delivery Reviews. 57 (2005): 1569-1582.

[2] Schmitz, T., Grabovac, V., Palmberger, T. F., Hoffer, M. H. and Bernkop-Schnurch, A. Synthesis and characterization of a chitosan-N-acetyl cysteine conjugate. International Journal of Pharmaceutics. 347 (2008): 79-85.

[3] Roldo, M., Hornol, M., Caliceti, P. and Bernkop-Schnurch, A. Mucoadhesive thiolated chitosan as platforms for oral controlled drug delivery: synthesis and in vitro evaluation. European Journal of Pharmaceutics and Biopharmaceutics. 57 (2004): 115-121.

[4] Peppas, N. A. and Huang, Y. Nanoscale technology of mucoadhesive interactions. Advanced Drug Delivery Reviews. 56 (2004): 1675-1687.

[5] Bernkop-Schnurch, A. and Steininger, S. Synthesis and characterisation of mucoadhwsive thiolated polymers. International Journal of Pharmaceutics. 194 (2000): 239 – 247.

[6] Bernkop-Schnurch, A. Mucoadhesive systems in oral drug delivery. Drug Discovery Today: Technologies. 2 (2005): 83-87.

[7] Dhawan, S., Singla, A. K. and Sinha, V. R. Evaluation of mucoadhesive properties of chitosan microspheres prepared by different methods. AAPS PharmSciTech. 5(4) (2004): 1-7.

[8] Leitner, V. M., Walker, G. F. and Bernkop-Schnurch, A. Thiolated polymers: evidence for the formation of disulphide bonds with mucus glycoproteins. European Journal of Pharmaceutics and Biopharmaceutics. 56 (2003): 207-214.

[9] Zhang, C., Ping, Q., Zhang, H. and Shen, J. Synthesis and characterization of water-soluble O-succinyl-chitosan. European Poymer Journal. 39 (2003): 1629-1634.

[10] Caner, H., Yilmaz, E. and Yilmaz, O. Synthesis, characterization and antibacterial activity of poly(N-vinylimidazole) grafted chitosan. Carbohydrate Polymers. 69 (2007): 318-325.

[11] Rossi, S., Ferrari, F., Bonferoni, M. C. and Caramella, C. Characterization of chitosan hydrochloride-mucin rheological interaction: influence of polymer concentration and polymer:mucin weight ratio. European Journal of pharmaceutical Sciences. 12 (2001): 479-485.

[12] Bernkop-Schnurch, A., Hornof, M. and Zoidl, T. Thiolated polymers-thiomers: synthesis and in vitro evaluation of chitosan-2-iminothiolane conjugates. International Journal of Pharmaceutics. 260 (2003): 229-237.

[13] Liu, L., Li, Y., Fang, Y. and Chen, L. Microwave – assisted graft copolymerization of ε-caprolactone onto chitosan via the phthaloyl protection method. Carbohydrate Polymers. 60 (2005): 351-356.

[14] Chen, L., Tian, Z. and Du, Y. Synthesis and pH sensitivity of carboxymethyl chitosan-based polyampholyte hydrogel for protein carrier matrices. Biomaterials. 25 (2004): 3725-3732.

[15] Jungbunzlauer ; gluconolactone. [Online]. 2003. Available from: http://www.jungbunzlauer.com/products-applications/products/gluconates/glucono-delta-lactone/general-information.html [2008, October 23]

[16] Human metabolome database; gamma-caprolactone. [Online]. 2005. Available from: http://www.hmdb.ca/metabolites/HMDB03843 [2008, November 10]

[17] Sahasathian, T., Kerdcholpetch, T., Chanweroch, A., Praphairaksit, N., Suwonjandee, N., and Muangsin, N. Sustained Release of Amoxicillin from Chitosan Tablets. Archives of Pharmacal Research. 30 (2007): 526-531.

[18] Gillman, A., Nies, T. W. and Taylor, P. The pharmaceutical basis of therapeutics. Vol. 1. 8[th]ed. New York: Pergamon Press, 1991

[19] O' Brien, W. M. Adverse reactions to nonsteroidal anti-inflammatory drugs: diclofenac compared with other nonsteroidal anti-inflammatory drugs. The American Journal of Medicine. 80 (1986): 70-80.

[20] Liu, Z., Lu, W., Qian, L., Zhang, X., Zeng, P. and Pan, J. In vitro and in vivo studies on mucoadhesive microspheres of amoxicillin. Journal of Controlled Release. 102 (2005): 135-144.

[21] Rajinikanth, P. S., Balasubramaniam, J. and Mishra, B. Development and evaluation of novel floating in situ gelling system of amoxicillin for eradication of *Helicobacter pylori*. International Journal of Pharmaceutics. 335 (2007): 114-122.

[22] Hilton, A. K. and Deasy, P. B. In vitro and in vivo evaluation of an oral sustained-release floating dosage form of amoxicillin trihydrate. International Journal of Pharmaceutics. 86 (1992): 79-88.

[23] Clausen, A. E. and Bernkop-Schnurch, A. Direct compressible polymethacrylic acid-starch compositions for site-specific drug delivery. Journal of Controlled Release. 75(1-2) (2001): 93-102.

[24] Chun, M., Sah, H. and Choi, H. Preparation of mucoadhesive microspheres containing antimicrobial agents for eradication of H.pylori. International Journal of Pharmaceutics. 297 (2005): 172-179.

[25] Tonnesen, H. H. and Karlsen, J. Alginate in drug delivery systems. Drug Development and Industrial Pharmacy. 28 (2002): 621-630.

[26] Sriamornsak, P. And Sungthongjeen, S. Modification of theophylline release with alginate gel formed in hard capsules. AAPS PharmSciTech. 8(3) (2007): (E1-E8)

[27] Murata, Y., Sasaki, N., Miyamoto, E. and Kawashima, S. Use of floating alginate gel beads for stomach-specific drug delivery. European Journal of Pharmaceutics and Biopharmaceutics. 50 (2000): 221-226.

[28] Madsen, F., Eberth, K. and Smart, J. D. A rheological examination of the mucoadhesive/mucus interaction: the effect of mucoadhesive type and concentration. Journal of Controlled Release. 50 (1998): 167-178.

[29] Smart, J. D. The basics and underlying mechanisms of mucoadhesion. Advanced Drug Delivery Reviews. 57 (2005): 1556-1568.

[30] Ahuja, R.P. and Khar, J. A. Mucoadhesive drug delivery systems. Drug Development and Industrial Pharmacy. 23 (1997): 489– 515.

[31] Mathiowitz, E., Chickering, D.E. Definitions, mechanisms and theories of bioadhesion, In Mathiowitz, E., Chickering, D.E., Lehr, C.-M. (Eds.). Bioadhesive Drug Delivery Systems: Fundamentals, Novel Approaches and Development, pp. 1 –10. New York: Marcel Decker, 1999.

[32] Peppas, N.A. and Sahlin, J.J. Hydrogels as mucoadhesive and bioadhesive materials: a review. Biomaterials. 17 (1996): 1553– 1561.

[33] Vasir, J. K., Tambwekar, K. and Garg, S. Bioadhesive microspheres a controlled drug delivery system. International Journal of Pharmaceutics. 255 (2003): 13-32.

[34] Wu, S. Formation of adhesive bond, Polymer Interface and Adhesion, New York: Marcel Dekker, 1982.

[35] Smart, J.D. The role of water movement and polymer hydration in mucoadhesion, In Mathiowitz, E., Chickering, D.E., Lehr, C.-M. (Eds.). Bioadhesive Drug Delivery Systems: Fundamentals, Novel Approaches and Development, pp. 11 –23. New York: Marcel Decker, 1999.

[36] Kim, C. Controlled release dosage form design. Pennsylvania: Technology Publishing Book, 2000.

[37] Brannon-Peppas, L. Biomaterials: Polymers in Controlled Drug Delivery [Online]. 1997. Available from: http://www.devicelink.com/mpb/archive/97/11/003.html [2009, Sebtember 4]

[38] Lankalapalli, S. and Kolapalli, V. R. M. Polyelectrolyte complexes: a review of their applicability in drug delivery technology. Indian Journal of Pharmaceutical Sciences. 71 (2009): 481-487.

[39] Batista, M. K. S., Pinto, L. F., Gomes, C. A. R. and Gomes, P. Novel highly-soluble peptide-chitosan polymers: chemical synthesis and spectral characterization. Carbohydrate Polymers. 64 (2006): 299-305.

[40] Moltugh, D. J. A guide to the seawood industry. (ROME: FAO, 2003).

[41] Wikipedia, the from encyclopedia; amoxicillin trihydrate. [Online]. 2001. Available from: http://www.en.wikipedia.org/wiki/Amoxicillin [2008, October 10]

[42] Lacy C. F., et al. Drug information handbook. 12th ed. Hudson: OH:Loxi Comp, 2004.

[43] Gerald, K. M. AHFS Drug Information 2004 Bethesda: ASHP, 2004.

[44] Sallmann, A. R. The history of diclofenac. The American Journal of Madicine. 80 (1986): 29-33.

[45] Thatte, M.R. Synthesis and antibacterial assessment of water-soluble hydrophobic chitosan derivatives bearing quaternary ammonium functionality. Master's Thesis, Department of Chemistry Faculty of Science Louisiana State University and A & M College, 2004.

[46] Xie, Y., Liu, X. and Chen, Q. Synthesis and characterization of water-soluble chitosan derivate and its antibacterial activity. Carbohydrate Polymers. 69 (2007): 142-147.

[47] Almeida, P. F. and Almeida, A. J. Cross-linked alginate-gelatine beads: a new matrix for controlled release of pindolol. Journal of Controlled Release. 97 (2004): 431-439.

[48] Thawachinee Buranachai, Controlled release of sodium diclofenac from chitosan/polyethylene glycol beads cosslinked with tripolyphosphate, Master's Thesis, Program of Pertochemistry and Polymer Science Faculty of Science Chulalongkorn University, 2006.

[49] Teerawat Sahasathian, Controlled release of amoxicillin from alginate-gelatin-chitosan beads, Master's Thesis, Program of Pertochemistry and Polymer Science Faculty of Science Chulalongkorn University, 2007.

[50] Hassan, E. E. and Gallo J. M. A simple rheological method for the *in vitro* assessment of mucin-polymer bioadhesive bond strength. Pharmaceutical Research. 7 (1990): 491-495.

[51] Ma, G., Yang, D., Zhou, Y., Xiao, M., Kennedy, J. F. and Nie, J. Preparation 9 and characterization of water-soluble N-alkylated chitosan. Carbohydrate Polymers. 74 (2008): 121-126.

[52] Luckachan, G. E. and Pillai, C. K. S. Chitosan/oligo L-lactide graft copolymers: Effect of hydrophobic side chains on the physic-chemical properties and biodegradability. Carbohydrate Polymers. 64 (2006): 254-266.

[53] Deacon, M. P., Mcgurk, S., Roberts, C. J., Williams, P. M., Tendler, S. J. B., Davies, M. C., Davis, S. S. and Harding, S. E. Atomic force microscopy of gastric mucin and chitosan mucoadhesive systems. Biochem. Journal. 348 (2000): 557-563.

[54] Lin, Y., Chen, Q. and Luo, H. Preparation and characterization of N-(2-34 carboxybenzyl)chitosan as a potential pH-sensitive hydrogel for drug delivery. Carbohydrate research. 342 (2007): 87-95.

[55] Bajpai, S. K., Sharma, S. Investigation of swelling/degradation behavior of alginate beads crosslinked with $Ca^{2+}$ and $Ba^{2+}$ ions. Reactive & Functional Polymers. 59 (2004): 129-140.

[56] Gomes, P., Gomes, C. A. R., Batista, M. K. S., Pinto, L. F. and Silva, P. A. P. Synthesis, structure characterization and properties of water-soluble N-(γ-propanoyl-amino acid)-chitosans. Carbohydrate Polymers. 71 (2008): 54-65.

[57] Anal, A. K. and Stevens, W. F. Chitosan-alginate multilayer beads for controlled release of ampicillin. International Journal of Pharmaceutics. 290 (2005): 45-54.

[58] Mladenovska, K., Cruaud, O., Richomme, P., Belamie, E., Raicki, R. S., Venier-Julienne, M.-C., Popovski, E., Benoit, J. P. and Goracinova, K. 5-ASA loaded chitosan-Ca-alginate microparticles: Preparation and physicochemical characterization. International Journal of Pharmaceutics. 345 (2007): 59-69.

[59] Piyakulawat, P., Praphairaksit, N., Chantarasiri, N. and Muangsin, N. Preparation and evaluation of chitosan/carrageenan beads for controlled release of sodium diclofenac. AAPS PharmSciTech. 8(4) (2007): E1-E11.

[60] Ostberg, T., Lund, E. M. and Graffner, C. Calcium alginate matrices for oral multiple unit administration: IV. Release characteristics in different media. International Journal of Pharmaceutics. 112 (1994): 241-248.

# APPENDICES

# APPENDIX A

**Degree of substitution**

The % substitution of MCC was calculated using the signal intensities obtained from the $^1$H- NMR. The equation that is applicable for the $^1$H- NMR spectrum in Figure 4.4 is as follows

$$\frac{Intregrate\ due\ to\ b,c,3,4,5,6}{Intregrate\ due\ to\ d} = \frac{Number\ of\ "c"\ hydrogen\ and\ sugar\ proton\ per\ sugar\ residue}{Number\ of\ "a"\ proton\ per\ sugar\ residue}$$

Assuming the degree of substitution to be Y%

$$\frac{Intregrate\ due\ to\ b,c,3,4,5,6}{Intregrate\ due\ to\ d} = \frac{\frac{2Y}{100} + 4_{sugar}}{\frac{3_a \times Y}{100}}$$

Rearranging the terms

$$Y = \frac{4_{sugar} \times 100}{3[\frac{Intregrate\ due\ to\ b,c,3,4,5,6}{Intregrate\ due\ to\ d} - \frac{2}{3}]}$$

*Where* Y was degree of substitution

The degree of subsitution of MCC was calculated using the signal intensities obtained from the $^1H$ *NMR.*

For example, degree of substitution of MCC 0.1 using the intensities of $^1H$ *NMR* spectrum was calculated from the peak area at 3.35 – 3.55 ppm of $-CH_{2b}$-, $-CH_c$- and $H_3 - H_6$ proton against 0.83 - 0.85 ppm of $-CH_{2d}$- *proton as follow equation:*

$$\frac{24.02}{1.00} = \frac{\frac{2Y}{100} + 4_{sugar}}{\frac{3_a \times Y}{100}}$$

$$Y = \frac{4_{sugar} \times 100}{3[\frac{24.02}{1.00} - \frac{2}{3}]}$$

$$Y = 5.71\ \%$$

The % substitution of MCG was calculated using the signal intensities obtained from the $^{1}$H- NMR. The equation that is applicable for the $^{1}$H- NMR spectrum in Figure 4.6 is as follows

$$\frac{Intregrate\ due\ to\ c, 3, 4, 5, 6}{Intregrate\ due\ to\ a} = \frac{Number\ of\ "c"\ hydrogen\ and\ sugar\ proton\ per\ sugar\ residue}{Number\ of\ "a"\ proton\ per\ sugar\ residue}$$

Assuming the degree of substitution to be Y%

$$\frac{Intregrate\ due\ to\ c, 3, 4, 5, 6}{Intregrate\ due\ to\ a} = \frac{\frac{2Y}{100} + 4_{sugar}}{\frac{1_a \times Y}{100}}$$

Rearranging the terms

$$Y = \frac{4_{sugar} \times 100}{\dfrac{Intregrate\ due\ to\ c, 3, 4, 5, 6}{Intregrate\ due\ to\ a} - 2}$$

*Where* Y was degree of substitution

The degree of subsitution of MCG was calculated using the signal intensities obtained from the $^{1}H$ *NMR.*

For example, degree of substitution of MCG 0.1 using the intensities of $^{1}H$ *NMR* spectrum was calculated from the peak area at 3.50 -3.70 ppm of $-CH_{2c}$- and $H_3$ – $H_6$ proton against 3.84 ppm of $-CH_a$- proton as follow equation:

$$\frac{18.77}{1.00} = \frac{\frac{2Y}{100} + 4_{sugar}}{\frac{1_a \times Y}{100}}$$

$$Y = \frac{4_{sugar} \times 100}{\frac{18.77}{1.00} - 2}$$

$$Y = 23.85 \ \%$$

# APPENDIX B

**Calibration curve**

Calibration curve of amoxicillin

The concentration versus peak area of amoxicillin determined by HPLC assay as the same condition described in Chapter III is presented in Table A1. The plot of calibration curve of amoxicillin is illustrated in Figure A1.

**Table A1** Absorbance of various concentrations of amoxicillin determined by HPLC

| Concentration (ppm) | Peak area |
|---|---|
| 5 | 78023 |
| 10 | 120365 |
| 20 | 222744 |
| 50 | 516324 |
| 100 | 1051519 |
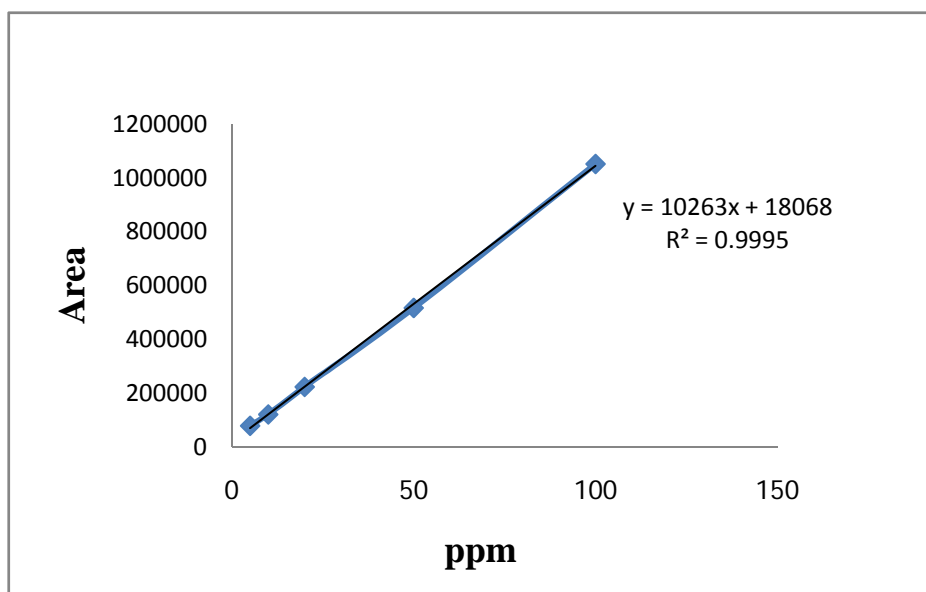


**Figure A1** Calibration curve of amoxicillin.

Calibration curve of sodium diclofenac

The concentration versus peak area of sodium diclofenac in 0.1 N HCl (pH 1.2), phosphate buffer pH 7.4 at 276 nm. are presented in Table A2 to A3. The plot of calibration curve of sodium diclofenac is illustrated in Figure A2 to A3.

**Table A2** Absorbance of sodium diclofenac drug in phosphate buffer pH 7.4 determined in 276 nm

| Concentration (ppm) | Absorbance |
|---|---|
| 5 | 0.1634 |
| 10 | 0.3303 |
| 15 | 0.4994 |
| 20 | 0.6645 |
| 25 | 0.8288 |
| 30 | 1.0027 |
| 35 | 1.1728 |
| 40 | 1.3372 |
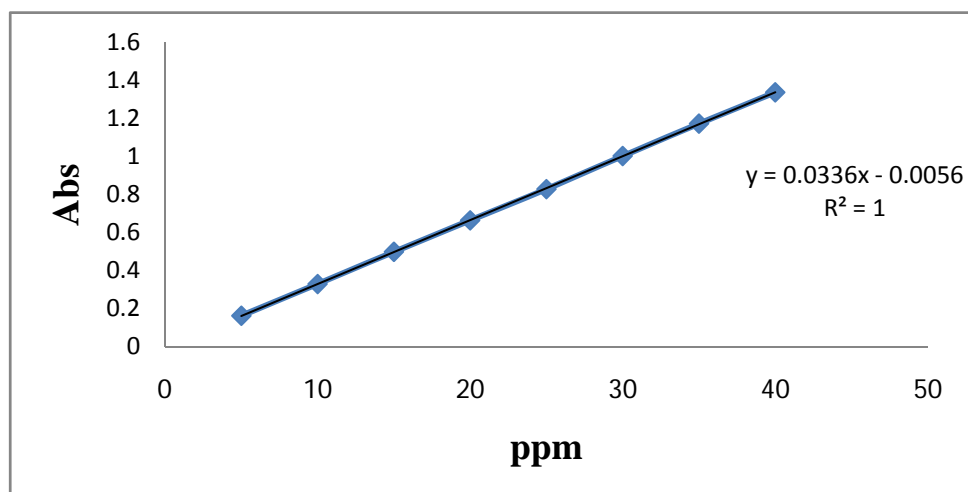


**Figure A2** Calibration curve of sodium diclofenac drug in phosphate buffer pH 7.4 determined in 276 nm

**Table A3** Absorbance of sodium diclofenac drug in 0.1 N HCl (pH 1.2) determined in 276 nm

| Concentration (ppm) | Absorbance |
|---|---|
| 2 | 0.0656 |
| 4 | 0.1220 |
| 6 | 0.1743 |
| 8 | 0.2356 |
| 10 | 0.2860 |



$$y = 0.0277x + 0.0104$$
$$R^2 = 0.9993$$
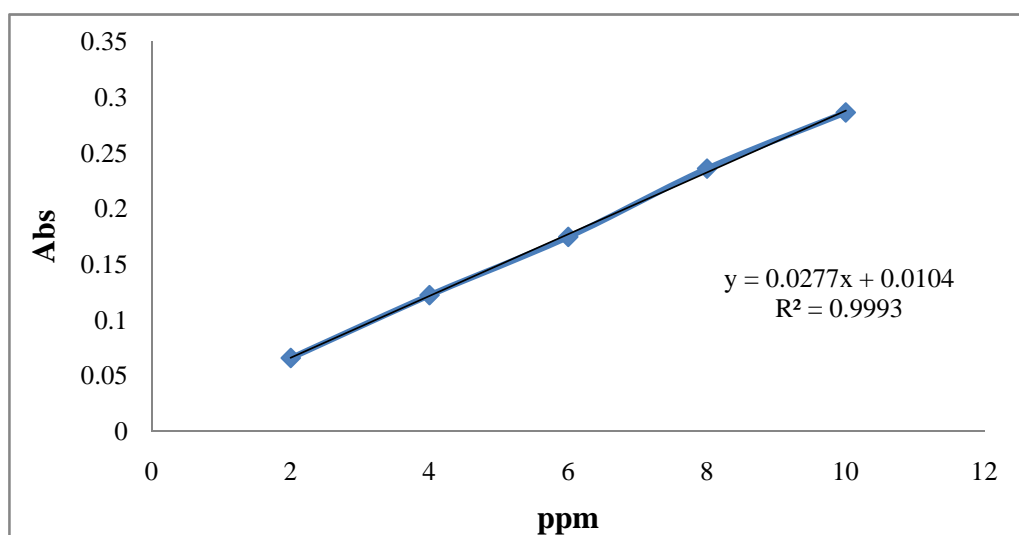
**Figure A2** Calibration curve of sodium diclofenac drug in 0.1 N HCl (pH 1.2) determined in 276 nm

# APPENDIX C

## Swelling ratio

**Table C1** The swelling raio of Chitosan film and MCG film in $H_2O$

| Time (min) | Chitosan | MCG 0.1 | MCG 0.3 | MCG 0.7 | MCG 1 |
|---|---|---|---|---|---|
| 0 | $0 \pm 0.00$ | $0 \pm 0.00$ | $0 \pm 0.00$ | $0 \pm 0.00$ | $0 \pm 0.00$ |
| 1 | $1.5 \pm 0.00$ | $1.5 \pm 0.00$ | $1.7 \pm 0.00$ | $1.7 \pm 0.00$ | $1.5 \pm 0.00$ |
| 2 | $1.5 \pm 0.00$ | $2 \pm 0.00$ | $1.7 \pm 0.00$ | $2.4 \pm 0.00$ | $3 \pm 0.00$ |
| 3 | $1.5 \pm 0.00$ | $2 \pm 0.00$ | $1.7 \pm 0.00$ | $2.4 \pm 0.00$ | $3 \pm 0.00$ |
| 4 | $1.5 \pm 0.00$ | $2 \pm 0.00$ | $1.7 \pm 0.00$ | $2.4 \pm 0.00$ | $3 \pm 0.00$ |
| 5 | $1.5 \pm 0.00$ | $2 \pm 0.00$ | $1.7 \pm 0.00$ | $2.4 \pm 0.00$ | $3 \pm 0.00$ |
| 6 | $1.5 \pm 0.00$ | $2 \pm 0.00$ | $1.7 \pm 0.00$ | $2.4 \pm 0.00$ | $3 \pm 0.00$ |
| 10 | $1.5 \pm 0.00$ | $2 \pm 0.00$ | $1.7 \pm 0.00$ | $2.4 \pm 0.00$ | $3 \pm 0.00$ |
| 15 | $1.5 \pm 0.00$ | $2 \pm 0.00$ | $1.7 \pm 0.00$ | $2.4 \pm 0.00$ | $3 \pm 0.00$ |

**Table C2** The swelling raio of Chitosan film and MCG film in phosphate buffer (pH 7.4)

| Time (min) | Chitosan | MCG 0.1 | MCG 0.3 | MCG 0.7 | MCG 1 |
|---|---|---|---|---|---|
| 0 | 0 ± 0.00 | 0 ± 0.00 | 0 ± 0.00 | 0 ± 0.00 | 0 ± 0.00 |
| 1 | 1.5 ± 0.00 | 1.6 ± 0.00 | 1.6 ± 0.00 | 1.7 ± 0.00 | 2.4 ± 0.00 |
| 2 | 1.5 ± 0.00 | 2 ± 0.00 | 1.7 ± 0.00 | 2.2 ± 0.00 | 2.8 ± 0.00 |
| 3 | 1.5 ± 0.00 | 2 ± 0.00 | 1.7 ± 0.00 | 2.2 ± 0.00 | 2.8 ± 0.00 |
| 4 | 1.5 ± 0.00 | 2 ± 0.00 | 1.7 ± 0.00 | 2.2 ± 0.00 | 2.8 ± 0.00 |
| 5 | 1.5 ± 0.00 | 2 ± 0.00 | 1.7 ± 0.00 | 2.2 ± 0.00 | 2.8 ± 0.00 |
| 6 | 1.5 ± 0.00 | 2 ± 0.00 | 1.7 ± 0.00 | 2.2 ± 0.00 | 2.8 3 ± 0.00 |
| 10 | 1.5 ± 0.00 | 2 ± 0.00 | 1.7 ± 0.00 | 2.2 ± 0.00 | 2.8 ± 0.00 |
| 15 | 1.5 ± 0.00 | 2 ± 0.00 | 1.7 ± 0.00 | 2.2 ± 0.00 | 2.8 ± 0.00 |

**Table C3** The swelling raio of Chitosan film and MCG film in 0.1 N HCl (pH 1.2)

| Time (min) | Chitosan | MCG 0.1 | MCG 0.3 | MCG 0.7 | MCG 1 |
|---|---|---|---|---|---|
| 0 | $0 \pm 0.00$ | $0 \pm 0.00$ | $0 \pm 0.00$ | $0 \pm 0.00$ | $0 \pm 0.00$ |
| 1 | $1.5 \pm 0.00$ | $2.4 \pm 0.00$ | $1.7 \pm 0.00$ | $1.8 \pm 0.00$ | $3 \pm 0.00$ |
| 2 | $1.5 \pm 0.00$ | $2.4 \pm 0.00$ | $2 \pm 0.00$ | $2.8 \pm 0.00$ | $3.2 \pm 0.00$ |
| 3 | $1.5 \pm 0.00$ | $2.4 \pm 0.00$ | $2 \pm 0.00$ | $2.8 \pm 0.00$ | $3.2 \pm 0.00$ |
| 4 | $1.5 \pm 0.00$ | $2.4 \pm 0.00$ | $2 \pm 0.00$ | $2.8 \pm 0.00$ | $3.2 \pm 0.00$ |
| 5 | $1.5 \pm 0.00$ | $2.4 \pm 0.00$ | $2 \pm 0.00$ | $2.8 \pm 0.00$ | $3.2 \pm 0.00$ |
| 6 | $1.5 \pm 0.00$ | $2.4 \pm 0.00$ | $2 \pm 0.00$ | $2.8 \pm 0.00$ | $3.2 \pm 0.00$ |
| 10 | $1.5 \pm 0.00$ | $2.4 \pm 0.00$ | $2 \pm 0.00$ | $2.8 \pm 0.00$ | $3.2 \pm 0.00$ |
| 15 | $1.5 \pm 0.00$ | $2.4 \pm 0.00$ | $2 \pm 0.00$ | $2.8 \pm 0.00$ | $3.2 \pm 0.00$ |

**Table C4** The swelling raio of Chitosan film and MCC film in $H_2O$

| Time (min) | Chitosan | MCG 0.1 | MCG 0.3 | MCG 0.7 | MCG 1 |
|---|---|---|---|---|---|
| 0 | 0 ± 0.00 | 0 ± 0.00 | 0 ± 0.00 | 0 ± 0.00 | 0 ± 0.00 |
| 1 | 1.5 ± 0.00 | 1.5 ± 0.00 | 1.7 ± 0.00 | 1.7 ± 0.00 | 1.5 ± 0.00 |
| 2 | 1.5 ± 0.00 | 2 ± 0.00 | 1.7 ± 0.00 | 2.4 ± 0.00 | 3 ± 0.00 |
| 3 | 1.5 ± 0.00 | 2 ± 0.00 | 1.7 ± 0.00 | 2.4 ± 0.00 | 3 ± 0.00 |
| 4 | 1.5 ± 0.00 | 2 ± 0.00 | 1.7 ± 0.00 | 2.4 ± 0.00 | 3 ± 0.00 |
| 5 | 1.5 ± 0.00 | 2 ± 0.00 | 1.7 ± 0.00 | 2.4 ± 0.00 | 3 ± 0.00 |
| 6 | 1.5 ± 0.00 | 2 ± 0.00 | 1.7 ± 0.00 | 2.4 ± 0.00 | 3 ± 0.00 |
| 10 | 1.5 ± 0.00 | 2 ± 0.00 | 1.7 ± 0.00 | 2.4 ± 0.00 | 3 ± 0.00 |
| 15 | 1.5 ± 0.00 | 2 ± 0.00 | 1.7 ± 0.00 | 2.4 ± 0.00 | 3 ± 0.00 |

**Table C5** The swelling raio of Chitosan film and MCC film in phosphate buffer (pH 7.4)

| Time (min) | Chitosan | MCG 0.1 | MCG 0.3 | MCG 0.7 | MCG 1 |
|---|---|---|---|---|---|
| 0 | 0 ± 0.00 | 0 ± 0.00 | 0 ± 0.00 | 0 ± 0.00 | 0 ± 0.00 |
| 1 | 1.5 ± 0.00 | 1.6 ± 0.00 | 1.6 ± 0.00 | 1.7 ± 0.00 | 2.4 ± 0.00 |
| 2 | 1.5 ± 0.00 | 2 ± 0.00 | 1.7 ± 0.00 | 2.2 ± 0.00 | 2.8 ± 0.00 |
| 3 | 1.5 ± 0.00 | 2 ± 0.00 | 1.7 ± 0.00 | 2.2 ± 0.00 | 2.8 ± 0.00 |
| 4 | 1.5 ± 0.00 | 2 ± 0.00 | 1.7 ± 0.00 | 2.2 ± 0.00 | 2.8 ± 0.00 |
| 5 | 1.5 ± 0.00 | 2 ± 0.00 | 1.7 ± 0.00 | 2.2 ± 0.00 | 2.8 ± 0.00 |
| 6 | 1.5 ± 0.00 | 2 ± 0.00 | 1.7 ± 0.00 | 2.2 ± 0.00 | 2.8 3 ± 0.00 |
| 10 | 1.5 ± 0.00 | 2 ± 0.00 | 1.7 ± 0.00 | 2.2 ± 0.00 | 2.8 ± 0.00 |
| 15 | 1.5 ± 0.00 | 2 ± 0.00 | 1.7 ± 0.00 | 2.2 ± 0.00 | 2.8 ± 0.00 |

**Table C6** The swelling raio of Chitosan film and MCC film in 0.1 N HCl (pH 1.2)

| Time (min) | Chitosan | MCG 0.1 | MCG 0.3 | MCG 0.7 | MCG 1 |
|---|---|---|---|---|---|
| 0 | 0 ± 0.00 | 0 ± 0.00 | 0 ± 0.00 | 0 ± 0.00 | 0 ± 0.00 |
| 1 | 1.5 ± 0.00 | 2.4 ± 0.00 | 1.7 ± 0.00 | 1.8 ± 0.00 | 3 ± 0.00 |
| 2 | 1.5 ± 0.00 | 2.4 ± 0.00 | 2 ± 0.00 | 2.8 ± 0.00 | 3.2 ± 0.00 |
| 3 | 1.5 ± 0.00 | 2.4 ± 0.00 | 2 ± 0.00 | 2.8 ± 0.00 | 3.2 ± 0.00 |
| 4 | 1.5 ± 0.00 | 2.4 ± 0.00 | 2 ± 0.00 | 2.8 ± 0.00 | 3.2 ± 0.00 |
| 5 | 1.5 ± 0.00 | 2.4 ± 0.00 | 2 ± 0.00 | 2.8 ± 0.00 | 3.2 ± 0.00 |
| 6 | 1.5 ± 0.00 | 2.4 ± 0.00 | 2 ± 0.00 | 2.8 ± 0.00 | 3.2 ± 0.00 |
| 10 | 1.5 ± 0.00 | 2.4 ± 0.00 | 2 ± 0.00 | 2.8 ± 0.00 | 3.2 ± 0.00 |
| 15 | 1.5 ± 0.00 | 2.4 ± 0.00 | 2 ± 0.00 | 2.8 ± 0.00 | 3.2 ± 0.00 |

**Table C7** The swelling raio of the beads in 0.1 N HCl (pH 1.2)

| Time (min) | Formulation A | Formulation B | Formulation C | Formulation D | Formulation E | Formulation F |
|---|---|---|---|---|---|---|
| 0 | 0 ± 0.00 | 0 ± 0.00 | 0 ± 0.00 | 0 ± 0.00 | 0 ± 0.00 | 0 ± 0.00 |
| 30 | 0 ± 0.00 | 0 ± 0.00 | 0 ± 0.00 | 0 ± 0.00 | 0 ± 0.00 | 0 ± 0.00 |
| 60 | 0 ± 0.00 | 0 ± 0.00 | 0 ± 0.00 | 0 ± 0.00 | 0 ± 0.00 | 0 ± 0.00 |
| 120 | 0 ± 0.00 | 0 ± 0.00 | 0 ± 0.00 | 0 ± 0.00 | 0 ± 0.00 | 0 ± 0.00 |
| 240 | 0 ± 0.00 | 0 ± 0.00 | 0 ± 0.00 | 0 ± 0.00 | 0 ± 0.00 | 0 ± 0.00 |
| 360 | 0 ± 0.00 | 0 ± 0.00 | 0 ± 0.00 | 0 ± 0.00 | 0 ± 0.00 | 0 ± 0.00 |
| 1440 | 0 ± 0.00 | 0 ± 0.00 | 0 ± 0.00 | 0 ± 0.00 | 0 ± 0.00 | 0 ± 0.00 |

**Table C8** The swelling raio of the beads in 0.1 N HCl (pH 1.2)

| Time (min) | Formulation G | Formulation H | Formulation I | Formulation J |
|:---:|:---:|:---:|:---:|:---:|
| 0 | $0 \pm 0.00$ | $0 \pm 0.00$ | $0 \pm 0.00$ | $0 \pm 0.00$ |
| 30 | $0 \pm 0.00$ | $0 \pm 0.00$ | $0 \pm 0.00$ | $0 \pm 0.00$ |
| 60 | $0 \pm 0.00$ | $0 \pm 0.00$ | $0 \pm 0.00$ | $0 \pm 0.00$ |
| 120 | $0 \pm 0.00$ | $0 \pm 0.00$ | $0 \pm 0.00$ | $0 \pm 0.00$ |
| 240 | $0 \pm 0.00$ | $0 \pm 0.00$ | $0 \pm 0.00$ | $0 \pm 0.00$ |
| 360 | $0 \pm 0.00$ | $0 \pm 0.00$ | $0 \pm 0.00$ | $0 \pm 0.00$ |
| 1440 | $0 \pm 0.00$ | $0 \pm 0.00$ | $0 \pm 0.00$ | $0 \pm 0.00$ |

**Table C9** The swelling raio of the beads in 0.1 N HCl (pH 1.2)

| Time (min) | Formulation K | Formulation L | Formulation M | Formulation N | Formulation O | Formulation P |
|---|---|---|---|---|---|---|
| 0 | 0 ± 0.00 | 0 ± 0.00 | 0 ± 0.00 | 0 ± 0.00 | 0 ± 0.00 | 0 ± 0.00 |
| 30 | 0 ± 0.00 | 0.20 ± 0.00 | 0.50 ± 0.00 | 0.33 ± 0.00 | 0 ± 0.00 | 0.25 ± 0.00 |
| 60 | 0 ± 0.00 | 0.20 ± 0.00 | 0.50 ± 0.00 | 0.67 ± 0.00 | 0.25 ± 0.00 | 0.50 ± 0.00 |
| 120 | 0 ± 0.00 | 0.20 ± 0.00 | 0.50 ± 0.00 | 0.67 ± 0.00 | 0.25 ± 0.00 | 0.50 ± 0.00 |
| 240 | 0 ± 0.00 | 0.20 ± 0.00 | 0.50 ± 0.00 | 0.67 ± 0.00 | 0.25 ± 0.00 | 0.50 ± 0.00 |
| 360 | 0 ± 0.00 | 0.20 ± 0.00 | 0.50 ± 0.00 | 0.67 ± 0.00 | 0.25 ± 0.00 | 0.50 ± 0.00 |
| 1440 | 0 ± 0.00 | 0.20 ± 0.00 | 0.50 ± 0.00 | 1.00 ± 0.00 | 0.25 ± 0.00 | 0.50 ± 0.00 |

**Table C10** The swelling raio of the beads in 0.1 N HCl (pH 1.2)

| Time (min) | Formulation Q | Formulation R | Formulation S | Formulation T |
|---|---|---|---|---|
| 0 | 0 ± 0.00 | 0 ± 0.00 | 0 ± 0.00 | 0 ± 0.00 |
| 30 | 0.33 ± 0.00 | 0.33 ± 0.00 | 0 ± 0.00 | 0.33 ± 0.00 |
| 60 | 0.67 ± 0.00 | 0.67 ± 0.00 | 0.25 ± 0.00 | 0.33 ± 0.00 |
| 120 | 0.67 ± 0.00 | 0.67 ± 0.00 | 0.25 ± 0.00 | 0.67 ± 0.00 |
| 240 | 0.67 ± 0.00 | 0.67 ± 0.00 | 0.25 ± 0.00 | 0.67 ± 0.00 |
| 360 | 0.67 ± 0.00 | 1.00 ± 0.00 | 0.25 ± 0.00 | 0.67 ± 0.00 |
| 1440 | 1.00 ± 0.00 | 1.00 ± 0.00 | 0.50 ± 0.00 | 0.67 ± 0.00 |

**Table C11** The swelling raio of the beads in phosphate buffer pH 7.4

| Time (min) | Formulation A | Formulation B | Formulation C | Formulation D | Formulation E | Formulation F |
|---|---|---|---|---|---|---|
| 0 | 0 ± 0.00 | 0 ± 0.00 | 0 ± 0.00 | 0 ± 0.00 | 0 ± 0.00 | 0 ± 0.00 |
| 30 | 0 ± 0.00 | 0 ± 0.00 | 0 ± 0.00 | 0 ± 0.00 | 0 ± 0.00 | 0 ± 0.00 |
| 60 | 0 ± 0.00 | 0.50 ± 0.00 | 0.50 ± 0.00 | 0.50 ± 0.00 | 0.50 ± 0.00 | 0.50 ± 0.00 |
| 120 | 0.50 ± 0.00 | 0.75 ± 0.00 | 0.75 ± 0.00 | 0.75 ± 0.00 | 0.75 ± 0.00 | 0.75 ± 0.00 |
| 240 | 0.75 ± 0.00 | 0.75 ± 0.00 | 1.25 ± 0.00 | 1.00 ± 0.00 | 1.25 ± 0.00 | 0.75 ± 0.00 |
| 360 | 1.00 ± 0.00 | 1.00 ± 0.00 | 1.25 ± 0.00 | 1.00 ± 0.00 | 1.25 ± 0.00 | 0.75 ± 0.00 |
| 1440 | 1.00 ± 0.00 | 1.00 ± 0.00 | 1.25 ± 0.00 | 1.00 ± 0.00 | 1.25 ± 0.00 | 0.75 ± 0.00 |

**Table C12** The swelling raio of the beads in phosphate buffer pH 7.4

| Time (min) | Formulation G | Formulation H | Formulation I | Formulation J |
|---|---|---|---|---|
| 0 | 0 ± 0.00 | 0 ± 0.00 | 0 ± 0.00 | 0 ± 0.00 |
| 30 | 0 ± 0.00 | 0 ± 0.00 | 0 ± 0.00 | 0 ± 0.00 |
| 60 | 0.25 ± 0.00 | 0.25 ± 0.00 | 0.25 ± 0.00 | 0.25 ± 0.00 |
| 120 | 0.50 ± 0.00 | 0.50 ± 0.00 | 0.75 ± 0.00 | 0.75 ± 0.00 |
| 240 | 0.75 ± 0.00 | 1.00 ± 0.00 | 1.00 ± 0.00 | 1.00 ± 0.00 |
| 360 | 0.75 ± 0.00 | 1.00 ± 0.00 | 1.00 ± 0.00 | 1.00 ± 0.00 |
| 1440 | 0.75 ± 0.00 | 1.00 ± 0.00 | 1.00 ± 0.00 | 1.00 ± 0.00 |

**Table C13** The swelling raio of the beads in phosphate buffer pH 7.4

| Time (min) | Formulation K | Formulation L | Formulation M | Formulation N | Formulation O | Formulation P |
|---|---|---|---|---|---|---|
| 0 | 0 ± 0.00 | 0 ± 0.00 | 0 ± 0.00 | 0 ± 0.00 | 0 ± 0.00 | 0 ± 0.00 |
| 30 | 0.25 ± 0.00 | 0.20 ± 0.00 | 0.50 ± 0.00 | 0.33 ± 0.00 | 0 ± 0.00 | 0.25 ± 0.00 |
| 60 | 0.50 ± 0.00 | 0.40 ± 0.00 | 1.00 ± 0.00 | 0.33 ± 0.00 | 0.50 ± 0.00 | 0.50 ± 0.00 |
| 120 | 1.00 ± 0.00 | 1.00 ± 0.00 | 1.50 ± 0.00 | 0.67 ± 0.00 | 1.00 ± 0.00 | 1.25 ± 0.00 |
| 240 | 1.50 ± 0.00 | 1.20 ± 0.00 | 1.75 ± 0.00 | 1.67 ± 0.00 | 1.00 ± 0.00 | 1.50 ± 0.00 |
| 360 | 1.75 ± 0.00 | 1.40 ± 0.00 | 1.75 ± 0.00 | 2.33 ± 0.00 | 1.50 ± 0.00 | 1.50 ± 0.00 |
| 1440 | 1.75 ± 0.00 | 1.40 ± 0.00 | 2.00 ± 0.00 | 2.33 ± 0.00 | 1.50 ± 0.00 | 1.50 ± 0.00 |

**Table C14** The swelling raio of the beads in phosphate buffer pH 7.4

| Time (min) | Formulation Q | Formulation R | Formulation S | Formulation T |
|---|---|---|---|---|
| 0 | 0 ± 0.00 | 0 ± 0.00 | 0 ± 0.00 | 0 ± 0.00 |
| 30 | 0.67 ± 0.00 | 0.67 ± 0.00 | 0.25 ± 0.00 | 0.33 ± 0.00 |
| 60 | 0.67 ± 0.00 | 0.67 ± 0.00 | 0.25 ± 0.00 | 0.67 ± 0.00 |
| 120 | 1.33 ± 0.00 | 1.00 ± 0.00 | 0.50 ± 0.00 | 1.33 ± 0.00 |
| 240 | 2.00 ± 0.00 | 1.67 ± 0.00 | 1.25 ± 0.00 | 2.00 ± 0.00 |
| 360 | 2.00 ± 0.00 | 1.67 ± 0.00 | 1.25 ± 0.00 | 2.33 ± 0.00 |
| 1440 | 2.00 ± 0.00 | 1.67 ± 0.00 | 1.50 ± 0.00 | 2.33 ± 0.00 |

# APPENDIX D

**Percentage of drug release**

**Table D1** Percentage of sodium diclofenac release in 0.1 N HCl (pH 1.2)

| Time (min) | Formulation A | | | | Formulation B | | | | Formulation C | | | | Formulation D | | | |
|---|---|---|---|---|---|---|---|---|---|---|---|---|---|---|---|---|
| | 1 | 2 | 3 | mean±SD | 1 | 2 | 3 | mean±SD | 1 | 2 | 3 | mean±SD | 1 | 2 | 3 | mean±SD |
| 0 | 0.43 | 0.39 | 0.33 | 0.38 ± 0.05 | 0.12 | 0.11 | 0.20 | 0.14 ± 0.05 | 0.10 | 0.15 | 0.07 | 0.10 ± 0.04 | 0.07 | 0.09 | 0.11 | 0.09 ± 0.02 |
| 15 | 0.59 | 0.48 | 0.40 | 0.48 ± 0.09 | 0.10 | 0.16 | 0.15 | 0.14 ± 0.03 | 0.34 | 0.35 | 0.30 | 0.33 ± 0.02 | 0.10 | 0.07 | 0.07 | 0.08 ± 0.02 |
| 30 | 0.62 | 0.45 | 0.61 | 0.56 ± 0.09 | 0.18 | 0.17 | 0.12 | 0.15 ± 0.03 | 0.36 | 0.37 | 0.34 | 0.35 ± 0.02 | 0.13 | 0.12 | 0.13 | 0.13 ± 0.01 |
| 60 | 0.54 | 0.38 | 0.33 | 0.42 ± 0.11 | 0.15 | 0.18 | 0.16 | 0.16 ± 0.02 | 0.42 | 0.44 | 0.45 | 0.43 ± 0.01 | 0.17 | 0.18 | 0.19 | 0.18 ± 0.01 |
| 90 | 0.51 | 0.48 | 0.56 | 0.52 ± 0.04 | 0.29 | 0.17 | 0.22 | 0.23 ± 0.06 | 0.48 | 0.42 | 0.37 | 0.42 ± 0.05 | 0.18 | 0.24 | 0.22 | 0.21 ± 0.03 |
| 120 | 0.57 | 0.49 | 0.48 | 0.51 ± 0.05 | 0.21 | 0.20 | 0.20 | 0.20 ± 0.00 | 0.46 | 0.39 | 0.41 | 0.42 ± 0.04 | 0.27 | 0.36 | 0.27 | 0.30 ± 0.05 |
| 240 | 0.69 | 0.60 | 0.67 | 0.65 ± 0.04 | 0.23 | 0.22 | 0.17 | 0.21 ± 0.03 | 0.54 | 0.50 | 0.53 | 0.52 ± 0.02 | 0.29 | 0.28 | 0.27 | 0.28 ± 0.01 |
| 360 | 0.76 | 0.80 | 0.77 | 0.78 ± 0.02 | 0.26 | 0.27 | 0.25 | 0.26 ± 0.01 | 0.60 | 0.57 | 0.62 | 0.60 ± 0.03 | 0.38 | 0.35 | 0.40 | 0.38 ± 0.03 |
| 480 | 0.97 | 0.90 | 0.84 | 0.90 ± 0.06 | 0.29 | 0.31 | 0.26 | 0.28 ± 0.03 | 0.70 | 0.65 | 0.62 | 0.66 ± 0.04 | 0.46 | 0.50 | 0.46 | 0.47 ± 0.02 |
| 1440 | 1.06 | 0.92 | 0.93 | 0.97 ± 0.08 | 0.39 | 0.41 | 0.38 | 0.39 ± 0.02 | 0.69 | 0.69 | 0.80 | 0.73 ± 0.06 | 0.56 | 0.54 | 0.54 | 0.55 ± 0.01 |

**Table D2** Percentage of sodium diclofenac release in 0.1 N HCl (pH 1.2)

| Time (min) | Formulation E | | | | Formulation F | | | | Formulation G | | | | Formulation H | | | |
|---|---|---|---|---|---|---|---|---|---|---|---|---|---|---|---|---|
| | 1 | 2 | 3 | mean±SD | 1 | 2 | 3 | mean±SD | 1 | 2 | 3 | mean±SD | 1 | 2 | 3 | mean±SD |
| 0 | 0.02 | 0.02 | 0.02 | 0.02 ± 0.00 | 0.02 | 0.02 | 0.02 | 0.02 ± 0.00 | 0.09 | 0.08 | 0.07 | 0.08 ± 0.01 | 0.15 | 0.04 | 0.06 | 0.08 ± 0.06 |
| 15 | 0.05 | 0.06 | 0.06 | 0.05 ± 0.01 | 0.13 | 0.09 | 0.12 | 0.11 ± 0.02 | 0.19 | 0.28 | 0.23 | 0.23 ± 0.04 | 0.23 | 0.24 | 0.24 | 0.24 ± 0.01 |
| 30 | 0.10 | 0.13 | 0.11 | 0.11 ± 0.02 | 0.16 | 0.15 | 0.18 | 0.16 ± 0.02 | 0.14 | 0.14 | 0.14 | 0.14 ± 0.00 | 0.26 | 0.30 | 0.27 | 0.28 ± 0.02 |
| 60 | 0.15 | 0.17 | 0.18 | 0.17 ± 0.02 | 0.21 | 0.18 | 0.21 | 0.20 ± 0.02 | 0.74 | 0.23 | 0.51 | 0.50 ±0.26 | 0.37 | 0.35 | 0.30 | 0.34 ± 0.04 |
| 90 | 0.22 | 0.21 | 0.19 | 0.20 ± 0.01 | 0.20 | 0.20 | 0.22 | 0.20 ± 0.01 | 0.20 | 0.26 | 0.22 | 0.23 ± 0.03 | 0.50 | 0.38 | 0.32 | 0.40 ± 0.09 |
| 120 | 0.23 | 0.20 | 0.25 | 0.23 ± 0.02 | 0.25 | 0.24 | 0.26 | 0.25 ± 0.01 | 0.40 | 0.32 | 0.35 | 0.35 ± 0.04 | 0.41 | 0.43 | 0.32 | 0.39 ± 0.06 |
| 240 | 0.30 | 0.34 | 0.31 | 0.31 ± 0.02 | 0.28 | 0.30 | 0.29 | 0.29 ± 0.01 | 0.29 | 0.81 | 0.58 | 0.56 ± 0.26 | 0.56 | 0.51 | 0.46 | 0.51 ± 0.05 |
| 360 | 0.38 | 0.38 | 0.38 | 0.38 ± 0.00 | 0.32 | 0.35 | 0.34 | 0.34 ± 0.02 | 0.33 | 0.34 | 0.39 | 0.35 ± 0.03 | 0.64 | 0.57 | 0.52 | 0.57 ± 0.06 |
| 480 | 0.44 | 0.47 | 0.45 | 0.45 ± 0.02 | 0.35 | 0.38 | 0.40 | 0.37 ± 0.02 | 0.40 | 0.44 | 0.39 | 0.41 ± 0.03 | 0.72 | 0.63 | 1.12 | 0.82 ± 0.26 |
| 1440 | 0.71 | 0.62 | 0.59 | 0.64 ± 0.06 | 0.43 | 0.45 | 0.46 | 0.45 ± 0.01 | 0.63 | 0.72 | 0.68 | 0.68 ±0.04 | 0.79 | 0.67 | 0.88 | 0.78 ± 0.10 |

**Table D3** Percentage of sodium diclofenac release in 0.1 N HCl (pH 1.2)

| Time (min) | Formulation I | | | | Formulation J | | | |
|---|---|---|---|---|---|---|---|---|
| | 1 | 2 | 3 | mean±SD | 1 | 2 | 3 | mean±SD |
| 0 | 0.32 | 0.15 | 0.24 | 0.24 ± 0.09 | 0.0231 | 0.0347 | 0.0441 | 0.03 ± 0.01 |
| 15 | 0.40 | 0.32 | 0.30 | 0.34 ± 0.05 | 0.0837 | 0.1278 | 0.1146 | 0.11 ± 0.02 |
| 30 | 0.29 | 0.22 | 0.23 | 0.25 ±0.04 | 0.1432 | 0.0818 | 0.1238 | 0.12 ± 0.03 |
| 60 | 0.48 | 0.81 | 0.62 | 0.64 ± 0.16 | 0.1276 | 0.0949 | 0.1309 | 0.12 ± 0.02 |
| 90 | 0.66 | 0.37 | 0.45 | 0.49 ± 0.14 | 0.5950 | 0.1407 | 0.3120 | 0.35 ± 0.22 |
| 120 | 0.34 | 0.37 | 0.36 | 0.36 ± 0.01 | 0.3777 | 0.1664 | 0.2740 | 0.27 ± 0.10 |
| 240 | 0.38 | 0.42 | 0.41 | 0.40 ± 0.02 | 0.3109 | 0.4192 | 0.3024 | 0.34 ± 0.06 |
| 360 | 0.46 | 0.89 | 0.58 | 0.64 ±0.22 | 0.2680 | 0.2124 | 0.2362 | 0.23 ± 0.03 |
| 480 | 0.54 | 0.64 | 0.64 | 0.61 ± 0.06 | 0.2935 | 0.2671 | 0.2914 | 0.28 ± 0.01 |
| 1440 | 0.68 | 0.78 | 0.71 | 0.72 ± 0.05 | 0.6526 | 0.5631 | 0.6517 | 0.62 ± 0.05 |

**Table D4** Percentage of sodium diclofenac release in phosphate buffer pH 7.4

| Time (min) | Formulation A | | | | Formulation B | | | | Formulation C | | | | Formulation D | | | |
|---|---|---|---|---|---|---|---|---|---|---|---|---|---|---|---|---|
| | 1 | 2 | 3 | mean±SD | 1 | 2 | 3 | mean±SD | 1 | 2 | 3 | mean±SD | 1 | 2 | 3 | mean±SD |
| 0 | 2.78 | 2.26 | 2.38 | 2.47 ± 0.27 | 0.27 | 0.28 | 0.36 | 0.30 ± 0.05 | 0.30 | 0.32 | 0.22 | 0.28 ± 0.06 | 0.13 | 0.13 | 0.13 | 0.13 ± 0.00 |
| 15 | 8.85 | 8.83 | 7.11 | 8.26 ± 1.00 | 3.02 | 2.48 | 2.55 | 2.68 ± 0.30 | 1.65 | 2.26 | 2.19 | 2.03 ± 0.33 | 1.19 | 1.16 | 1.73 | 1.36 ± 0.32 |
| 30 | 11.32 | 11.99 | 9.72 | 11.0 ± 1.16 | 4.54 | 4.09 | 4.14 | 4.26 ± 0.25 | 3.63 | 3.28 | 3.27 | 3.39 ± 0.21 | 2.34 | 2.13 | 2.24 | 2.24 ± 0.11 |
| 60 | 21.93 | 21.87 | 19.44 | 21.0 ± 1.42 | 11.60 | 10.82 | 10.85 | 11.09±0.44 | 7.88 | 7.44 | 8.32 | 7.88 ± 0.44 | 5.46 | 5.07 | 4.88 | 5.13 ± 0.30 |
| 90 | 28.54 | 29.36 | 27.24 | 28.38± .07 | 18.92 | 18.68 | 18.49 | 18.70±0.21 | 12.89 | 11.79 | 11.41 | 12.03±0.76 | 8.09 | 7.45 | 7.38 | 7.64 ± 0.39 |
| 120 | 35.93 | 37.92 | 34.54 | 36.1 ± 1.70 | 25.58 | 26.11 | 25.61 | 25.77±0.30 | 18.15 | 16.64 | 16.75 | 17.18±0.84 | 12.66 | 10.92 | 11.84 | 11.80±0.87 |
| 240 | 54.99 | 60.86 | 59.76 | 58.54±3.12 | 48.56 | 49.44 | 47.19 | 48.40±1.13 | 31.22 | 28.92 | 31.48 | 30.54±1.41 | 27.37 | 25.08 | 25.00 | 25.82±1.35 |
| 360 | 69.82 | 76.60 | 73.49 | 73.30±3.40 | 65.59 | 64.90 | 62.25 | 64.25±1.76 | 41.47 | 40.55 | 45.08 | 42.37±2.40 | 39.70 | 38.70 | 38.31 | 38.90±0.71 |
| 480 | 76.65 | 82.74 | 79.76 | 79.72±3.04 | 73.32 | 77.66 | 76.53 | 75.84±2.25 | 51.47 | 52.24 | 58.58 | 54.10±3.90 | 51.92 | 51.58 | 49.79 | 51.10±1.15 |
| 1440 | 71.43 | 80.22 | 77.06 | 76.24±4.45 | 96.96 | 96.47 | 97.23 | 96.89±0.38 | 92.63 | 100.84 | 102.86 | 98.78±5.42 | 90.57 | 93.13 | 97.73 | 93.8 ± 3.63 |

**Table D5** Percentage of sodium diclofenac release in phosphate buffer pH 7.4

| Time (min) | Formulation E | | | | Formulation F | | | | Formulation G | | | | Formulation H | | | |
|---|---|---|---|---|---|---|---|---|---|---|---|---|---|---|---|---|
| | 1 | 2 | 3 | mean±SD | 1 | 2 | 3 | mean±SD | 1 | 2 | 3 | mean±SD | 1 | 2 | 3 | mean±SD |
| 0 | 0.14 | 0.13 | 0.24 | 0.17 ± 0.06 | 0.13 | 0.13 | 0.13 | 0.13 ± 0.00 | 0.33 | 0.38 | 0.38 | 0.36 ± 0.03 | 0.26 | 0.22 | 0.40 | 0.30 ± 0.09 |
| 15 | 1.77 | 1.94 | 2.35 | 2.02 ± 0.30 | 0.99 | 1.01 | 0.77 | 0.92 ± 0.13 | 1.36 | 1.35 | 1.39 | 1.37 ± 0.02 | 2.54 | 3.39 | 2.34 | 2.76 ± 0.53 |
| 30 | 2.90 | 2.56 | 2.77 | 2.74 ± 0.17 | 1.65 | 2.07 | 1.69 | 1.81 ± 0.23 | 1.98 | 1.58 | 1.88 | 1.81 ±0.20 | 4.11 | 5.24 | 4.03 | 4.46 ± 0.61 |
| 60 | 7.86 | 7.15 | 7.27 | 7.43 ± 0.38 | 4.29 | 4.58 | 3.97 | 4.28 ± 0.30 | 6.12 | 7.16 | 6.59 | 6.63 ± 0.52 | 12.20 | 12.80 | 11.53 | 12.18±0.64 |
| 90 | 12.05 | 10.92 | 10.93 | 11.30±0.65 | 7.53 | 6.96 | 5.66 | 6.72 ± 0.96 | 11.35 | 11.71 | 11.55 | 11.54±0.18 | 20.69 | 20.83 | 20.33 | 20.62±0.25 |
| 120 | 15.79 | 15.38 | 15.46 | 15.54±0.21 | 11.05 | 9.85 | 8.35 | 9.75 ± 1.35 | 17.06 | 19.16 | 17.95 | 18.06±1.05 | 29.04 | 29.67 | 30.02 | 29.58±0.23 |
| 240 | 28.16 | 30.10 | 30.75 | 29.67±1.35 | 25.77 | 20.95 | 20.62 | 22.45±2.88 | 31.13 | 35.04 | 32.85 | 33.00±1.96 | 53.16 | 58.27 | 58.30 | 56.58±0.99 |
| 360 | 40.11 | 44.19 | 44.68 | 42.99±2.51 | 38.77 | 35.16 | 35.39 | 36.44±2.02 | 47.95 | 50.89 | 47.12 | 48.65±1.98 | 71.91 | 74.72 | 74.59 | 73.74±0.53 |
| 480 | 48.77 | 54.93 | 54.91 | 52.87±3.55 | 49.58 | 45.70 | 47.50 | 47.59±1.94 | 56.56 | 63.01 | 61.78 | 60.45±3.43 | 81.22 | 89.03 | 86.99 | 85.75±1.66 |
| 1440 | 92.57 | 104.84 | 99.38 | 98.93±6.15 | 95.21 | 93.77 | 99.68 | 96.22±3.08 | 97.04 | 96.55 | 96.31 | 96.63±0.38 | 92.85 | 93.64 | 99.20 | 95.23±2.86 |

**Table D6** Percentage of sodium diclofenac release in phosphate buffer pH 7.4

| Time (min) | Formulation I | | | | Formulation J | | | |
|---|---|---|---|---|---|---|---|---|
| | 1 | 2 | 3 | mean±SD | 1 | 2 | 3 | mean±SD |
| 0 | 0.70 | 0.69 | 0.65 | $0.68 \pm 0.03$ | 1.10 | 0.97 | 1.13 | $1.06 \pm 0.09$ |
| 15 | 1.23 | 0.88 | 1.04 | $1.05 \pm 0.18$ | 1.90 | 2.10 | 1.88 | $1.96 \pm 0.14$ |
| 30 | 1.51 | 1.23 | 1.28 | $1.34 \pm 0.15$ | 2.16 | 1.57 | 1.77 | $1.83 \pm 0.40$ |
| 60 | 3.29 | 2.72 | 2.97 | $2.99 \pm 0.29$ | 5.23 | 4.57 | 4.59 | $4.80 \pm 0.50$ |
| 90 | 5.29 | 4.62 | 4.79 | $4.90 \pm 0.34$ | 8.09 | 6.93 | 7.28 | $7.43 \pm 0.83$ |
| 120 | 8.17 | 8.39 | 8.14 | $8.23 \pm 0.13$ | 13.76 | 10.67 | 12.10 | $12.18 \pm 2.07$ |
| 240 | 16.19 | 17.70 | 16.64 | $16.84 \pm 0.77$ | 25.94 | 35.29 | 25.02 | $28.75 \pm 6.23$ |
| 360 | 28.44 | 31.52 | 29.55 | $29.84 \pm 1.56$ | 37.01 | 38.50 | 36.02 | $37.18 \pm 1.60$ |
| 480 | 39.85 | 40.75 | 41.58 | $40.72 \pm 0.87$ | 49.68 | 47.40 | 47.06 | $48.05 \pm 2.45$ |
| 1440 | 89.76 | 89.73 | 88.25 | $89.25 \pm 0.86$ | 98.50 | 95.99 | 104.53 | $99.67 \pm 1.97$ |

**Table D7** Percentage of amoxicillin trihydrate release in 0.1 N HCl (pH 1.2)

| Time (min) | Formulation K | | | | Formulation L | | | | Formulation M | | | | Formulation N | | | |
|---|---|---|---|---|---|---|---|---|---|---|---|---|---|---|---|---|
| | 1 | 2 | 3 | mean±SD | 1 | 2 | 3 | mean±SD | 1 | 2 | 3 | mean±SD | 1 | 2 | 3 | mean±SD |
| 0 | 3.42 | 3.29 | 3.40 | 3.37± 0.07 | 3.80 | 3.79 | 3.88 | 3.82± 0.05 | 3.39 | 3.88 | 3.80 | 3.69± 0.26 | 4.42 | 4.48 | 4.44 | 4.44± 0.03 |
| 30 | 6.24 | 7.75 | 6.92 | 6.97±0.75 | 12.19 | 9.67 | 11.90 | 11.25±1.38 | 18.67 | 9.41 | 11.15 | 13.07±4.92 | 8.76 | 9.65 | 9.47 | 9.29± 0.47 |
| 60 | 34.71 | 33.31 | 34.23 | 34.08±0.71 | 36.09 | 35.69 | 36.17 | 35.98±0.26 | 50.34 | 32.83 | 37.17 | 40.11±9.12 | 21.58 | 21.27 | 21.73 | 21.53±0.23 |
| 120 | 56.31 | 52.14 | 55.68 | 54.71±2.25 | 67.69 | 65.28 | 69.25 | 67.41±2.00 | 79.65 | 58.90 | 60.97 | 66.51±11.46 | 47.86 | 47.47 | 48.73 | 48.02±0.65 |
| 240 | 65.01 | 57.55 | 59.65 | 60.73±3.85 | 79.19 | 75.66 | 79.63 | 78.16±2.18 | 82.80 | 67.77 | 70.00 | 73.52 ± 8.11 | 60.83 | 63.87 | 63.27 | 62.66±1.61 |
| 360 | 69.26 | 68.97 | 68.96 | 69.06±0.17 | 84.12 | 84.84 | 85.34 | 84.77±0.61 | 84.12 | 74.35 | 76.48 | 78.32 ± 5.14 | 70.88 | 73.14 | 71.72 | 71.91±1.14 |
| 1440 | 90.67 | 89.91 | 90.39 | 90.32±0.39 | 103.63 | 103.57 | 103.78 | 103.66±0.11 | 90.09 | 89.54 | 89.52 | 89.72 ± 0.33 | 91.34 | 91.85 | 91.59 | 91.59±0.25 |

**Table D8** Percentage of amoxicillin trihydrate release in 0.1 N HCl (pH 1.2)

| Time (min) | Formulation O | | | | Formulation P | | | | Formulation Q | | | | Formulation R | | | |
|---|---|---|---|---|---|---|---|---|---|---|---|---|---|---|---|---|
| | 1 | 2 | 3 | mean±SD | 1 | 2 | 3 | mean±SD | 1 | 2 | 3 | mean±SD | 1 | 2 | 3 | mean±SD |
| 0 | 4.31 | 4.33 | 4.46 | 4.36 ± 0.08 | 3.34 | 3.28 | 3.38 | 3.33 ± 0.05 | 3.30 | 3.95 | 3.86 | 3.70 ± 0.35 | 3.47 | 3.91 | 4.30 | 3.89 ± 0.42 |
| 30 | 15.15 | 12.09 | 17.01 | 14.75±2.48 | 19.63 | 18.40 | 19.96 | 19.33±0.83 | 13.64 | 6.82 | 9.90 | 10.12±3.42 | 12.80 | 7.82 | 13.80 | 11.48±3.20 |
| 60 | 34.49 | 29.59 | 35.68 | 33.25±3.23 | 44.86 | 43.79 | 44.99 | 44.55±0.66 | 37.16 | 21.35 | 31.98 | 30.17±8.06 | 36.94 | 22.89 | 39.34 | 33.06±8.88 |
| 120 | 63.57 | 60.13 | 65.02 | 62.91±2.51 | 69.66 | 66.93 | 70.66 | 69.08±1.93 | 53.18 | 44.89 | 52.86 | 50.31±4.69 | 53.88 | 43.78 | 55.17 | 50.94±6.24 |
| 240 | 73.61 | 72.25 | 75.53 | 73.80±1.65 | 78.86 | 77.19 | 78.17 | 78.07±0.84 | 58.93 | 55.21 | 62.63 | 58.92±3.71 | 59.56 | 54.64 | 63.78 | 59.33±4.57 |
| 360 | 73.72 | 73.58 | 75.64 | 74.31±1.15 | 84.70 | 82.40 | 82.35 | 83.15±1.35 | 64.63 | 63.03 | 69.93 | 65.87±3.61 | 61.72 | 62.61 | 68.84 | 64.39±3.88 |
| 1440 | 94.20 | 94.02 | 95.09 | 94.43±0.57 | 90.55 | 89.83 | 90.77 | 90.38±0.49 | 96.34 | 96.33 | 89.05 | 93.91±4.21 | 94.61 | 94.78 | 96.45 | 95.28±1.02 |

**Table D9** Percentage of amoxicillin trihydrate release in 0.1 N HCl (pH 1.2)

| Time (min) | Formulation S | | | | Formulation T | | | |
|---|---|---|---|---|---|---|---|---|
| | 1 | 2 | 3 | mean±SD | 1 | 2 | 3 | mean±SD |
| 0 | 3.28 | 3.95 | 3.52 | 3.59 ± 0.34 | 4.16 | 4.13 | 4.09 | 4.13 ± 0.03 |
| 30 | 10.01 | 7.67 | 8.57 | 8.75 ± 1.18 | 11.57 | 11.56 | 11.60 | 11.57 ± 0.02 |
| 60 | 24.41 | 20.38 | 22.45 | 22.41 ± 2.02 | 26.61 | 26.11 | 26.69 | 26.47 ± 0.32 |
| 120 | 42.90 | 38.68 | 42.38 | 41.32 ± 2.30 | 51.53 | 52.57 | 52.19 | 52.10 ± 0.53 |
| 240 | 52.91 | 49.28 | 52.67 | 51.62 ± 2.03 | 62.93 | 59.36 | 62.97 | 61.75 ± 2.07 |
| 360 | 58.72 | 57.24 | 58.52 | 58.16 ± 0.80 | 65.31 | 66.94 | 66.35 | 66.20 ± 0.82 |
| 1440 | 94.77 | 97.51 | 96.63 | 96.30 ± 1.40 | 92.07 | 92.50 | 92.37 | 92.32 ± 0.22 |

**Table D10** Percentage of amoxicillin trihydrate release in phosphate buffer pH 7.4

| Time (min) | Formulation K | | | | Formulation L | | | | Formulation M | | | | Formulation N | | | |
|---|---|---|---|---|---|---|---|---|---|---|---|---|---|---|---|---|
| | 1 | 2 | 3 | mean±SD | 1 | 2 | 3 | mean±SD | 1 | 2 | 3 | mean±SD | 1 | 2 | 3 | mean±SD |
| 0 | 1.13 | 1.16 | 1.07 | 1.12± 0.04 | 0.43 | 0.43 | 0.41 | 0.42± 0.01 | 0.43 | 0.45 | 0.42 | 0.43± 0.01 | 0.29 | 0.30 | 0.28 | 0.29± 0.01 |
| 30 | 2.30 | 1.93 | 2.79 | 2.34± 0.43 | 6.20 | 6.92 | 6.39 | 6.51± 0.37 | 3.89 | 4.02 | 4.03 | 3.98± 0.07 | 1.00 | 0.90 | 0.76 | 0.89± 0.12 |
| 60 | 17.20 | 16.24 | 17.36 | 16.93±0.60 | 19.46 | 19.99 | 19.49 | 19.65±0.29 | 18.57 | 18.73 | 18.88 | 18.73±0.16 | 17.86 | 17.76 | 17.68 | 17.77±0.09 |
| 120 | 71.02 | 71.30 | 71.42 | 71.25±0.21 | 51.23 | 51.48 | 50.87 | 51.20±0.30 | 46.30 | 46.49 | 46.46 | 46.41±0.10 | 50.52 | 50.26 | 50.29 | 50.36±0.14 |
| 240 | 95.48 | 96.12 | 95.76 | 95.79±0.32 | 84.97 | 85.49 | 84.98 | 85.15±0.30 | 81.56 | 81.76 | 81.76 | 81.70±0.12 | 93.63 | 93.31 | 93.52 | 93.48±0.16 |
| 360 | 100.98 | 100.48 | 97.54 | 99.67±1.85 | 100.38 | 98.39 | 98.31 | 99.03±1.18 | 94.84 | 94.92 | 94.92 | 94.89±0.05 | 98.88 | 100.04 | 100.35 | 99.75±0.77 |
| 1440 | 81.33 | 81.11 | 81.30 | 81.25±0.12 | 82.13 | 82.10 | 81.59 | 81.94±0.30 | 75.86 | 75.98 | 75.97 | 75.94±0.07 | 82.54 | 82.31 | 82.51 | 82.45±0.12 |

**Table D11** Percentage of amoxicillin trihydrate release in phosphate buffer pH 7.4

| Time (min) | Formulation O | | | | Formulation P | | | | Formulation Q | | | | Formulation R | | | |
|---|---|---|---|---|---|---|---|---|---|---|---|---|---|---|---|---|
| | 1 | 2 | 3 | mean±SD | 1 | 2 | 3 | mean±SD | 1 | 2 | 3 | mean±SD | 1 | 2 | 3 | mean±SD |
| 0 | 0.24 | 0.25 | 0.23 | 0.24 ± 0.01 | 0.46 | 0.47 | 0.44 | 0.46 ± 0.02 | 0.32 | 0.34 | 0.31 | 0.32 ± 0.01 | 0.30 | 0.30 | 0.29 | 0.30 ± 0.01 |
| 30 | 5.58 | 5.62 | 5.59 | 5.60 ± 0.02 | 3.25 | 3.24 | 3.31 | 3.27 ± 0.04 | 2.52 | 2.34 | 2.47 | 2.44 ± 0.09 | 3.46 | 3.57 | 3.53 | 3.52 ± 0.05 |
| 60 | 19.26 | 19.39 | 19.47 | 19.38±0.11 | 18.25 | 18.06 | 18.24 | 18.19±0.11 | 18.00 | 13.36 | 15.49 | 15.62±2.32 | 14.53 | 13.72 | 14.26 | 14.17±0.41 |
| 120 | 60.10 | 60.44 | 60.19 | 60.24±0.18 | 48.28 | 48.33 | 48.42 | 48.35±0.07 | 51.57 | 40.75 | 48.10 | 46.81±5.52 | 42.28 | 39.68 | 40.93 | 40.96±1.30 |
| 240 | 86.21 | 86.82 | 86.34 | 86.46±0.32 | 91.75 | 91.77 | 91.90 | 91.80±0.08 | 86.58 | 79.76 | 84.84 | 83.73±3.55 | 82.67 | 84.04 | 84.80 | 83.84±1.08 |
| 360 | 99.65 | 100.61 | 99.71 | 99.99±0.54 | 98.93 | 99.42 | 99.23 | 99.20±0.25 | 93.39 | 86.72 | 89.99 | 90.03±3.34 | 93.29 | 90.90 | 93.96 | 92.72±1.61 |
| 1440 | 93.05 | 93.69 | 90.63 | 92.46±1.61 | 88.93 | 89.14 | 89.22 | 89.09±0.15 | 92.67 | 85.77 | 89.98 | 89.47±3.48 | 82.44 | 78.79 | 82.27 | 81.17±2.06 |

**Table D12** Percentage of amoxicillin trihydrate release in phosphate buffer pH 7.4

| Time (min) | Formulation S | | | | Formulation T | | | |
|---|---|---|---|---|---|---|---|---|
| | 1 | 2 | 3 | mean±SD | 1 | 2 | 3 | mean±SD |
| 0 | 0.45 | 0.47 | 0.43 | 0.45 ± 0.02 | 0.31 | 0.30 | 0.28 | 0.30 ± 0.01 |
| 30 | 4.62 | 4.41 | 4.52 | 4.52 ± 0.10 | 1.13 | 1.24 | 1.11 | 1.16 ± 0.07 |
| 60 | 21.90 | 21.73 | 21.78 | 21.80 ± 0.09 | 14.84 | 10.75 | 13.92 | 13.17 ± 2.15 |
| 120 | 54.19 | 54.48 | 54.39 | 54.35 ± 0.15 | 43.06 | 53.29 | 52.36 | 49.57 ± 5.66 |
| 240 | 75.75 | 76.10 | 75.88 | 75.91 ± 0.18 | 92.15 | 85.43 | 89.57 | 89.25 ± 3.06 |
| 360 | 78.16 | 78.23 | 78.28 | 78.22 ± 0.06 | 99.23 | 98.68 | 98.20 | 98.90 ± 0.61 |
| 1440 | 68.03 | 69.84 | 68.12 | 68.66 ± 1.02 | 68.98 | 65.58 | 65.90 | 67.02 ± 1.70 |

**VITA**

Name           : Miss Metawee Srilaphan

Date of Birth  : August 23, 1981

Nationality    : Thai

Education       : 2000 – 2003 Bachelor's Degree of Science in Chemistry,
                 Chandrakasem Rajabhat University, Bangkok, Thailand

                 2006 – 2009 Master's Degree of Science in Program of
                 Petrochemistry and Polymer Science, Chulalongkorn University,
                 Bangkok, Thailand

Grant          : Graduate Thesis Grant of Chulalongkorn University